DANMARKS OG GRØNLANDS GEOLOGISKE UNDERSØGELSE RAPPORT 2006/28

# Rock physics analysis of sonic velocities in basalts from Faroes and Icelandic wells

Contribution to the SeiFaBa Project
Funded by the Sindri Group

Peter Japsen & Gary Mavko

CONFIDENTIAL
FORTROLIG

GEOLOGICAL SURVEY OF DENMARK AND GREENLAND
MINISTRY OF THE ENVIRONMENT

G E U S

DANMARKS OG GRØNLANDS GEOLOGISKE UNDERSØGELSE RAPPORT 2006/28

# Rock physics analysis of sonic velocities in basalts from Faroes and Icelandic wells

## Contribution to the SeiFaBa Project Funded by the Sindri Group

Peter Japsen[1] & Gary Mavko[2]

[1] Danmarks og Grønlands Geologiske Undersøgelse (GEUS)
[2] Stanford University

Released 01.01.08

GEOLOGICAL SURVEY OF DENMARK AND GREENLAND
MINISTRY OF THE ENVIRONMENT

G E U S

# 1. Introduction

The SeiFaBa project ('Seismic and petrophysical properties of Faroes Basalt', 2002–2006) was funded by the Sindri Group as part of the programmes for licensees within the Faroese area and addressed the problem of seismic imaging in basalts with special focus on the subaerially extruded flood basalts. This study reports properties from three Faroese wells (see cross plots of well data in Appendix A): The Glyvursnes-1 (GL-1) well was drilled to 700 m by SeiFaBa outside Tórshavn in 2002 (Figs 1.1, 1.2; Waagstein & Andersen 2004). During the same operations, the existing 660 m deep Vestmanna-1 (VM-1) well was reamed and logged. The purpose of the experiments at these wells is to provide a link from the hand-specimen scale of the core-log, through the slightly larger averaging of borehole logs to seismic scales. A full range of wireline logs are also available for the Faroese Lopra-1/1A (LP-1) borehole that was drilled to 2.2 km in 1981 and deepened to 3.6 km in 1996 without reaching the base of the volcanic rocks (e.g. Hald & Waagstein 1984; Christie et al. 2002). Geochemical analysis and ultrasonic measurements have been carried out on samples from the three Faroese drillhole by the SeiFaBa project (Japsen & Waagstein 2005; Olsen 2005; Olsen et al. 2005).

An acoustic logging program was run in three wells in west Iceland in December 1998. The logging program and VSP surveys were a co-operation between Norsk Hydro, the Icelandic energy authorities (Orkustofnun) and Schlumberger. Orkustofnun selected three existing geothermal boreholes in western Iceland, each c. 1 km deep that penetrated different geological sequences dominated by hyaloclastites (HH-1 at Haukholt in the Hreppar district), flood basalts (LL-3 at Laugaland in the Holt district) and a mixed environment (LA-10 in Thorlákshöfn) (see Fig. 1.3 and further details in Appendix B). The logs became available for the SeiFaBa project after Orkustofnun became partner in the project in 2005.

The lavas on the Faroes are 59–55 million years old and are divided into the Lower, Middle and Upper Basalt formations; the UBF, MBF and LBF, respectively (Rasmussen & Noe-Nygaard 1970; Waagstein 1988; Larsen et al. 1999; Waagstein *et al*. 2002). The lavas on Iceland are of late Cenozoic age (Jóhanneson & Saemundsson 1998) and the three wells studied penetrate volcanic rocks of Pliocene to Holocene age (Fridleifsson & Gudlaugsson 1998; Vilmundardóttir et al. 1999a, b).

In this report we compare and discuss well log and core data from the Faroese wells and log data from the Icelandic wells. Our emphasis is on sonic properties, and how they relate to depth, composition, and pore space properties. We find that the acoustic properties for all data sets are fairly well-described in terms of a single set of mineral end-point properties expressed as mineral density and elastic moduli. The main deviation from the general data trend is probably related to alteration of the basalt matrix accompanied with filling of vesicles with zeolites and clay. Such deviations are observed for the Middle and Lower Basalt Formations on the Faroes.

# 2. Well data and stratigraphic interpretation

## 2.1 Faroese wells

An extensive logging program was run in the Glyvursnes and Vestmanna boreholes in 2002, comparable to that previously run in the Lopra well (1981, 1996) (see plots of the log data in Appendix A). It includes optical televiewer, caliper, natural gamma, resistivity, neutron porosity, density, full wave sonic, spectral gamma (of poor quality) and temperature/conductivity. The processing of the full wave sonic log for these two wells was difficult.

The stratigraphy of the basalts in the GL-1 and VM-1 wells was established from the full core in these wells (Waagstein 1983; Waagstein & Andersen 2004). The Vestmanna and Glyvursnes boreholes penetrate the lowermost 550 m and the uppermost 450 m of the 1,400 m thick MBF, respectively. In both sections the MBF is characterised by compound flows composed of thin flow-units of variable porosity and by rare thin beds of tuff. The overlying section at about 230 to 285 m in GL-1 consists of a few relatively thick plagioclase-phyric flow-units which are morphologically more similar to the flows of the LBF, although the latter are near-aphyric.

The Glyvursnes, Vestmanna and Lopra boreholes represent sections of increasing age and depth of burial. The Glyvursnes core displays variable degrees of mineralisation of vesicles and voids, while the Vestmanna core is more completely mineralised (Jørgensen 1984). The depth of burial is clearly reflected by increasing paleotemperatures as estimated from the zeolite parageneses found in Vestmanna and Lopra (Jørgensen 1984; Waagstein *et al*. 2002).

A detailed stratigraphy of basalt flows, sediment/tuff layers and dolerite dykes was established for the Lopra-1 hole drilled in 1981 based on drill cuttings and cores and compared with the density, porosity, resistivity and gamma ray log-response (Hald & Waagstein 1984; Nielsen *et al*. 1984). A more extensive logging program including a full wave sonic log was run in the deepened hole from 200 m to TD. The new logs have been used to establish a detailed stratigraphy for the flood basalt sequence between 200 m and 2500 m by dividing the lava flows into massive and porous parts (Boldreel 2006). The porous upper part of a flow is characterised by high values of the neutron porosity log, low values of density, low P- and S-velocities and intermediate values of the caliper, this in contrast to the rather massive part characterised by high values of density, high P- and S- wave velocities and low values of the neutron porosity. The basal zone is seldom identified due to the small vertical extent of the zone. In addition 52 intervals with >1% potassium were mapped at the flow boundaries and interpreted as altered basalt or tuffaceous sediments. These intervals were also identified from the high values of neutron porosity and caliper in combination with low values of density, P- and S-velocity. Two dolerite dikes intruding the basalt column were identified by having the highest values of density, P- and S-velocities and lowest values of the neutron porosity. Preliminary rock physics analysis of the Lopra-1 data was presented by Japsen et al. (2005) and a similar analysis of log data from the three Faroes wells by Mavko & Japsen (2005).

Ultrasonic measurements were carried out on several core samples from the three Faroes wells. P- and S-wave velocities were measured on 43 1.5” samples: 13 from VM-1, 25 from GL-1 and 5 from LP-1 (Olsen 2005; Olsen et al. 2005). Conventional core analysis covering gas permeability, He-porosity and grain density determination was also carried out. The velocities were measured at different hydrostatic pressure conditions to reach the in situ pressure condition where all minor fractures are closed (100, 200 and 300 bar). All samples here measured in a water saturated state and some also in a gas saturated state. Here we compare only results for water saturated samples at 300 bar. A preliminary analysis of ultrasonic and geochemical properties of cores samples from the Glyvursnes-1 and Vestmanna-1 was presented by Japsen & Waagstein (2005).

## 2.2 Icelandic wells

Three Icelandic wells drilled for production of geothermal energy (see Appendix B) were logged in a cooperation project between Norsk Hydro, Orkustofnun and Schlumberger. The field work was conducted from December 1 to 9 1998 (Kanestrøm 1999). A suite of logs were acquired in the three wells: dipole sonic imager (DSI), litho-density log (LDL), combined seismic imager (CSI), temperature (CPLT) and caliper (TCS), but no neutron porosity log (see plots of the log data in Appendix A).

The HH-1 well has a TD of 1320 m. Because of high temperature at TD (170º C) the logging stopped at 1120 m. The drilled section consists of 85% hyaloclastite. According to the geological report for the borehole, the well is located in ‘one of the hottest low-temperature systems’ in Iceland, the Hreppar district, S. Iceland (Vilmundardóttir et al. 1999a). The geothermal gradient is about 140ºC/km. The lithostratigraphy rest solely on analysis of cuttings and no thin sections were available for e.g. analysis of hydrothermal alteration. The volcanics at Haukholt are belong to the Hreppar Formation and are mainly of Pleistocene age (c. 2 m.y. old), but the deepest rocks are of late Pliocene age (c. 3 m.y. old). The drillhole penetrated hyaloclastites with lava interbeds, the latter signalling interglacials in most cases. A considerable part of the rocks are reworked hyalocrystalline tuffs, interbedded with primary volcaniclastic rocks and lavas. The rocks exposed at the surface contain chabaite and analcime in lava vesicles, implying that the surface rocks are within the chabazite-thomsonite alteration zone (40-70ºC). The presence of this zeolite zone on the surface witnesses that erosion in the order of 4-500 m has taken place.

The LA-10 well was drilled in 1987 and logged to TD in 1998 (995 m). The drilled section consists of 45% submarine and 45% subaerial Pleistocene basalt. According to the geological report for the borehole, the well is located in Thorlákshöfn on the eastern flank of the active riftzone in W Iceland, the Reykjanes-Langjökull rift zone (Fridleifsson & Gudlaugsson 1998). The upper 70 m are composed of highly permeable pillow lava originating from onshore post-glacial lavaflows which were rapidly quenched by flowing into the sea. Shallow-marine sediments are interbedded with and underlying the pillow lava formation. The unconformable ‘basement’ underneath is composed of late Pleistocene lavas and hyaloclastites. Very little amount of water can be obtained by pumping. The geothermal gradient is 90ºC/km. Chabasite is the most common low-temperature zeolite (498-682 m).

The LL-3 well was drilled in 1977 and logged to TD in 1998 (1091 m). The drilled section consists of 95% subaerial basalt. According to the geological report for the borehole, the well is located in the Laugaland area on the western flank of the active eastern rift zone in SW Iceland (Vilmundardóttir et al. 1999b). The nearest active volcano is Mount Hekla, 40 km to the NE. The bedrock belongs to the oldest part of the Hreppar Formation of Late Pliocene – Early Pleistocene age (3.2 – 0.8 Ma). The bedrock in the Laugaland area is considered to be 3.0 – 2.5 m.y. old. The Hreppar Formation is composed of lava flows with interbeds of hyaloclastites from glaciations periods and also some sedimentary beds. In the older parts of the formation, interglacial lava flows dominate over hyaloclastites as it is documented by the borehole where only thin (<30 m) beds of hyaloclastites are present. The borehole penetrated a regular pile of subaerial lavaflows containing less than 5% sedimentary interbeds, hyaloclastites, breccia and dikes. The water yield of the rock is poor, but two main water-conducting geothermal systems can be identified: The upper system (50-220 m) has a temperature of 60-75ºC and the lower system (635-920 m) has a temperature of 90-92ºC. The well is not intersected with water-conducting fracture zones. The secondary minerals place the rocks in the mesolite/scolesite alteration zone.

## 2.3 Quality control of well log data

The density and acoustic logs were quality-controlled and edited (Gommesen 2005; Gommesen & Ahmed 2005). The well logs are characterized by shallow readings in the bore hole and may therefore be influenced by, for example, borehole rugosity (calculated as the caliper values minus the bit size). Furthermore the logs were analysed for apparent malfunctions, such as cycle skipping in the sonic readings, and for missing readings. Generally, the log readings are deleted at the top of the hole, around the casing shoes or when the logging stops. The log readings are in some cases also deleted in the very bottom of the hole.

Density and sonic tool readings may be affected by e.g. washouts. An efficient approach to detect logging intervals affected by poor bore hole conditions is through cross plot analysis. From cross plots of e.g. bulk density versus Vp or Vp versus Vs (or Poisson's ratio) outliers may be identified, and be compared to the responses of the remaining curves of the log suite to identify any abnormal elastic behaviour. Especially for the LP-1 well, poor bore hole conditions are related to abnormal log readings. By comparing bulk density versus Vp and Vp versus Vs with the rugosity of the bore hole, we observe that readings of Vp are stable whereas readings of bulk density and Vs are very sensitive to the hole conditions, eventually resulting in low values of density and Vs (picking too late shear wave arrivals), respectively.

The quality of the Icelandic well log data is generally good. However, data that deviates from the general trends are observed in HH-01 and LL-03. Noteworthy is also that there is no resistivity and neutron porosity data available for the three wells. Calliper log is also missing for LA-10.

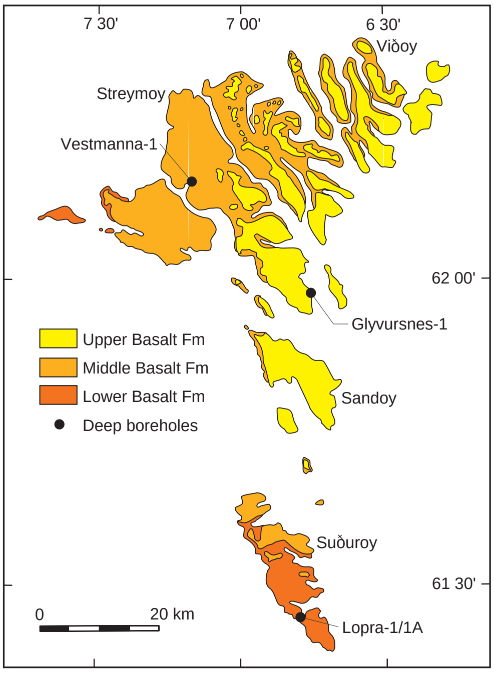


Figure 1.1. Geological map of the Faroe Islands showing the location of deep boreholes and the distribution of the three Palaeogene basalt formations (modified after Waagstein 1998).

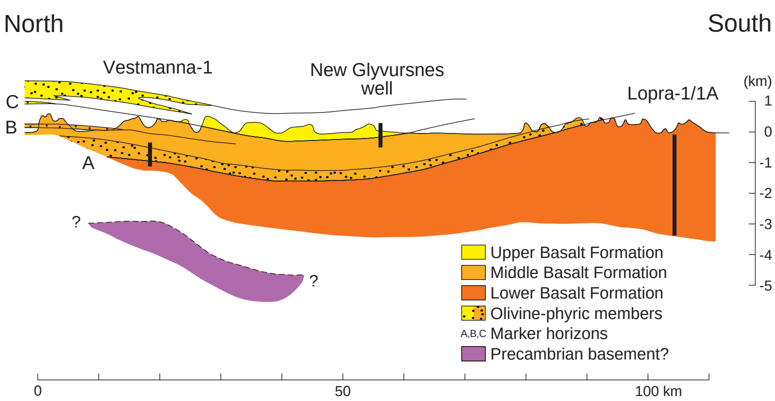


Figure 1.2. Stratigraphical position of deep boreholes in the Faroe Islands (modified after Waagstein 1988).


Figure 1.3. Location of the three Icelandic wells (from Kanestrøm 1999). Further details in Appendix B.

# 3. Basic observations

Plots of well logs and cross plots of well log data from the three Faroese wells (flood basalts) and the three Icelandic wells (different environments) are shown in Appendix A.

## 3.1 Properties estimated from core data

### 3.1.1 Well-defined Vp-φ and Vp-Vs relations irrespective of basalt formation

The plots of the ultrasonic data measured on core samples indicate that the data set represent rocks of broadly identical composition with regards to their acoustic properties – irrespective of basalt formation. Vp plot along well-defined trends versus porosity and do not show great variations with respect to well (basalt formation) nor basalt facies, only data from sediment samples may deviate, the Vp-Vs trend is very well-defined (Figs 3.1a,b, 3.2a,b). The relation between Vp and Vs is particularly sensitive to differences in rock composition (and fluid content), but such differences are not apparent from the plots.

### 3.1.2 Scattered trend of Vp versus density

However, there is a significant scatter when Vp is plotted versus density for the samples (Figs. 3.1c, 3.2c). If we assume a single relation between Vp and porosity, this result indicates a significant scatter in the grain densities of the individual samples because

$$\rho = \rho_{gr} \cdot (1 - \phi)$$

where $\rho$ is density (g/ccm), $\rho_{gr}$ is grain density and $\varphi$ is porosity (see Fig. 4.1c). There is indeed a large scatter in the measured values of grain density that varies from 2.7 to almost 3.1 g/ccm for the investigated samples. The dependency of density on grain density is illustrated by Fig. 3.3a that shows that lower bound of Vp-density data is defined by samples with maximum grain density and that data points with lower density for a given velocity are characterized by a smaller grain density. Fig. 3.3b highlights the considerable span in grain densities from 2.7 to 3.1 g/ccm and that even samples from massive cores span a wide range of grain densities. Low grain densities are likely to represent altered samples with a high percentage of light minerals such as clay (e.g. 2.55 g/ccm) and zeolites (e.g. Narolite 2.25 g/ccm) in contrast to the main constituents of basalt pyroxene (3.3 g/ccm) and plagioclase (c. 2.6 g/ccm) (data from Mavko et al. 1998).

There is a strong bias in the selection of the samples towards massive lava flows because these units are easier to investigate (due to the low porosity) and because they were selected to investigate the properties of the different flow units; moreover samples of lava crust and breccia were difficult to investigate due to large vesicles. Consequently, altered rock material that is likely to occur more frequently in the crust of lava flows and in breccia are not well presented in the data set. Examples of altered rocks are the crustal sample G-35 (grain density of only 2.7 g/ccm, Vp c. 5 km/s, depth 346 m) and the two samples of massive flow units, G-36 and G-77 (grain density less than 2.9 g/ccm, Vp greater than 6 km/s, depths 353 and 669 m) (cf. Olsen 2005; Olsen et al. 2005). In thin section sample G-35 is seen to be characterized by vesicles filled with zeolites and clay whereas the plagio-clase is altered and the plagioclase is fresh (R. Waagstein pers. comm.).

## 3.2 Properties estimated from Faroese log data

- In GL-1 the gamma ray is low (<20 API) and fairly constant and systematically higher for the sediments. The P-wave sonic is highest in the massives and lowest in the sediments. The bulk density is systematically lower than in Lopra-1, indicating systematically higher porosity, and possibly a change in mineralogy. The density also shows smaller fluctuations than were observed in Lopra-1. Distinct changes in the character of the logs occur at 45 m and 300 m whereas the interface between the Upper and the Middle Basalt Formations is at 355 m (Waagstein & Andersen 2004).

- In VM-1 the gamma ray is constant and low (c. 10 API), but systematically higher in the sediments than in the basalts, as with the other wells. The density and density fluctuations are smaller than in Lopra-1, similar to Glyvursnes-1. Again, the P-wave sonic is highest in the massives and lowest in the sediments. The Vp/Vs ratio in Vestmanna-1 is much more uniform than in either Lopra-1 or Glyvursnes-1, though there are abrupt Vp/Vs spikes.

- In LP-1 we observe that the gamma ray log varies over a wide range (<40 API) and that it is systematically higher in the sediments than in the various basalt layers. Apparently the gamma level varies from flow unit to flow unit. The bulk density shows large fluctuations with depth, indicating primarily large variations in porosity. However, the upper limit of density is fairly uniform with depth and probably indi-cates that the density asymptotically approaches the mineral density as the porosity approaches zero. The sonic Vp is highest for the massive basalts, intermediate for the basalt topflows, and lowest for the sediments.

We observe a general velocity increase with depth in well GL-1 below c. 350 m within the MBF (below the level of the thick high-velocity flow units). This change is partly due to shift to a higher Vp-rho trend and partly due to increased density (reduced porosity) which add up to an increase in velocity to match the high Vp values found in VM-1 for the MBF. This will be discussed more in the following sections.

## 3.3 Properties estimated from Icelandic log data

- In HH-1 (85% hyaloclastites) the gamma ray is low through most of the drilled sec-tion (<20 API), but is markedly higher (c. 40 API) in the tuffaceous interval around 800 m which is also characterized by low densities. Bulk densities vary from 2 to more than 3 g/ccm and are typically low in the tuffs (small density variations). The upper density limit of c. 3 g/ccm probably indicates low density zones with porosity near zero. Vp closely follows the variations in density and the trend of the Vp-Vs ratio is well defined around a mean value that decreases slightly with depth from 2 near the surface to c. 1.8. There is no clear lithological discrimination in terms of the Vp-Vs ratio and this observation supports that the sediments are reworked tuffs and volcanic rocks.

- In LA-10 (45% submarine, 45% subaerial basalts) the gamma ray values are low (< 20 API) throughout the drilled section, but vary in a stepwise manner with depth. Density varies from 2 to 3 g/ccm with large variations across short depth intervals corresponding to the characteristic porosity variation over individual lava flows. The density variation is small over tuff units. Vp variations reflect closely variations in density and is thus controlled by porosity. There is a wide scatter in the Vp-Vs ratio that probably reflects bad velocity (Vs) readings.

- In LL-3 (95% subaerial basalts) the gamma ray are fairly high (10-30 API) and scattered. Density varies over short distances with a total range from 2.2 to 3 g/ccm only a tuff unit near the surface has a constant, low density. Vp closely mimics these variations that are due to the porosity profile across individual flows. The general level of the Vp-Vs ratio drops from near 2 at the surface to 1.8 at the base of the well.

## 3.4 Comparison of Faroese and Icelandic log data

### 3.4.1 Two Vp-density trends

Based on the Faroese and Icelandic log data we can distinguish two main Vp-rho relations for flood basalts:

- a trend of relative low Vp compared to rho. This trend is observed for the UBF in the GL-1 well where e.g. Vp<4 km/s for 2.6 g/ccm (Fig. 3.4a) and for the LL-3 well (Appendix A).
- a trend of relative high Vp compared to rho. This trend is observed for the LBF in the LP-1 well where e.g. Vp≈5.3 km/s for 2.6 g/ccm (Appendix A).

Moreover, the properties of the MBF appear to be transitional between the two trends. The GL-1 data from this interval represents both the high and the low trend (Fig. 3.4b), whereas the VM-1 data represent a very high Vp-rho trend (Fig. 3.4c). For the GL-1 well we observe a clear variation of Vp with depth below c. 550 m (Fig. 3.6). However, towards the base of VM-1, we observe a ‘reversal’ of the Vp-rho trend within the thin sequence of the LBF penetrated by the well.

The difference between the two trends means that identical values of density give different Vp. Somehow the structure of the basalt appear to be ‘stiffer’ in the deeper stratigraphic level and it is thus tempting to suggest that the difference between the two trends represents a change related to diagenetic changes at depth and this will be investigated in the following.

### 3.4.2 High gamma-level correlates with low Vp relative to density

For intervals with large variations in gamma it is clearly seen that high gamma readings corresponds to relatively low Vp (for given rho) (Figs 3.7, 3.8). We observe this for the LL-3 well (250-300 m) where a marked interval with high gamma has smaller values of Vp than the interval just above where gamma is smaller and density identical (Fig. 3.7). No relation with the scattered Vp/Vs data can be seen in this well. High gamma for low Vp accompanied with low Vp-Vs may also be observed on crossplots of Vp versus density for well LP-1 (1500-1800 m) (Fig. 3.7).

The observed relations: high gamma – low Vp – high Vp/Vs are similar to those seen for sandstone where quartz has low gamma and shale high gamma values. Shale reduces Vp and even more Vs and hence increases Vp/Vs (e.g. Han et al. 1986). From the blocky appearance of the gamma log for LL-3 (and LP-1) it seems likely that these variations are related to the primary composition of the flows.

## 3.5 Comparison of Faroese log and core data

We can use the core data to investigate the relations between the log data because there is agreement between the log and core data from the Faroese wells. The log measurements in the wells have been estimated at the same depths as where the core samples were taken: e.g. density, Vp and Vs. The log readings are compared with the lab data and show a high degree of consistency (Figs 3.9a-c). There is almost a 1:1 correlation for the density data in contrast to the bias between the two datasets shown by Japsen & Waagstein (2005). This improvement is due to the recalibration of the density logs in GL-1 and VM-1 as described by Waagstein & Japsen (2005). The correlation between Vp and Vs for the two datasets is also very good, even though Vp for the core data are slightly biased towards higher velocities whereas the Vs data are closer to a 1:1 correlation (see Japsen & Waagstein 2005 for further details). The bias of the Vp data may be due different scales because the finer sampling of spikes in the core material than for the log measurement. There is no difference in the correlation between the core and log data between Glyvursnes-1 and Vestmanna-1.

A comparison of log and core data in a plot of Vp versus density reveals a strong bias in the selection of the core samples relative to the log data for the entire logged sections in the GL-1 and VM-1 wells (Figs 3.10, 3.11): The low-density part of the relatively high Vp-density trend for the MBF in the two wells is only represented by one sample (G-35). The match between the two datasets is affected by the slight shift towards higher velocities for the core data. The analysis of the Vp-density relation for the core data shows that the outlying samples towards low densities are characterized by low grain density. Hence we can conclude that the relatively high Vp-density trend defined for the log data in these wells for the MBF also must be characterized by low grain densities (and hence low densities). This means that the basalt of the MBF must be significantly altered – partly due to presence of light minerals such as clay and zeolites and partly due to alteration of the rock matrix.

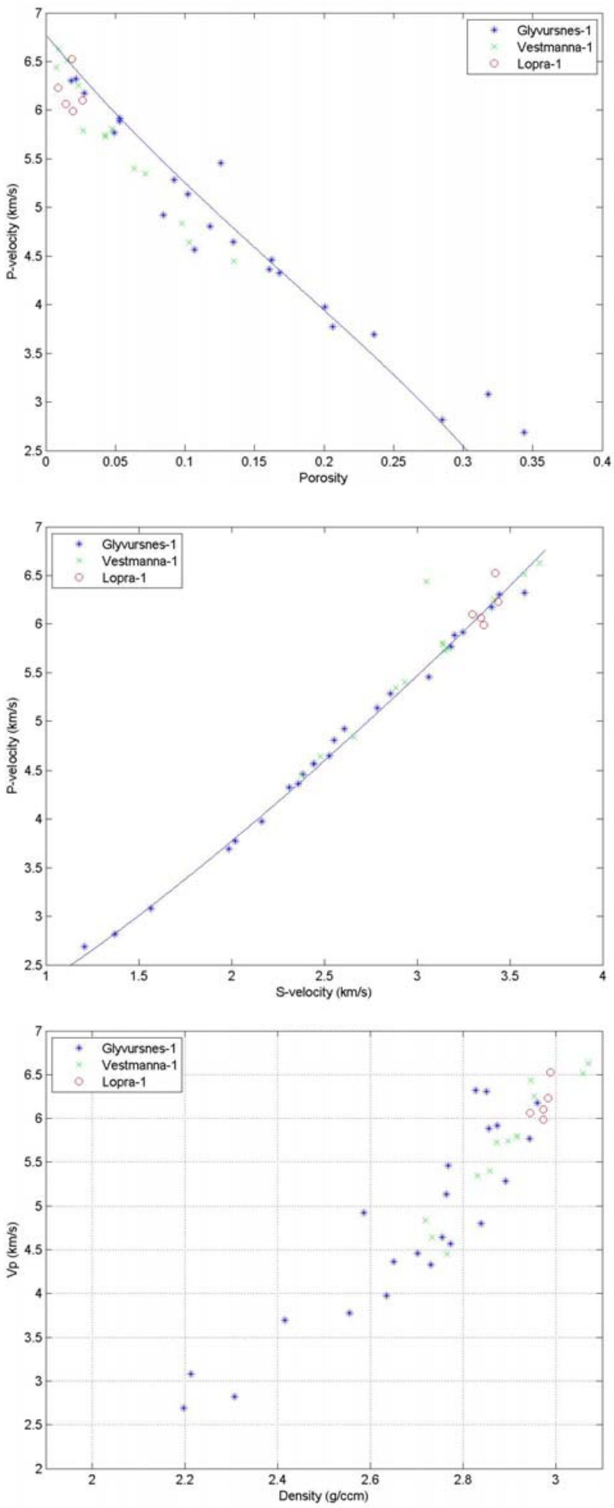


Figure 3.1. Plots of ultrasonic data for water saturated core samples measured at 300 bar (colorcoded by well). (a) Vp versus porosity. (b) Vp versus Vs. (c) Vp versus density. The well-defined trends seen in the plots of Vp versus porosity and Vs indicate that the data set represent rocks of broadly identical composition irrespective of basalt formation (well). However, the scatter seen in the plot of Vp versus density indicate variations in grain density are important for a fixed velocity-porosity data point. Upper Hashin-Shtrikman bound shown for reference (Japsen & Waagstein 2005).

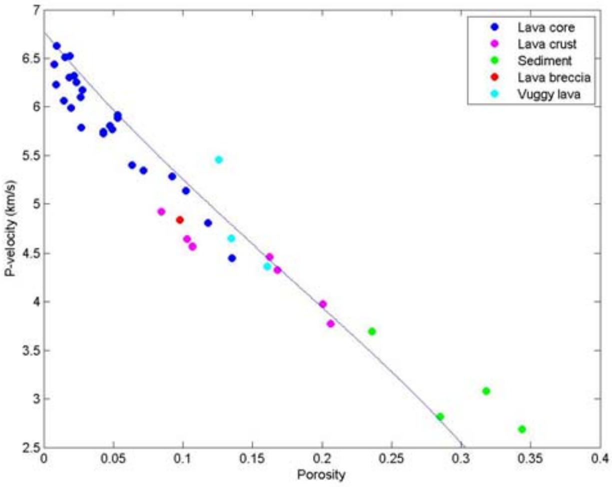


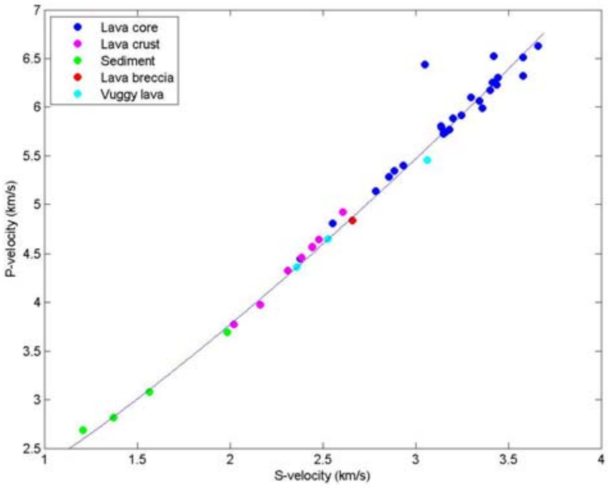


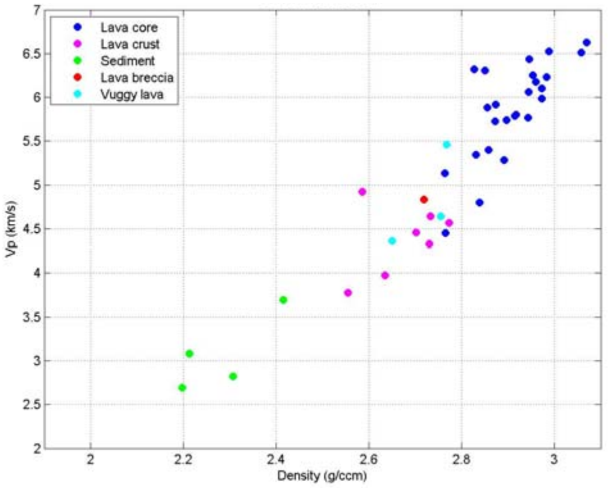


Figure 3.2. Plots of ultrasonic data for water saturated core samples measured at 300 bar (colorcoded by lithology). (a) Vp versus porosity. (b) Vp versus Vs. (c) Vp versus density. The well-defined trends seen in the plots of Vp versus porosity and Vs indicate that the data set represent rocks of broadly identical composition irrespective of lithology. However, the scatter seen in the plot of Vp versus density indicate variations in grain density are important for a fixed velocity-porosity data point (e.g. massive core data). Upper Hashin-Shtrikman bound shown for reference (Japsen & Waagstein 2005).

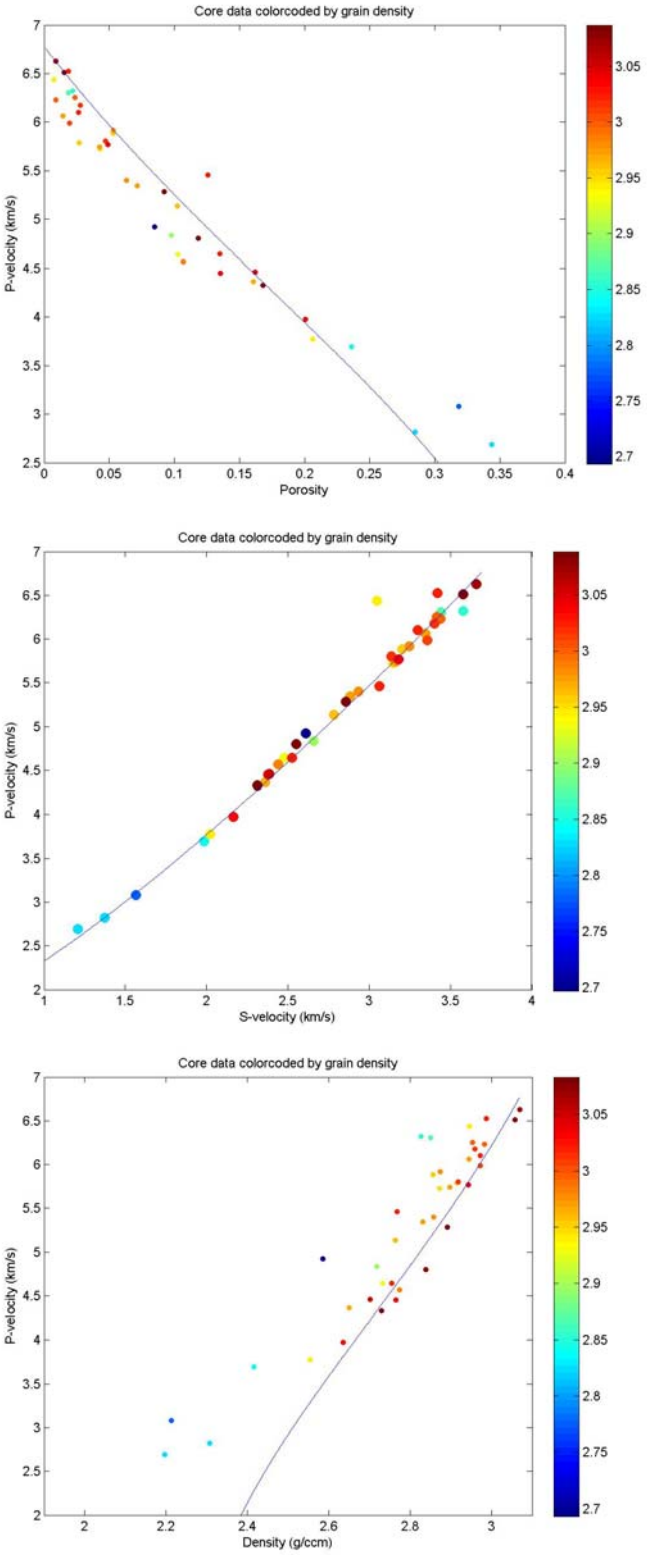


Figure 3.3. Plots of ultrasonic data for water saturated core samples measured at 300 bar colorcoded by grain density. (a) Vp versus porosity. (b) Vp versus Vs. (c) Vp versus density. Data for the basalt samples define a fairly well-defined velocity versus porosity trend and tight Vp-Vs trend whereas there is a pronounced scatter in the plot of velocity versus density. This scatter corresponds to a clear separation in grain densities. The upper bound of the data trend is represented by the upper Hashin-Shtrikman model (thin black line) (Japsen & Waagstein 2005).

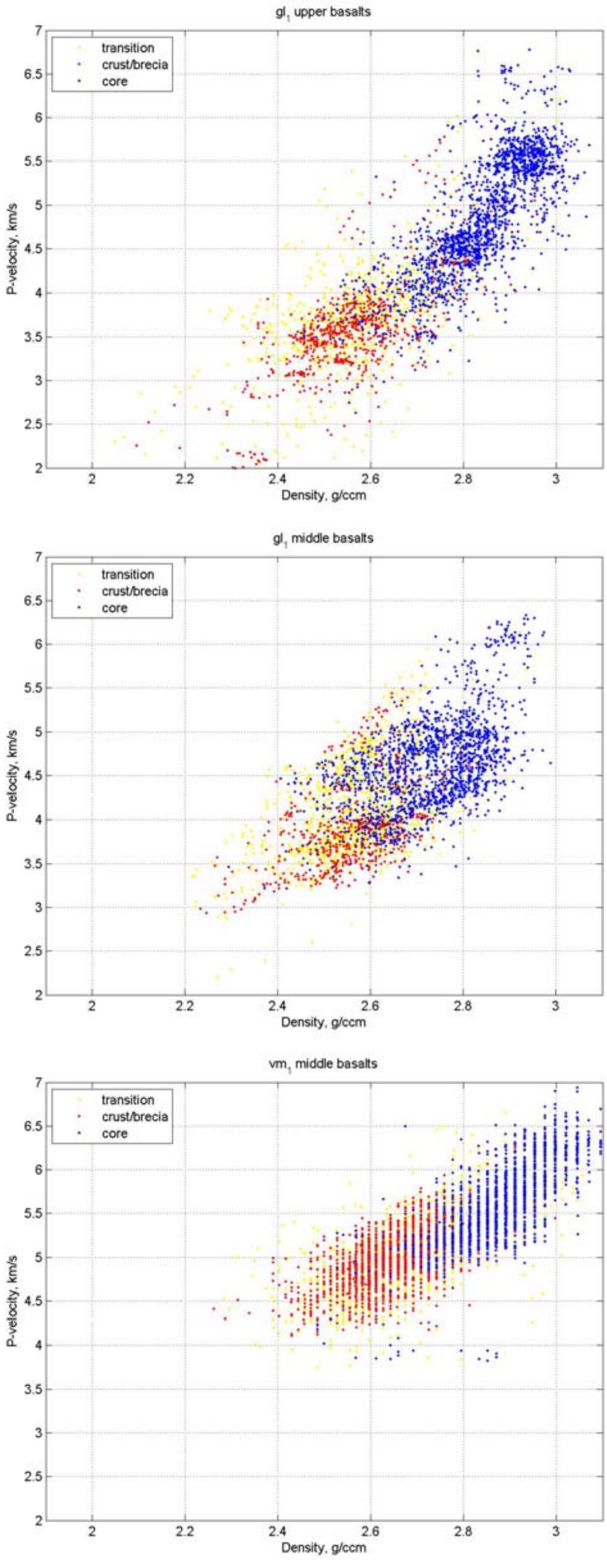


Figure 3.4. Vp versus density for (a) well GL-1, UBF. (b) well GL-1, MBF. (c) well VM-1, MBF. The log data plot along two trends of Vp versus density: a trend of relatively low Vp compared to rho (cf. Fig. a) and a trend of relative low Vp compared to rho (cf. Fig. c). The data for MBF in well GL-1 represents the overlapping trends (Fig. b). This transition represents a reduction in grain density rather than different relations between Vp and porosity (cf. Fig. 3.10).

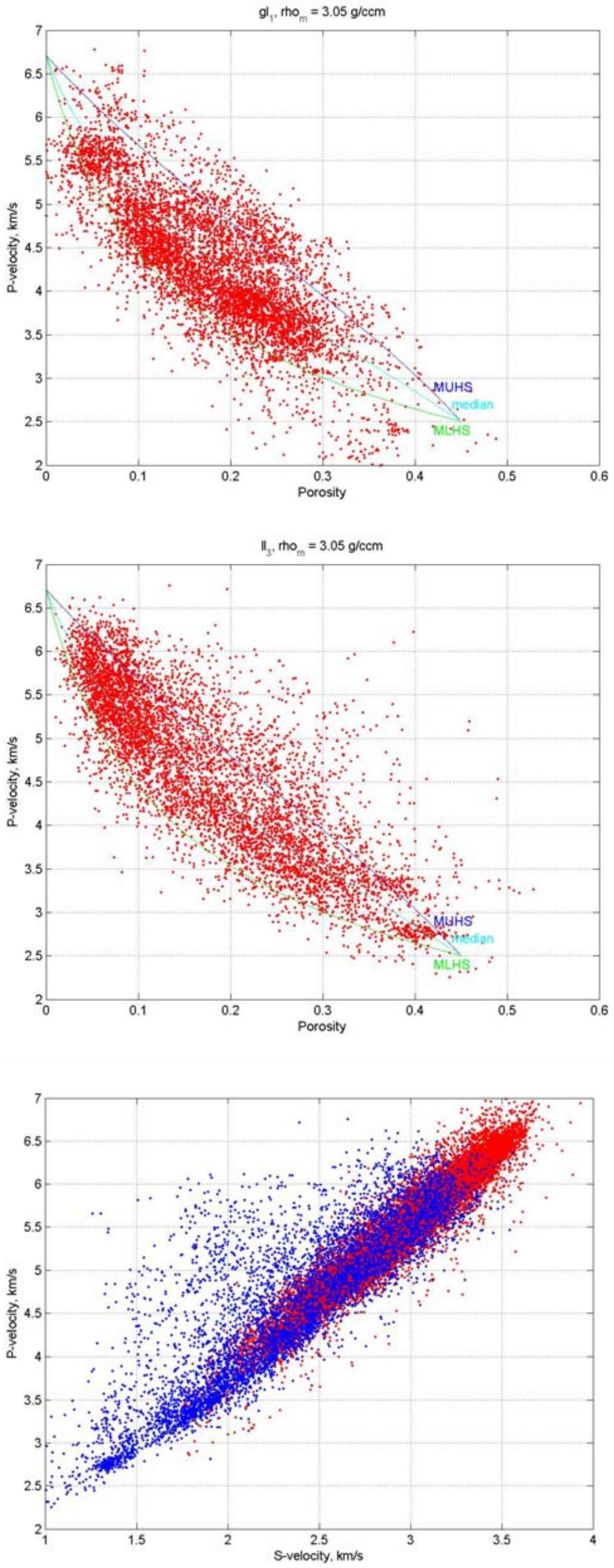


Figure 3.5. Comparison between data from (a) the GL-1 and (b) the LL-3 wells in plots of velocity versus porosity and (c) Vp-Vs data from the LP-1 (red) and LL-3 (blue) wells. Note the identical data trends for the two wells (the cluster of high-velocity data around a porosity of 20% represent altered basalt of the MBF). The reference lines in Figs a and b are computed for the MUHS, median and MLHS model described in the text.

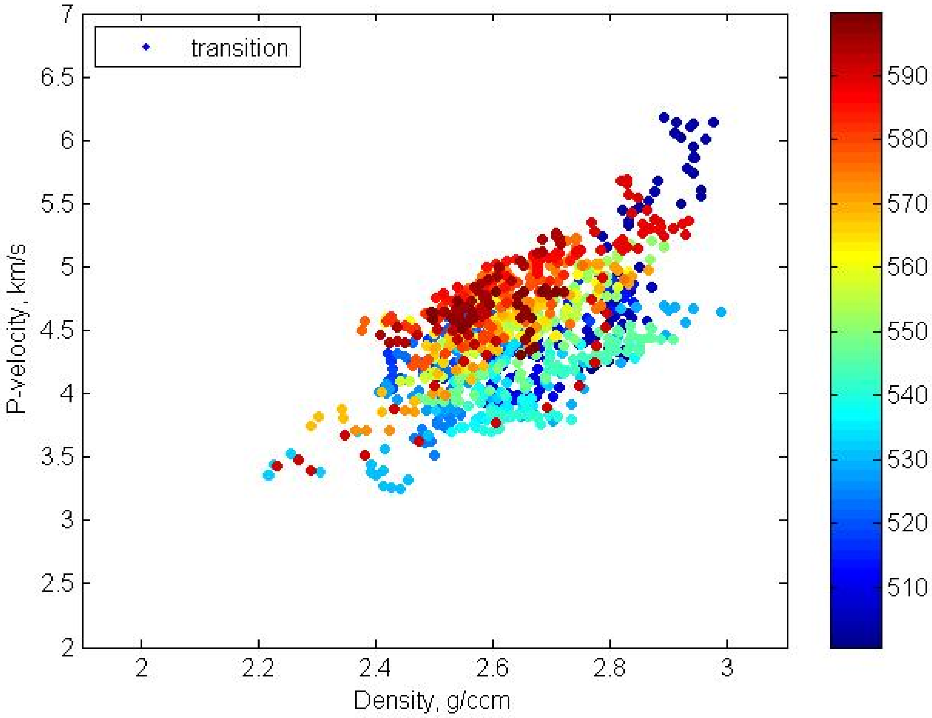


Fig. 3.6. Vp versus density for the MBF in GL-1 colorcoded by depth (500-600 m). For intermediate densities of e.g. 2.6 g/ccm there is a clear distinction between a shallow interval with low Vp and a deep interval with high Vp. This probably reflects alteration of the deeper basalts with zeolite infilling.

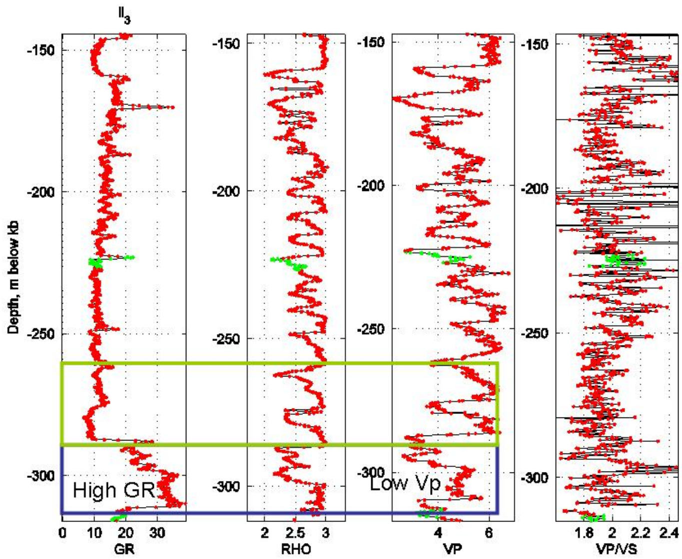


Fig. 3.7. Plot of logs for well LL-3 (detail for the depth interval 150 to 310 m). Note that a marked interval with high gamma has smaller values of Vp than the interval just above where gamma is smaller and density identical. No relation with the scattered Vp/Vs data can be seen in this well.

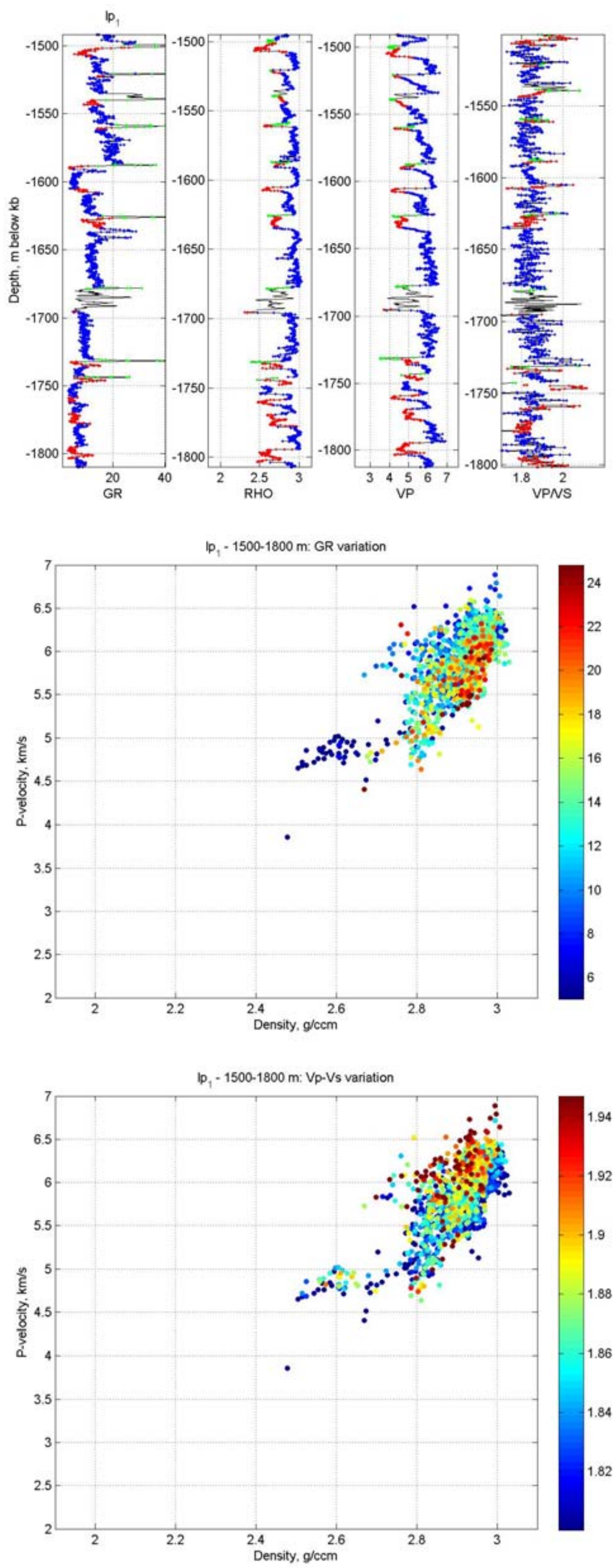


Fig. 3.8. (a) Plot of logs for well LP-1 (detail for the depth interval 1500 to 1800 m); cross-plots of Vp versus density for well LP-1 colorcoded by (b) gamma and (c) Vp-Vs ratio (1500-1800 m, massives only). High gamma readings correspond to values of Vp that are relatively low for a given density and to relatively low Vp-Vs ratio.

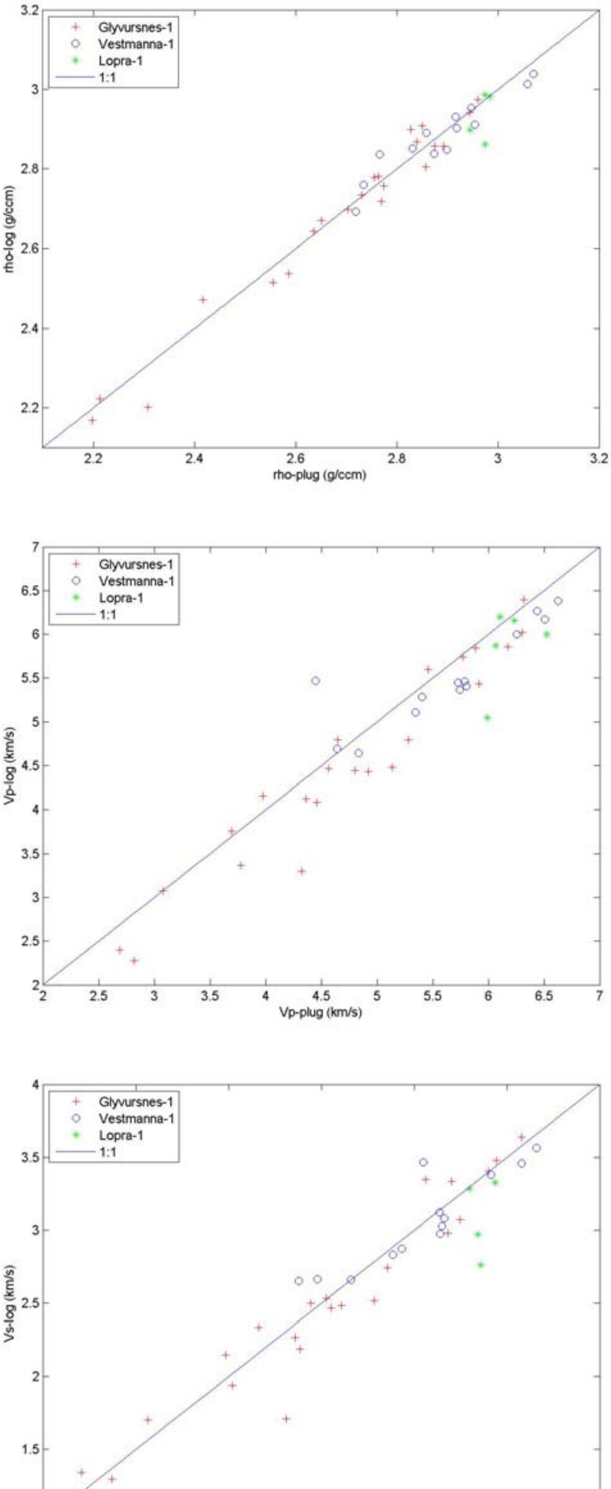


Figure 3.9. Plot of log versus water saturated core data at 300 bar estimated at the same depth. (a) Density. (b) Vp. (c) Vs. There is good consistency between the two data sets, but especially Vp for the core data are shifted towards high velocities relative to the log data.

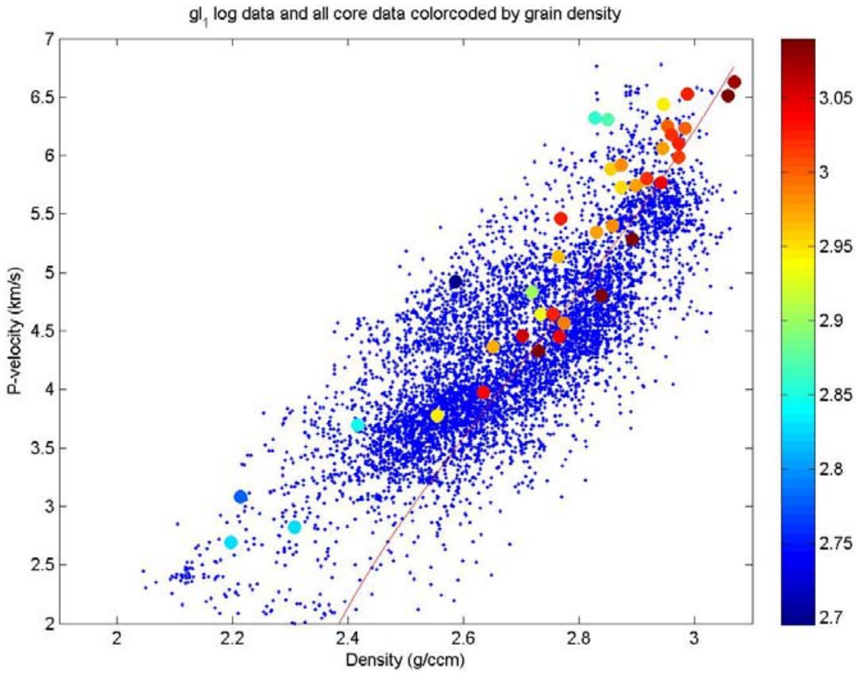


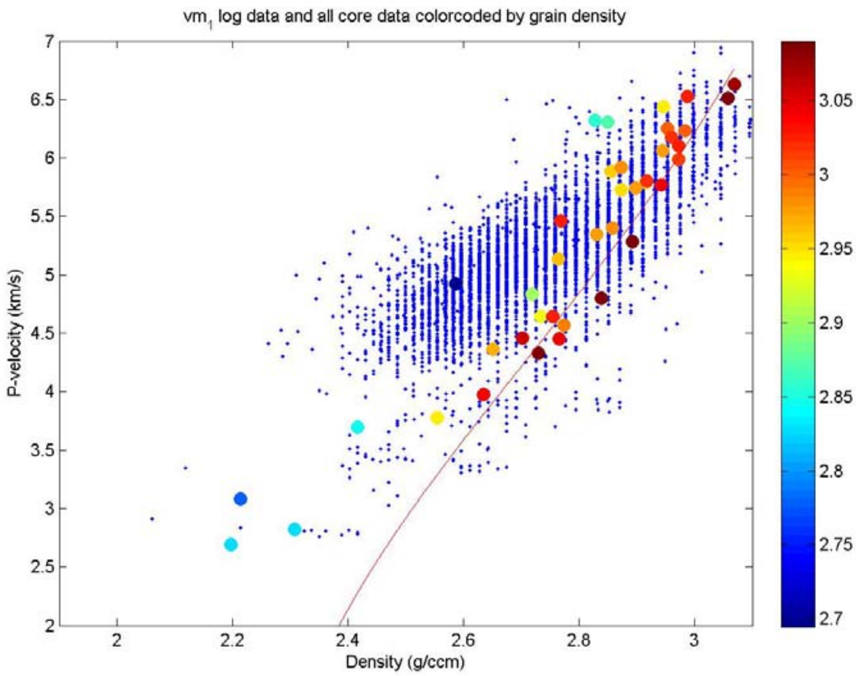


Figure 3.10. Plot of Vp versus density for water saturated core data at 300 bar (all samples) and log data for (a) The Glyvursnes-1 well. (b) The Vestmanna-1 well. (c) The low-density part of the relatively high Vp-density trend for the Middle Basalt Formation in the two wells is only represented by one sample.

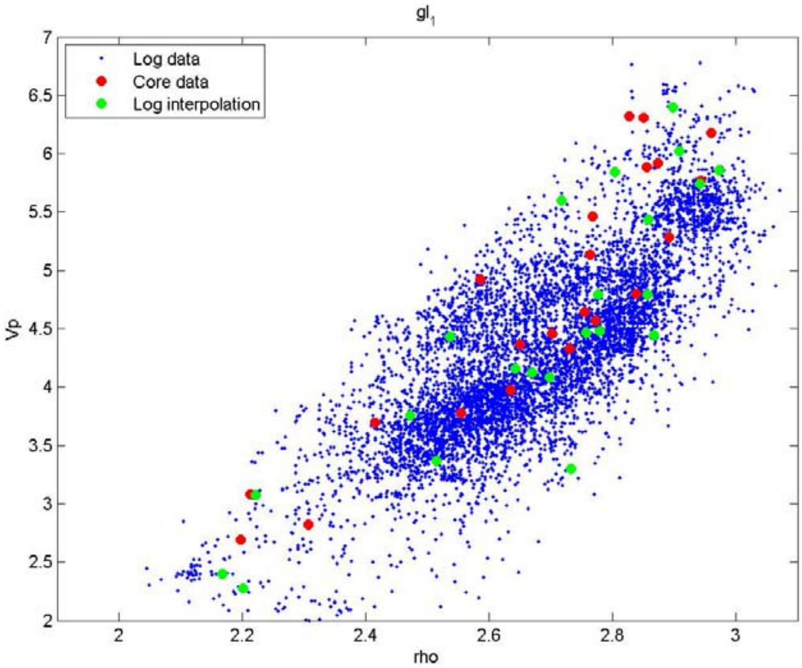


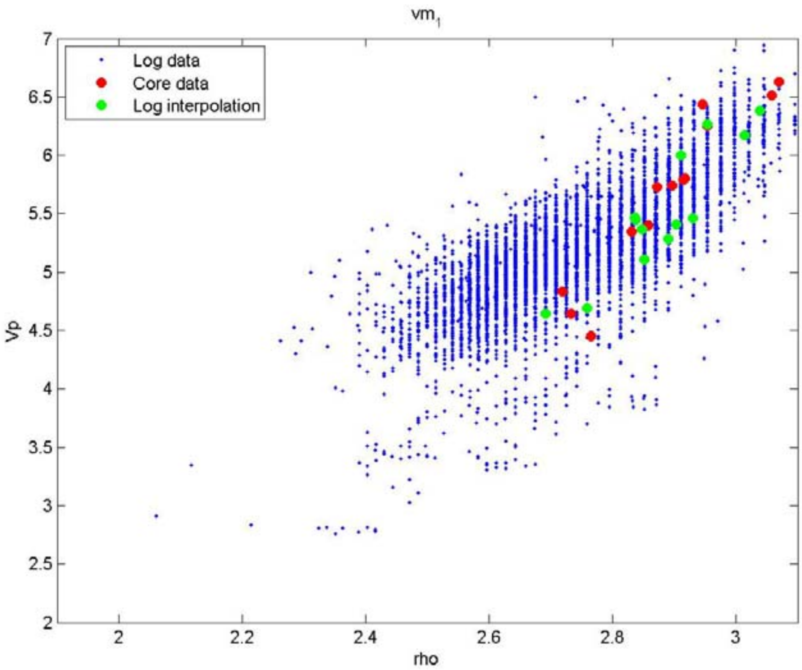


Figure 3.11. Plot of Vp versus density for water saturated core data at 300 bar (red circles) and log data estimated by interpolation at the same depth as the core sample (green circle) compared with log data (blue dots) for (a) The Gluvursnes-1 well. (b) The Vestmanna-1 well. The plots demonstrate the bias in the sampling of the core data relative to the entire drilled section with respect to density properties. The difference between the red and green circles illustrates the difference in the two data sets that is also demonstrated in Fig. 3.9.

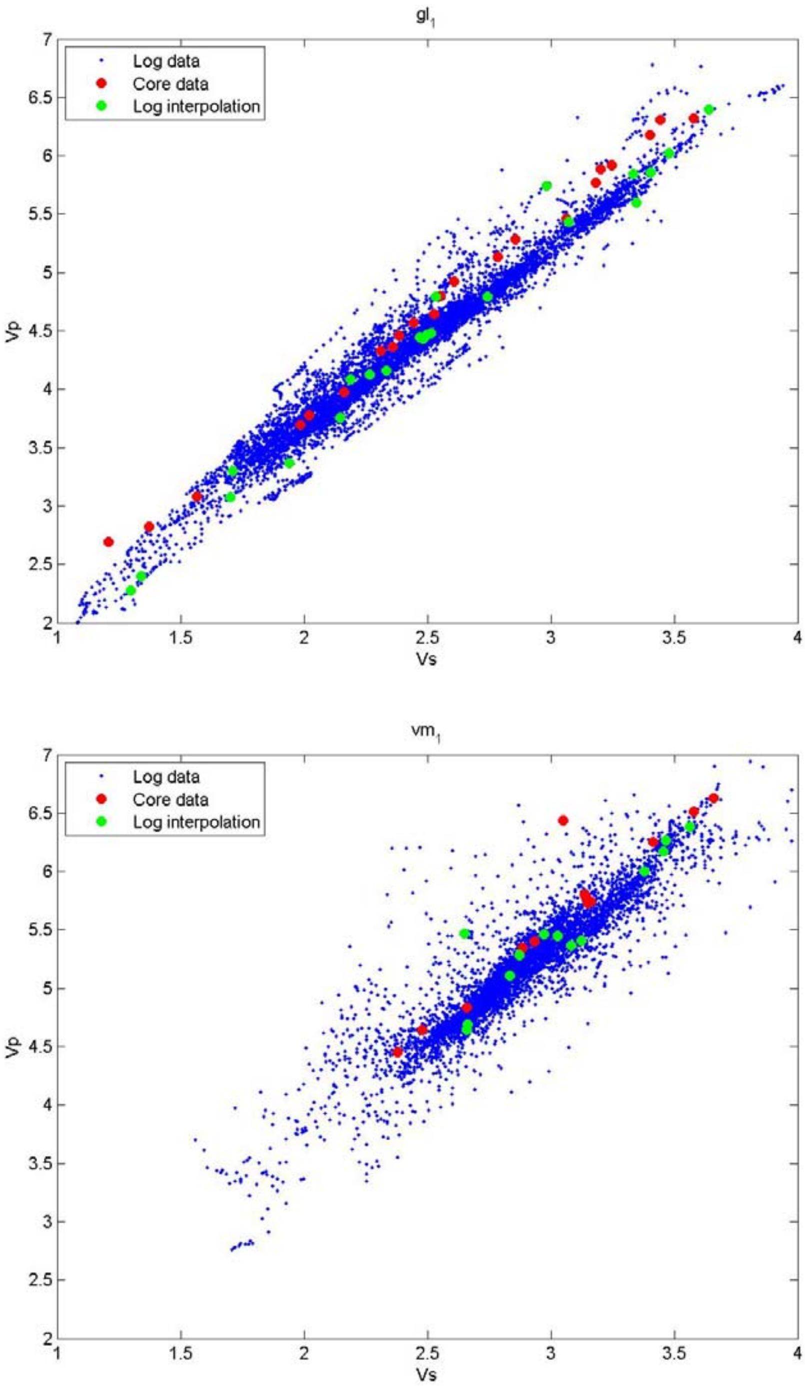


Figure 3.12. Plot of Vp versus Vs for water saturated core data at 300 bar (red circles) and log data estimated by interpolation at the same depth as the core sample (green circle) compared with log data (blue dots) for (a) The Gluvursnes-1 well. (b) The Vestmanna-1 well. The plots demonstrate the uniformity in the sampling of the core data relative to the entire drilled section with respect to velocity properties (and hence to porosity). The log data for the GL-1 well is shifted towards higher values of Vs (or lower Vp) compared to the core data. The difference between the red and green circles illustrates the difference in the two data sets that is also demonstrated in Fig. 3.9.

# 4. Rock physics modelling

## 4.1 Matrix densities

### 4.1.1 Faroese basalt

Matrix (or grain) density, $\rho_m$ (g/ccm), of 40 core samples from the 3 Faroese wells have been estimated, giving an average value of 3.00 g/ccm for samples of massive lava flows (Olsen 2005; Olsen et al. 2005). Plots of grain density variations show that the variation in grain density is systematically related to bulk density and to alteration of the rock as discussed below (Figs. 3.3, 4.1). We observe that the highest grain densities mark a lower bound in the plot of Vp versus density and thus that only the highest grain densities may be considered representative for the unaltered matrix. In Fig. 4.1a we observe a number of data points with a grain density of almost 3.1 g/ccm, but these values may also indicate anomalous high contents of heavy minerals and are thus not necessarily representative for the bulk properties of the unaltered basalt. In Fig. 4.1b we compare measured values of He-porosity with the bulk densities of the samples with the data points colorcoded by grain density with indication of the relation between density and porosity for a grain density of 3.05 g/ccm. This value may be taken as a fair approximation of the property of the unaltered basalt with the higher values as outliers above the line and increasingly lower values corresponding to more altered rock, below the line. A grain density of 3.05 g/ccm compares well with the 3.07 g/ccm estimated by Mavko et al. (2004) as the empirical upper limit of the log densities of the LBF in the LP-1 well. There are no indications of systematic variations in acoustic properties between the three basalt formations, nor between the three Faroese wells (Figs 3.1, 3.2). However, the matrix density exceeds 3.05 g/ccm in some of the drilled intervals; e.g. in well VM-1 where bulk densities reach 3.1 g/ccm between 440 and 490 m depth (see Appendix A).

From Fig. 4.1a we see that the samples of lava crust have the same range of maximum grain densities as massive lavas, which is to be expected because lava crust and core are part of the same lava flow. Apparently, both lava crust and core may be severely altered as indicated by the low grain densities of two core samples (G-36 and G-77, c. 2.87 g/ccm) and one crust sample (G-35, 2.7 g/ccm). It is possible that the high-porous lava crust is more prone to alterations because ground water may flow more easily here, but we adopt the same grain density as for the massive lava flows 3.05 g/ccm. This value is also assumed for breccia and for transitional and undefined lithologies as well as hyaloclastites. For sediments we assign the mean sample value of 2.8 g/ccm. For the dolerites in well LP-1 the matrix density appear to slightly smaller than for the surrounding basalt and we assign these rocks a matrix density of 3.02 g/ccm (see Appendix A).

We can calculate porosity, $\phi$, from bulk density, ρ, by the following expression:

$$\phi = \frac{\rho_m - \rho}{\rho_m - \rho_w}$$

where we substitute the above values for the matrix (or grain) density, $\rho_m$, and where $\rho_w$ = 1 g/ccm is the density of fresh water saturating the basalt. For bulk densities above 3.05 g/ccm we assign zero porosity. The resulting minimum porosities for e.g. the LP-1 well are very close to 0% (see Fig. 4.2). This is a reasonable result considering the tightness of the massive basalt flows and the measured minimum He-porosities of c. 1 for the core samples (Olsen 2005; Olsen et al. 2005). Note that variations in grain density of 0.02 g/ccm will result in maximum variations in the estimation of porosity of 1 p.u. and are thus not important for the analysis presented here.

In the LP-1 well high gamma readings were used as one parameter to distinguish sediments based on the log parameters (Boldreel 2006). We have assigned a low matrix density for all sediments and we thus get very low porosities for the data interpreted to be sediments in the LP-1 possibly indicating that this matrix density is too low or that too many data points have been interpreted as sediments (see Fig. 4.3 where not only data points for basalt flows are shown). Similarly low porosities are not estimated for sediments in the GL-1 and VM-1 (see plots of velocity versus porosity in Appendix A).

### 4.1.2 Icelandic basalt

Grain densities of Icelandic basalts have been studied by the Icelandic energy authorities. According to email correspondence with Omar Sigurdsson from ISOR in Reykjavík, the following observations have been made (there are no core samples from well LL-3):

Fresh basalt lavas:

- mean grain density 3.06 g/ccm with std 0.05, min = 2.95 g/ccm, max = 3.15 g/ccm (16 samples from various locations).
- mean grain density 3.07 g/ccm with std 0.01, min = 3.05 g/ccm, max = 3.09 g/ccm (85 samples from Oskjuhlid).

Basalt lavas with small alteration as zeolites and smectite:

- mean grain density 2.88 g/ccm with std 0.09, min = 2.69 g/ccm, max = 3.00 g/ccm (36 samples from various locations).

Basalt intrusions with similar alteration:

- mean grain density 2.89 g/ccm with std 0.08, min = 2.73 g/ccm, max 3.00 g/ccm (18 samples).

Reported densities from the Iceland-Research-Drilling Project (IRDP) well in Reydarfjordur, east Iceland (e.g. Drury 1985) for lavas are 3.02 g/ccm with std 0.18 (part of those lavas could have zeolite alteration). Density for basaltic intrusions in that well was reported to be 3.04 g/ccm with std 0.16.

A typical grain density for fresh Icelandic basalt lava measured on core samples is thus 3.06 g/ccm, so 3.05 g/ccm is a very reasonable pick (Omar Sigurdsson pers. comm.).

According to the geological reports for the Icelandic wells reworked tuffs and lavas are termed sediments (e.g. Vilmundardóttir et al 1999a). We therefore assign the grain density of unaltered basalt (3.05 g/ccm) to this lithology. This choice agrees with plot of Vp versus density for well HH-1 where most data points for sediments plot along the trend for basalt, but scattered points for sediments plot towards relatively low densities and thus probably corresponds to chemically altered basalt matrix with low grain density (Appendix A).

## 4.2 Ellipsoidal inclusion model based on data from Lopra-1

In this section, we analyze the observations by comparing them with rock physics models. One set of models represents the pore space as a collection of ellipsoidal inclusions, ranging from flat penny-shaped cracks to spherical pores. The equations that we implement are for the self-consistent formulation of Berryman (1995). The effective rock bulk and shear moduli of an N-phase composite are given by:

$$\sum_{i=1}^{N} x_i (K_i - K^*_{SC}) P^{*i} = 0$$

$$\sum_{i=1}^{N} x_i (\mu_i - \mu^*_{SC}) Q^{*i} = 0$$

where i refers to the *ith* material, $x_i$ its volume fraction, P and Q are geometric factors given in Table 4.1, and the superscript $^{*i}$ on P and Q indicates that the factors are for an inclusion of material i in a background medium with self-consistent effective moduli $K^*_{SC}$ and $\mu^*_{SC}$. These equations are coupled and must be solved by simultaneous iteration.

In the modelling, spherical pores are represented with an aspect ratio of 1; these are the stiffest possible shapes, leading to high velocities for a given porosity. In basalts, these would correspond well to vesicles. Successively smaller aspect ratios represent flattened spherical pores (oblate spheroids), which are successively more compliant. Aspect ratios less than about 0.1 are often referred to as “penny-shaped” cracks. In our application, we assume two phases, mineral and water.

In using these inclusion models, it is important to remember that they are quite idealized, and should not be interpreted too literally. In real rocks there are seldom ellipsoidal pores, though the approximation is probably better in vesicular volcanics than most others. Also, the ellipsoidal models do not explicitly allow for pore connectivity. Nevertheless, these models are useful elastic analogs, and we believe that the trends predicted by them, such as from stiffer pores to more compliant pores, are valid. In our discussion below, the fact that sonic data are consistent with a penny-shaped crack model does not mean that there must be cracks in the rocks. Poorly cemented, compliant grain contacts will yield the same elastic behaviour.

When comparing theoretical curves for the ellipsoidal inclusion model with well log data, we find that the results are very sensitive to the assumed mineral properties. Figure 4.2 shows plots of Vp versus Vs, Vp versus phi, and Vs versus phi for Lopra-1 data for massive lava flows and crust. The porosities were estimated from measured bulk densities using a matrix density 3.05 g/ccm. Superimposed are the predictions of the ellipsoidal inclusion model, for average pore aspect ratios of [1, 0.3, 0.1, 0.03, 0.01]. For these curves, we assumed the following matrix properties:

$$K_m = 83.4 \text{ GPa}, G_m = 40.1 \text{ GPa and } \rho_m = 3.05 \text{ g/ccm} \qquad \text{(eq. 1)}$$

where K is bulk modulus and G is shear modulus. The values corresponds to Vp = 6.7 km/s and Vs = 3.63 km/s.

The zero-porosity end-member was estimated from varying the mineral end-point value of Vp while keeping the Vp-Vs ratio fixed at 1.847 – the average log-value measured for the massive lava flows in the LP-1 well. The model is very sensitive to the mineral end-point properties, and other mineral end-point values were also tested, but the above choice was selected because it resulted in consistent estimates of aspect ratio based on both Vp and Vs data (it does not make physical sense that the P-waves are seeing different pore aspect ratios than the S-waves). In Figure 4.2 we observe that the data cloud for the massive lava flows (phi<15%) plot between the lines of aspect ratios of 0.03 and 0.3, even though the line of 0.1 plot slightly lower in the plot of Vp compared to that of Vs. The mineral-end point for the curves match the low-porosity end of the data cloud. The plot of Vp versus Vs also shows a nice agreement between data and model: there is agreement between the mineral end-point and the curves for small aspect ratios define a lower bound for the data trend indicating that stiffer pore shapes result in higher Vp-Vs ratios. The model curves capture the overall trend of the Vp versus Vs data. The mineral properties selected for the model represent an intermediate value in between the values for the main constituents of basalt, pyroxene (K = 110 GPa, G = 63 GPa, $\rho$ = 3.31 g/ccm) and plagioclase (K = 76 GPa, G = 26 GPa, $\rho$ = 2.63 g/ccm) (data from Mavko et al. 1998).

In Appendix A we compare the inclusion model established for the Lopra data with the log data for the other wells. For the GL-1 and the VM-1 wells we observe a general good agreement between the data and the model given by equation (1) for the plots of Vp, Vs and porosity. For the VM-1 well we see a good agreement between the mineral end-point and the data cloud with porosities close to zero and furthermore, that the predicted aspect ratios are similar for both Vp and Vs. This is highlighted by the plot of Vp versus Vs where the VM-1 data plot in a narrow range that coincides with the model and the LP-1 data. However, the GL-1 data appear to be biased towards relatively high values of Vs (especially for high velocities). Relatively few GL-1 data points plot near the mineral end-point. The three Icelandic wells plot very similarly relative to model in the plots of Vp and Vs versus porosity and in particularly in the plots of Vp versus Vs. The predicted high porosities of the Icelandic rocks reveals that the high-porosity rocks (irrespective of lithology) tend to have higher aspect ratios than the low porosity rocks. This behaviour is not understood.

## 4.3 Modified Hashin-Shtrikman bounds based on data from Lopra-1 and LL-3

Walls et al. (1998) found that a modified upper Hashin-Shtrikman (MUHS) model predicts the velocity-porosity behaviour of chalk as estimated from well log data from the Ekofisk field. Even though chalk and basalt are two rocks with nothing in common as lithologies, they share the property that the data trend is upwards concave in the velocity-porosity plane: The velocity-porosity gradient is large for small porosities, but small for high porosities and this result in the characteristic bended trend for e.g. the GL-1 and LL-3 wells that span a wide range of porosities (Fig. 4.3). This behaviour may be modelled by modified Hashin-Shtrikman bounds. See plots of velocity versus porosity for all wells in Appendix A where data points for all lithologies are shown in the same colour to emphasize that most data points fall within the modified upper and lower Hashin-Shtrikman bounds.

The model describes how the dry bulk and shear moduli, *K* and *G* increase as porosity is reduced from a maximum value, $\phi_{max}$, to zero porosity. The upper and lower Hashin-Shtrikman bounds give the narrowest possible range on the modulus of a mixture of grains and pores without specifying the geometries of the constituents (Hashin & Shtrikman 1963). The upper bound represents the stiffest possible pore shapes for porosity ranging from 0% to 100%, whereas the modified upper bound is defined for porosity up to a maximum value less than 100%. Here we refer to the high-porosity end member ($K_{\varphi max}$, $G_{\varphi max}$) as the maximum porosity ($\varphi$max) rather than as the critical porosity, which is defined as the porosity limit above which a sedimentary rock can only exist as a suspension (Nur *et al.* 1998). The low-porosity end-members ($K_s$, $G_s$) are the moduli of the solid at zero porosity. The modified upper Hashin-Shtrikman model is given by the dry-rock bulk and shear modulus, $K^{MUHS}$ and $G^{MUHS}$:

$$K^{MUHS} = \left[ \frac{\phi/\phi_{max}}{K_{\phi\max} + \frac{4}{3}G_s} + \frac{1-\phi/\phi_{max}}{K_s + \frac{4}{3}G_s} \right]^{-1} - \frac{4}{3}G_s$$

$$G^{MUHS} = \left[ \frac{\phi/\phi_{max}}{G_{\phi\max} + Z_s} + \frac{1-\phi/\phi_{max}}{G_s + Z_s} \right]^{-1} - Z_s, \qquad \text{(eq. 2)}$$

$$\text{where} \quad \mathrm{Z_s} = \frac{G_s}{6} \cdot \frac{9K_s + 8G_s}{K_s + 2G_s}$$

The modified lower bounds for the dry rock effective bulk and shear moduli ($K^{LMHS}$, $G^{LMHS}$) can be found from the modified lower Hashin-Shtrikman model (MLHS):

$$K^{MLHS} = \left[ \frac{\phi/\phi_{\max}}{K_{\phi\max} + \frac{4}{3}G_{\phi\max}} + \frac{1-\phi/\phi_{\max}}{K_s + \frac{4}{3}G_{\phi\max}} \right]^{-1} - \frac{4}{3}G_{\phi\max}$$

$$G^{MLHS} = \left[ \frac{\phi/\phi_{\max}}{G_{\phi\max} + Z_{\phi\max}} + \frac{1-\phi/\phi_{\max}}{G_s + Z_{\phi\max}} \right]^{-1} - Z_{\phi\max}, \qquad \text{(eq. 3)}$$

$$\text{where } Z_{\phi\max} = \frac{G_{\phi\max}}{6} \cdot \frac{9K_{\phi\max} + 8G_{\phi\max}}{K_{\phi\max} + 2G_{\phi\max}}$$

From this model we can calculate the modified upper and lower bounds on the moduli of the dry rock for a given porosity and then estimate the moduli for the saturated rock using Gassmann's relations (see Mavko et al. 1998) and the appropriate fluid properties (e.g. $\rho_w$ = 1 g/ccm and $K_w$=2.25 GPa for brine), and finally calculate Vp and Vs.

We chose the matrix properties given by equation (1) as the low-porosity end-member and estimate the high-porosity end-member by comparison with data from the LP-1 and LL-3 wells (see Appendix A). A consistent fit between model and data from these wells is found for the following properties:

$K_{\varphi max}$ = 5.55 GPa, $G_{\varphi max}$ = 3.2 GPa, $\varphi_{max}$ = 45% (eq. 4)
$K_s$ = 83.4 GPa, $G_s$ = 40.1 GPa and $\varphi$ = 0%

From the velocity-porosity plots of this model compared to log data (Appendix A) we see that most data points fall within the upper and lower bounds. In particular the model matches data for both the LP-1 and LL-3 wells that were used to define the model parameters, but the similarity between the data for these very different flood basalt series is striking.

The calculated velocity-porosity data typically plot in between the modified upper and lower Hashin-Shtrikman bounds, and we can thus calculate a median model defined by its dry moduli ($K^{MMHS}$, $G^{MMHS}$) as the mean of the upper and lower bounds:

$$K^{MMHS} = (K^{MUHS} + K^{MLHS})/2, \quad G^{MMHS} = (G^{MUHS} + G^{MLHS})/2, \qquad \text{(Eq. 5)}$$

This model may eventually be used as a velocity-porosity transform. From the plots of the modified Hashin-Shtrikman models in Appendix A it is apparent that there is quite an ambiguity in the relation between velocity and porosity estimated from bulk density; e.g. Vp=5.3 km/s corresponds to calculated porosities ranging from c. 10% to c. 20% for the lower and the upper bound respectively. However, a significant part of this range in porosities is due to variations in grain densities (see the Discussion section) where the apparently high porosities corresponds to altered basalt with low grain densities. The real porosity for these altered basalts is thus less than estimated from a fixed grain density of 3.05 g/ccm. From the study of core samples we know that the relation between He-porosity and velocity is very well-defined. Sonic velocity is thus a good measure of porosity and the suggested median velocity-porosity model may thus provide reasonable estimates of basalt porosity from sonic data.

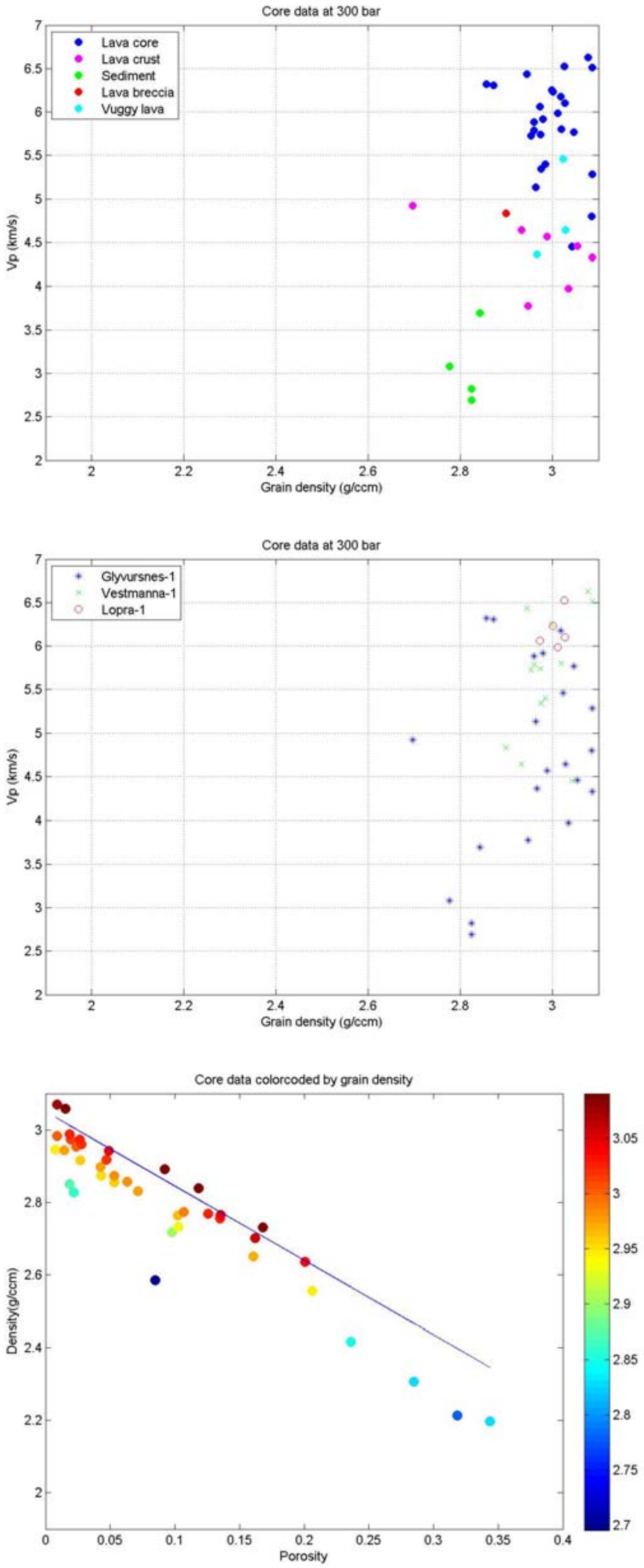


Figure 4.1. Plots of ultrasonic data for water saturated core samples measured at 300 bar. (a) Vp versus colorcoded by lithology. (b) Vp versus grain density with indication of well names. (c) Density versus He-porosity colorcoded by grain density. Straight line shows relation for grain density of 3.05 g/ccm. Both massive lava and lava crust show a range of grain densities, but the variation is not specific for any well.

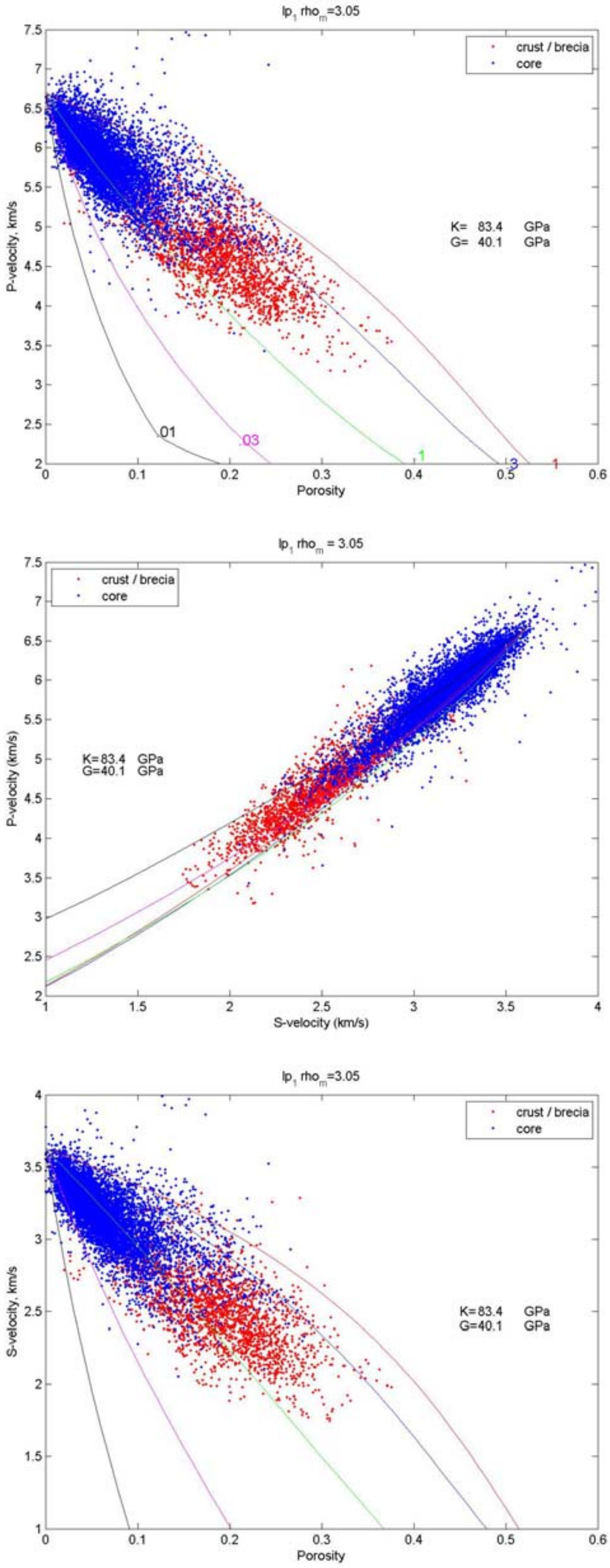


Figure 4.2. Comparison of sonic data from Lopra-1 with ellipsoidal inclusion rock model (eq. eq. 1). Adjusted mineral properties gives data-model consistency in both Vp-porosity and Vs-porosity planes. Only data for massive flows (blue) and crust/breccia (red) shown for simplicity.

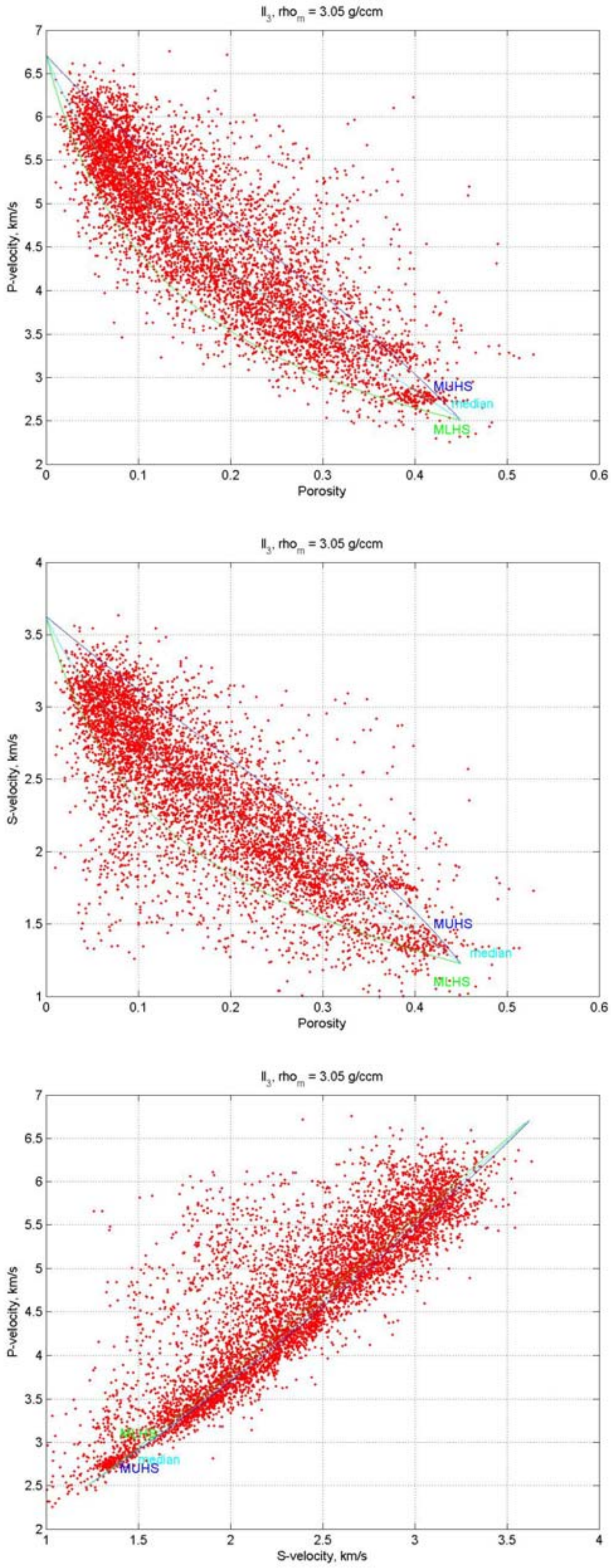


Figure 4.3. Comparison of sonic data from LL-3 with the modified upper and lower Hashin-Shtrikman bounds (MUHS, MLHS; eqs 2-4) as well as the mean of the upper and lower bounds (median; eq. 5). Data points from all lithologies are shown in the same colour to emphasize that most data points fall within the modified upper and lower bounds.

Table 4.1. Coefficients P and Q for some specific shapes. The subscripts m and i refer to the background and inclusion materials [from Berryman (1995)].

| Inclusion shape | $P^{mi}$ | $Q^{mi}$ |
|---|---|---|
| Spheres | $\dfrac{K_m + \frac{4}{3}\mu_m}{K_i + \frac{4}{3}\mu_m}$ | $\dfrac{\mu_m + \zeta_m}{\mu_i + \zeta_m}$ |
| Needles | $\dfrac{K_m + \mu_m + \frac{1}{3}\mu_i}{K_i + \mu_m + \frac{1}{3}\mu_i}$ | $\dfrac{1}{5}\left(\dfrac{4\mu_m}{\mu_m + \mu_i} + 2\dfrac{\mu_m + \gamma_m}{\mu_i + \gamma_m} + \dfrac{K_i + \frac{4}{3}\mu_m}{K_i + \mu_m + \frac{1}{3}\mu_i}\right)$ |
| Disks | $\dfrac{K_m + \frac{4}{3}\mu_i}{K_i + \frac{4}{3}\mu_i}$ | $\dfrac{\mu_m + \zeta_i}{\mu_i + \zeta_i}$ |
| Penny cracks | $\dfrac{K_m + \frac{4}{3}\mu_i}{K_i + \frac{4}{3}\mu_i + \pi\alpha\beta_m}$ | $\dfrac{1}{5}\left(1 + \dfrac{8\mu_m}{4\mu_i + \pi\alpha(\mu_m + 2\beta_m)} + 2\dfrac{K_i + \frac{2}{3}(\mu_i + \mu_m)}{K_i + \frac{4}{3}\mu_i + \pi\alpha\beta_m}\right)$ |

$$\beta = \mu\frac{(3K+\mu)}{(3K+4\mu)} \qquad \gamma = \mu\frac{(3K+\mu)}{(3K+7\mu)} \qquad \zeta = \frac{\mu}{6}\,\frac{(9K+8\mu)}{(K+2\mu)}$$

# 5. Discussion

## 5.1 Influence of basalt alterations on the physical properties

The analysis of log and core data from the three Faroes wells has shown

1. Consistency between the log and core data (almost 1:1 correlation between estimates of Vp, Vs and density at identical depths; Fig 3.9).
2. One data trend irrespective of basalt formation and borehole expressed as Vp-$\varphi$ (core data) and as Vp-Vs (core and log data) (Figs 3.2a, b, 3.1a, b).
3. A scattered Vp-density trend for core data (Figs 3.2c, 3.1c). Strong correlation between spread in density and grain density indicates that alteration of the rock matrix affects Vp-density relation (Fig. 3.3).
4. Two Vp-density trends for log data: A low trend characterizing the UBF in GL-1 and a high trend characterizing the MBF in VM-1. The MBF in GL-1 represents the transition between the two trends and the LBF in VM-1 plots along the low trend (Figs 3.4).

These observations show that the two Vp-density trends established from the well log data are related to alterations in the rock matrix: The low trend represents basalt with unaltered matrix with high grain density and the high trend represents altered basalt with a low grain density (Fig. 3.10). However, the two Vp-density trends represent the same Vp-porosity trend (Fig. 3.3a) where we observe that the scatter in porosity for a given velocity does not correspond to any clear variation in grain density.

The filling of vesicles with zeolites is a likely candidate for explaining these changes in the physical properties in basalt. Zeolites are framework silicates that are derived from low-temperature alteration of basalt and are redistributed by percolating water. Specific zeolites assemblages thus reflect distinct temperature conditions and the distribution by percolating water may explain why specific zones may be protected from growth of zeolites due to specific hydraulic conditions.

The possible changes due to alteration of basalt are illustrated schematically by Fig. 5.1. Altered samples (indicated by black circles) are characterized by low grain density due to the presence of light minerals such as clay and zeolites in the vesicles and probably also due to the alteration of the minerals in the matrix. In the plot of Vp versus density the altered samples deviate from the data trend as indicated by the horizontal black arrow (Fig. b), whereas the same samples do not deviate significantly from the data trend in the plot of Vp versus porosity. How can we explain these differences in terms of the physical changes of the sample due to the alteration processes?

- The infilling of vesicles with zeolites reduces porosity (horizontal red arrow in Fig. a), but also leads to a better grain contacts and thus to an increase in velocity (vertical red arrows in Figs a and b). If the formation of zeolites is due to influx of mass into the sample, the density of the sample will increase due to the replacement of brine with zeolite (vertical red arrow in Fig. b).

- The alteration of the matrix minerals removes mass and thus leads to a reduction of the bulk density (horizontal blue arrow in Fig. b) and probably reduces the sonic velocity of the mineral and thus of the matrix (vertical blue arrow in Figs a and b). The alteration of the matrix minerals does however, probably not lead to changes in porosity.

The dominant net effect of these processes is to move the altered sample along the velocity-porosity trend as porosity is reduced (strong alteration may apparently move a data point slightly towards lower porosities; indicated by the horizontal black arrow in Fig. a). The addition of zeolites thus leads to reduction of porosity and increase in velocity. If the addition of zeolites is due to influx of mass, the density of the rock will increase (net removal of mass will reduce density). This means that the outlying data points in the plot of Vp versus density must represent samples with relatively high velocity compared to density (rather than relatively low density compared velocity), because addition of zeolites increases velocity and only changes density of low-porosity basalts slightly.

## 5.2 Comparison of the properties of the UBF and the MBF

In Figure 5.3 we compare the suite of logs obtained from the GL-1 and VM-1. The GL-1 section represents the transition from UBF to MBF whereas the VM-1 section represents the transition from MBF to LBF. The VM-1 logs are plotted 300 m below the GL-1 logs to emphasize an intermediate part of the MBF which is not penetrated by the two wells, but which is known elsewhere on the Faroes (cf. Petersen et al. 2006). We observe that the MBF in GL-1 represents a gradual increase of velocity with depth from the low velocities in the UBF (apart from velocity peaks representing thick lava flows) to the high velocities in the MBF in VM-1, below which there is a drop in velocity for the LBF in VM-1. Concordant with this increase in Vp we observe an increase in density (both minimum and maximum) even though the numerical value of the increase is less prominent than that of the corresponding velocity. This is however, not surprising because of the steep density-velocity gradient for high-density basalt (e.g. Fig. 3.2c).

In Figure 3.4 we compare the log data from the GL-1 and VM-1 wells in plots of Vp versus density subdivided for the UBF and the MBF in the two wells. We observe the previously discussed shift from the low Vp-density trend for the UBF in GL-1 to high trend for the MBF in VM-1 with the MBF in GL-1 as a transition between the two. The differences in the log pattern shown in Figure 5.3 indicate that the shift from the low Vp-density trend to the high trend is accompanied by a general increase in density and velocity. This underlines that the net effect of the alteration of the basalts accompanied by zeolite infilling is an increase in velocity. The increase in density with depth does not reflect stratigraphic variations in the lava-flow thickness within the MBF because the mean flow thickness of the MBF in GL-1 and VM-1 is identical 2.2 m and not much different from the mean thickness of 3.4 m for the UBF in GL-1 (Waagstein & Andersen 2004).

The change in physical properties with depth does thus most likely reflect influx of mass into the deeper basalt sequences due to redistribution of mass related to diagenetic processes. The two basic observations of depth-related shifts

a. to a higher velocity-density trend, and
b. to a generally higher velocity level,

supports the interpretation that light material (e.g. zeolites) are added and causes an increase in bulk density (and a reduction in grain density) and thus higher sonic velocity. The added material may eventually be derived from alteration of basalts at more shallow levels.

## 5.3 A model for estimating grain density from velocity-density data

We can evaluate the influence of varying grain density on the velocity-density relation if we assume a simple velocity-porosity transform. In Fig. 3.2a we see that the velocity-porosity relation for basalt samples may be approximated by a linear relation; e.g. passing through Vp=6.5 km/s for zero porosity and 3.75 km/s for a porosity, $\phi$, of 0.2. We get

$$V_P = 6.5 - 13.75 \cdot \phi \qquad \text{(Eq. 6)}$$

This relation can be transformed into a relation between velocity and density, $\rho$, (and grain density, $\rho_{gr}$) by introducing the following expression for porosity where the density of water is 1 g/ccm:

$$\phi = \frac{\rho_m - \rho}{\rho_m - 1}$$

In Figure 5.4 the predicted relation between velocity and density is plotted for a range of grain densities between 2.7 and 3.05 g/ccm. Note the general good fit between the datapoints and the model that predict rocks with smaller grain densities to plot the left in the diagram. We can thus explain the scatter of the datapoints in a plot of velocity versus density as due to differences in grain density. Application of the model may be used to estimate grain densities from log data.

## 5.4 Comparison of the properties of the UBF and Icelandic flood basalt

In Figure 5.5 we compare the suite of logs obtained from the Faroese well GL-1 and the Icelandic well LL-3. The LL-3 drillhole penetrated 95% flood basalts of Plio-Pleistocene age whereas the GL-1 section represents the transition from UBF to MBF of Palaeogene age. We observe that the densities measured in the Icelandic well cover a wide range with an upper limit close to 3 g/ccm throughout most of the well, whereas the densities in the Faroese well show a more narrow range and that they only reach 3 g/ccm in limited depth intervals within the UBF and that densities are well below that value in the MBF. This pattern is repeated by the sonic log which reaches 6 km/s throughout the section penetrated by the LL-3 well whereas this value is only reached in narrow zone in the GL-1 well.

We can also compare the data from the two wells in the velocity-porosity plane where we observe that the data from the UBF and Icelandic flood basalts follow the same trend (Fig. 3.5). The densities in the UBF in the GL-1 well range from 2.4 to 3 g/ccm whereas the Icelandic data range from 2.2 to 3 g/ccm. For the high densities we observe that the bulk of data points in the Icelandic well are close to 3 g/ccm where as the centre of the data cloud for GL-1 is closer to 2.9 g/ccm, This small deviation in densities are however, reflected in a pronounced difference in sonic velocities: The maximum values for GL-1 are generally below 6 km/s, whereas they plot between 6 and 6.5 km/s for the LL-3 well. This means that only a small increase in density causes a strong response in velocity and this is also seen as the steep trend of the data cloud for the LL-3 well for densities above 2.8 g/ccm.

How can we understand that the maximum velocities in the Faroese flood basalts in GL-1 are smaller than those of the Icelandic flood basalts in LL-3? The analysis indicates that the grain densities and moduli of the basalt matrix in the two drilled sections must be close to the same value because they plot along the same Vp-porosity trend (the similarity of the grain densities for unaltered basalt is independently supported by core data as discussed above). This implies that the smallest porosities are reached in the Icelandic basalts because more data points are close to 3 g/ccm and hence that velocities above 6 km/s are more frequently reached. Part of the explanation behind this observation appears to be that the flow units in the Icelandic basalts have a greater thickness than the Faroese Upper Basalt Formation. The plot of the logs in the GL-1 well (Appendix A) shows a number of thick flows indicated by intervals of high density (e.g. around 250 m) but the mean flow thickness for the UBF is only 3.4 m (e.g. around a depth of 300 m) (Waagstein & Andersen 2003). The flows in the LL-3 well are however, in the order of 10 m throughout the well (Appendix A) and hence low porosities and velocities above 6 km/s are more frequently reached. An additional contribution to the high velocities in the LL-3 well may be due to compositional differences; cf. Vp>6 km/s for densities close to 3 g/ccm in the upper 100 m of that well, whereas Vp< 6 km/s for comparable densities in GL-1 around a depth of 250 m.

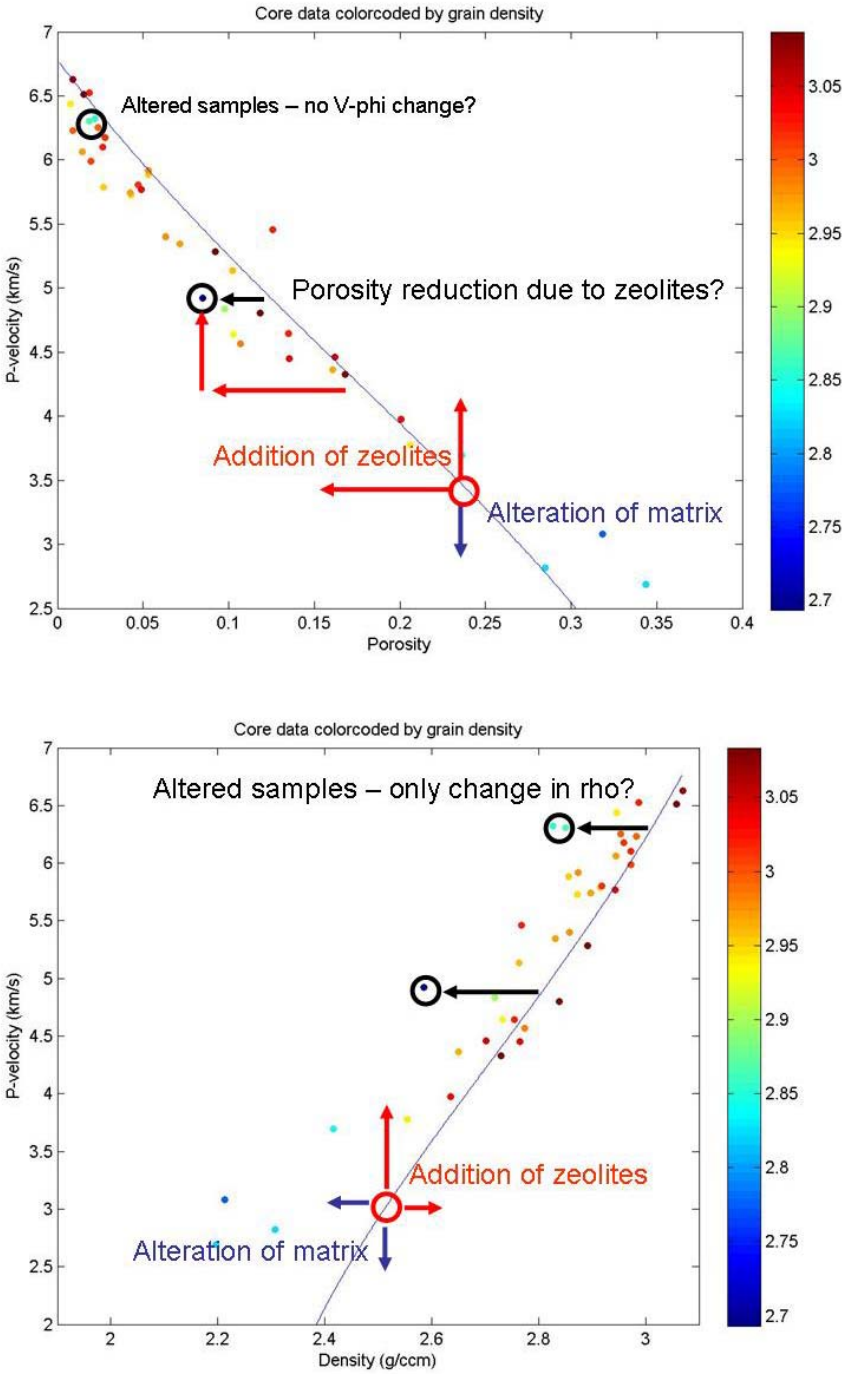


Figure 5.1. Schematic illustration of the influence of basalt alteration on physical properties. (a) Vp versus porosity. (b) Vp versus density. (c) Lab data for basalt samples colorcoded by grain density. Black circles indicate 3 samples with minimum grain densities and their density deviation from the data trend is indicated by black arrows. Expected changes due to infilling of zeolites are marked by red arrows and changes due to alteration of the matrix minerals by blue arrows relative to a data point on the data trend. The upper bound of the data trend is represented by the upper Hashin-Shtrikman model (thin black line) based on the core data (Japsen & Waagstein 2005).

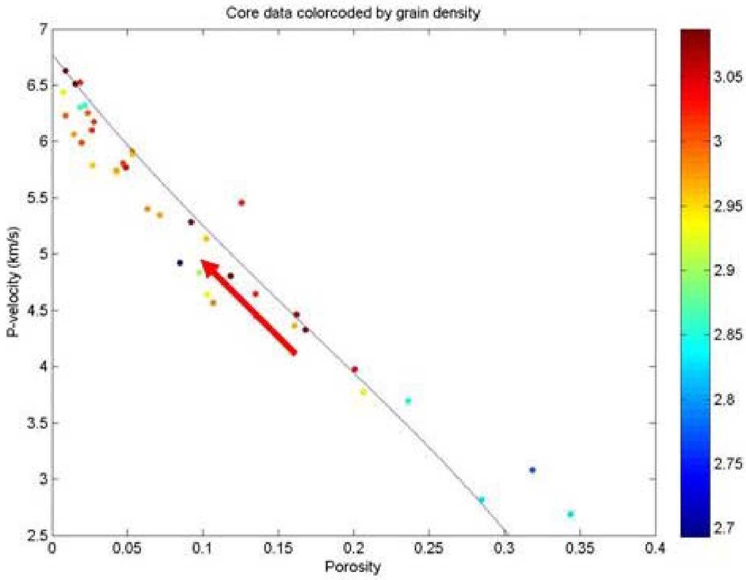


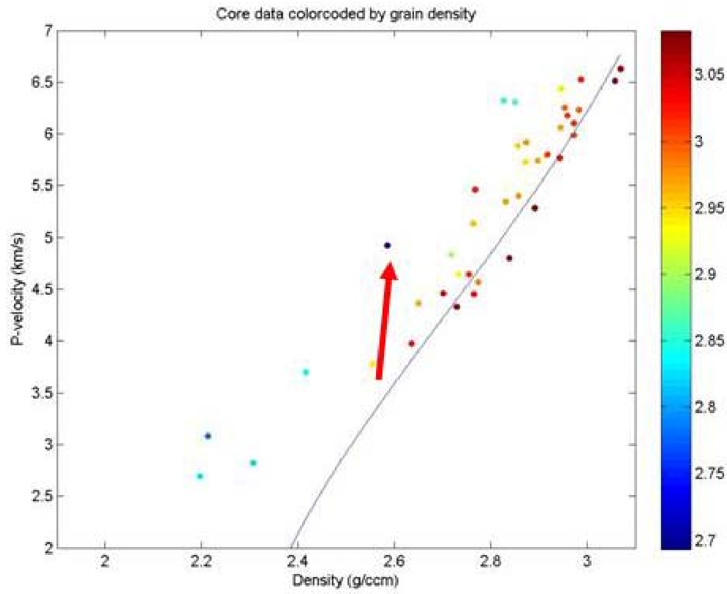


Figure 5.2. Schematic illustration of the net influence of basalt alteration on physical properties. (a) Vp versus porosity. (b) Vp versus density.

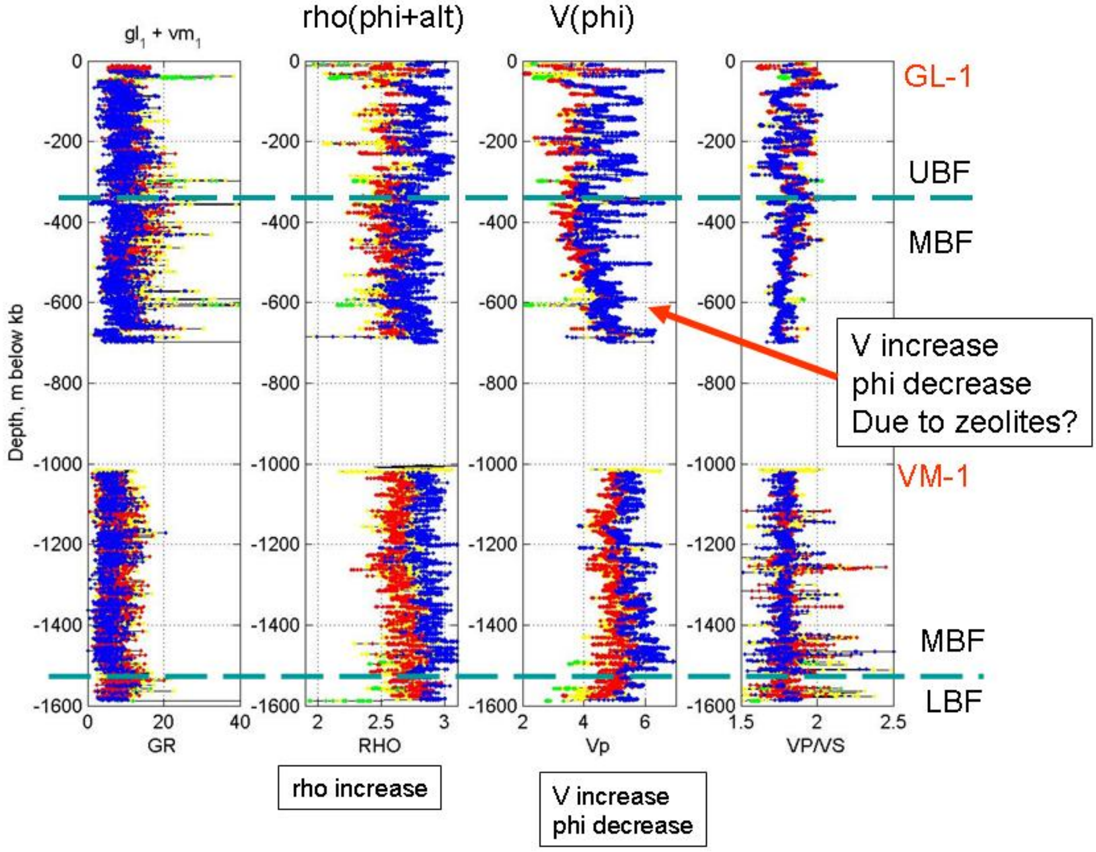


Figure 5.3. Composite plot of logs from the GL-1 and VM-1 wells. The GL-1 section represents the transition from UBF to MBF whereas the VM-1 section represents the transition from MBF to LBF. The VM-1 logs are plotted 300 m below those from GL-1 to emphasize the intermediate part of MBF which is elsewhere on the Faroes, but which is not penetrated by any of the two wells. Note that the MBF in GL-1 represents a gradual increase of velocity with depth from the generally low velocities in the UBF to the high velocities in the MBF in VM-1. There is a drop in velocity in the LBF in VM-1. The increase in Vp corresponds to an increase in density (both minimum and maximum).

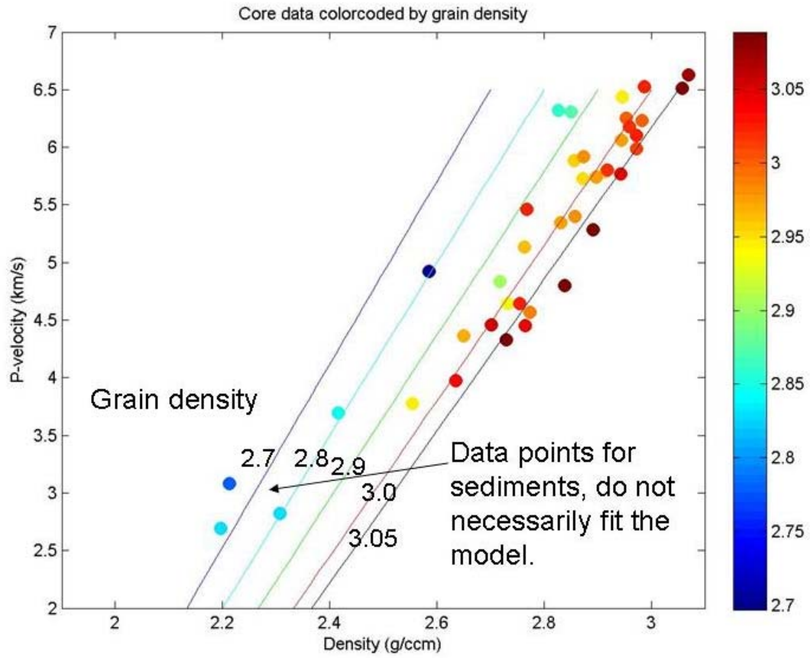


Figure 5.4. Plot of ultrasonic data for water saturated core samples measured at 300 bar: Vp versus density colorcoded by grain density. Straight lines represent different grain densities for a linear velocity-porosity trend given by equation (6). Note the general good fit between the datapoints and the model that predict rocks with smaller grain densities to plot the left in the diagram.

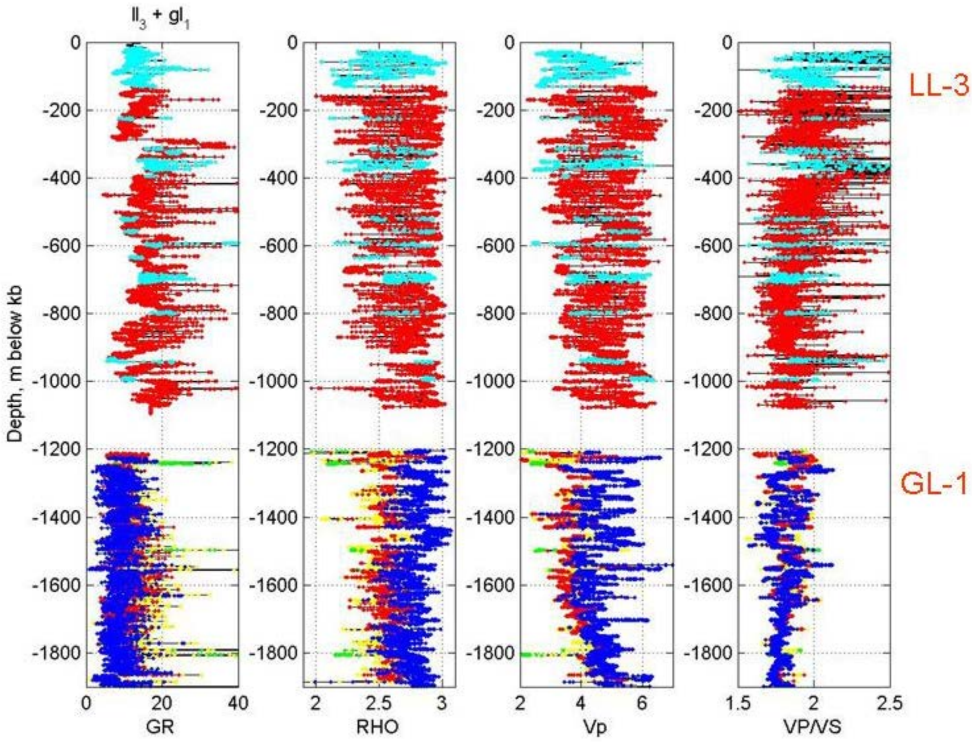


Figure 5.5. Composite plot of logs from the LL-3 and the GL-1 wells separated by an arbitrary depth interval.

# 6. Summary

We have analysed the acoustic properties of basalts based on sonic log data from three Faroese and three Icelandic boreholes and ultrasonic laboratory measurements on 43 1.5" core samples from the three Faroese boreholes. The Faroese boreholes are Lopra-1/1A (LP-1), Vestmanna-1 (VM-1) and Glyvursnes-1 (GL-1); respectively 3.6, 0.6 and 0.7 km deep. The Icelandic boreholes are the geothermal wells HH-1, LA-10 and LL-3; respectively 1.3, 1.0 and 1.1 km deep. The Faroese drillholes cover the Palaeogene basalts of the Lower, Middle and Upper Basalt Formations (UBF, MBF and LBF, respectively) and the rocks are mainly subaerial flood basalts apart from hyaloclastites below c. 2.5 km depth in the LP-1 well. The Icelandic wells penetrate volcanic rocks of Plio-Pleistocene age and cover a mixed environment: HH-1 (95% hyaloclastites), LA-10 (45% submarine and 45% subaerial basalts) and LL-3 (95% subaerial basalts).

We find a tight correlation between sonic Vp and He-porosity based on core data irrespective of basalt facies and well (only data for sediment samples deviate) and this supports the result of previous studies that porosity is the primary control on sonic velocity in basalt. The core data also reveal a well-defined relation between Vp and Vs, which is to be expected from rocks of broadly similar composition. However, there is a significant scatter in plots of Vp versus density and this scatter is related to the range of grain (matrix) densities from 2.7 to 3.1 g/ccm estimated for the samples. Low grain densities represent altered samples with high content of light minerals and this is confirmed by visual inspection of a thin section of a highly altered sample where zeolite and clay and pyroxene is altered whereas plagioclase remains fresh.

We can distinguish two main Vp-density relations for flood basalts based on the log data: (1) a trend of relatively low Vp compared to density (the UBF in the GL-1 well; the flood basalts in the LL-3 well) and (2) a trend of relatively high Vp compared to density (the LBF in the LP-1 well). The properties of the MBF are transitional between the two trends. The GL-1 data from this interval represents both the high and the low trend, whereas the VM-1 data represent a very high trend. However, towards the base of VM-1, we observe a 'reversal' of the Vp-density trend within the thin sequence of the LBF penetrated by the well.

There is agreement between the log and core data estimated at identical depths: There is almost a 1:1 correlation for the density data (note that the core data were used to calibrate the density log) and the correlation between Vp and Vs for the two datasets is also very good, even though Vp for the core data are slightly biased towards higher velocities. There is however, a strong bias in the selection of the core samples: The low-density part of the relatively high Vp-density trend for the MBF is only represented by one sample. But the analysis of the Vp-density relation for the core data shows that the outlying samples towards low densities are characterized by low grain density. Hence we can conclude that the relatively high Vp-density trend defined for the log data in these wells for the MBF also must be characterized by low grain densities. This means that the low Vp-density trend represents basalt with unaltered matrix with high grain density and the high trend represents altered basalt with a low grain density.

The transition from the low Vp-density trend of fresh basalts to the high trend of altered basalts within the MBF occurs concurrently with an increase of the sonic velocity and density with depth even though there is no increase in the flow thickness. This shows that the transition from fresh to altered basalt is accompanied by an increase in velocity and density and thus probably also by net influx of mass leading to higher densities (growth of zeolites). Two opposite processes probably takes place: (1) The infilling of vesicles with zeolites reduces porosity, but may also lead to better grain contacts and thus to an increase in velocity. If the formation of zeolites is due to influx of mass into the sample, the density of the sample will increase due to the replacement of brine with zeolite. (2) The alteration of the matrix minerals removes mass and thus leads to a reduction of the bulk density and probably reduces the sonic velocity of the mineral and thus of the matrix. The alteration of the matrix minerals does however, probably not lead to changes in porosity. The dominant net effect of these processes is to increase velocity as porosity is reduced. This means that data points along a high Vp-density trend represents samples with relatively high velocity compared to density (rather than low density compared velocity), because filling of prore space with light materials increases velocity and only changes density of low-porosity basalts slightly.

Maximum values of velocity and density of Icelandic flood basalts are generally higher than for the unaltered Faroese basalts of the UBF. This is observed both on plots of these parameters versus depth and on plots in the velocity-porosity plane where we observe that the data from the UBF and Icelandic flood basalts follow the same trend. The latter observation indicates that the grain densities and moduli of the basalt matrix in the two drilled sections must be close to the same value. Thus the smallest porosities are reached in the Icelandic basalts, and this probably reflects that the flow units in the Icelandic basalts have a greater thickness (several flows in the order of 10 m thickness) than the Faroese UBF (a few thick flows, but a mean flow thickness of only 3 m).

Matrix (or grain) density for the core samples varies systematically with bulk density and alteration of the rocks. We observe that the highest grain densities mark a lower bound in the plot of Vp versus density and thus that only the highest grain densities may be considered representative for the unaltered matrix. A grain density of 3.05 g/ccm is a fair approximation of the property of the unaltered basalt with higher values (almost 3.1 g/ccm) interpreted as outliers related to anomalous content of heavy minerals and lower values (minimum 2.7 g/ccm) corresponding to more altered rock. For sediments in Faroese wells we assign the mean sample value of 2.8 g/ccm. A typical grain density for fresh Icelandic basalt lava measured on core samples is 3.06 g/ccm, so 3.05 g/ccm is a reasonable pick (Omar Sigurdsson pers. comm.), and we also apply that value for volcanic sediments in Icelandic wells. For the dolerites in well LP-1 the matrix density appear to smaller than for the surrounding basalt and we assign a matrix density of 3.02 g/ccm for these rocks in all wells. We can convert measured log density to porosity based on these values for the matrix density for different lithologies and a pore water density of 1 g/ccm.

We estimate the mineral end-point properties of flood basalt with zero porosity by comparing log data from the LP-1 well with the self-consistent formulation of Berryman (1995) where the models represents the pore space as a collection of ellipsoidal inclusions, ranging from flat penny-shaped cracks to spherical pores. The fact that sonic data are consistent with a penny-shaped crack model does not mean that there must be cracks in the rocks. Poorly cemented, compliant grain contacts will yield the same elastic behaviour. When comparing theoretical curves with well log data, we find that the results are very sensitive to the assumed mineral properties, and that the following matrix properties yield consistent values of aspect ratios based on both Vp and Vs data (Vp and Vs versus porosity, Vp versus Vs): K = 83.4 GPa, G = 40.1 GPa and $\rho$ = 3.05 g/ccm where K is bulk modulus, G is shear modulus and $\rho$ is density. Comparison of the inclusion model with the log data for the both Faroese and Icelandic wells reveals good agreement between the mineral end-point and the data points with porosities close to zero and furthermore, that the predicted aspect ratios are similar for both Vp and Vs. However, the GL-1 data appear to be biased towards relatively high values of Vs. The three Icelandic wells plot very similarly relative to the model in the plots of Vp and Vs versus porosity and in particularly in the plots of Vp versus Vs.

A modified upper and lower Hashin-Shtrikman model has been estimated to predict the velocity-porosity behaviour of basalt because the data trend is upwards concave in the velocity-porosity plane (a characteristic bended trend for the wells that span a wide range of porosities) (see Walls et al. 1998). The model describes how the dry bulk and shear moduli, K and G increase as porosity is reduced along either a lower or an upper bound from a maximum value, $\phi$max, to mineral end-point properties at zero porosity. We have tested a model with the following properties at the maximum porosity of 45%: K = 5.55 GPa, G = 3.2 GPa, and find that most data points for all wells fall within the upper and lower bounds defined by this model. There is however, a considerable ambiguity in the relation between velocity and porosity estimated from bulk density. A significant part of this range in porosities is due to variations in grain densities where the apparently high porosities correspond to altered basalt with low grain densities. Sonic velocity is thus a proxy for the porosity of basalt and a median model defined by the mean of the upper and lower bounds may thus provide reasonable estimates of basalt porosity from sonic data.

# 7. References


Berryman, J.G., 1995: Mixture theories for rock properties, in: A Handbook of Physical Constants, Ahrens, T.J., ed., American Geophysical Union, Washington, 236 pp.

Boldreel, L.O. 2006: Wire-line log-based stratigraphy of flood basalts from the Lopra-1/1A well, Faroe Islands. In press for Geological Survey of Denmark and Greenland Bulletin 9.

Christie, P., Gollifer, I. & Cowper, D. 2006: Borehole seismic studies of a volcanic succession from the Lopra-1/1A borehole in the Faroe Islands, northern North Atlantic. In press for Geological Survey of Denmark and Greenland Bulletin 9.

Borehole seismic results from the Lopra deepening project. Journal of Conference Abstracts 7, 138.

Drury, M.J. 1985: The Iceland-research-drilling-project crustal section - physical properties of some basalts from the Reydarfjordur borehole, Iceland. Canadian Journal of Earth Sciences 22, 1588-1593.

Fridleifsson, G.Ó. & Gudlaugsson, S.Th. 1998: Borehole LN-10 Thorlákshöfn. Geological report. Orkustofnun, OS-98071 (prepared for Norsk Hydro), 14 pp.

Gommesen, L. 2005: SeiFaBa well log analysis, lithology and rock physics. Ødegaard A/S Report 04.26074.01, 23 pp.

Gommesen, L. & Ahmed M. 2005: SeiFaBa log analysis of Icelandic wells, Lithology and Rock Physics. Ødegaard A/S Report 03.24036.02, 29 pp.

Hald, N. & Waagstein, R. 1984: Lithology and chemistry of a 2-km sequence of Lower Tertiary tholeiitic lavas drilled on Suduroy, Faroe Islands (Lopra-1). In: Berthelsen, O. Noe-Nygaard, A. & Rasmussen, J. (eds) The deep drilling project 1980–1981 in the Faeroe Islands. Føroya Frodskaparfelag, Torshavn, 15–38.

Han, D.H., Nur,A. & Morgan,D. 1986: Effects of porosity and clay content on wave velocities in sandstones. Geophysics 51, 2093-2107.

Hashin, Z. & Shtrikman, S. 1963: A variational approach to the elastic behaviour of multiphase materials. Journal of the mechanics and physics of solids 11, 127–140.

Japsen, P. 2005: Seismic and petrophysical propterties of Faroes basalt. SeiFaBa workshop September 29 2005. GEUS rapport 2005/57 (confidential). 24 pp.

Japsen, P. & Waagstein, R. 2005: Preliminary analysis of ultrasonic and geochemical properties of core samples from Glyvursnes-1 and Vestmanna-1, Faroe Islands. Contribution to the SeiFaBa project. Funded by the Sindri Group. Danmarks og Grønlands Geologiske Undersøgelse Rapport 2005/19 (confidential). 39 pp.

Japsen, P., Andersen, C., Andersen, H.L., Andersen, M.S., Boldreel, L.O., Mavko, G., Mohammed, N.G., Pedersen, J.M., Petersen, U.K., Rasmussen, R., Shaw, F., Springer, N., Waagstein, R., White, R.S. & Worthington M. 2005: Preliminary results from investigations of seismic and petrophysical properties of Faroes basalts in the SeiFaBa project. In: Doré, A.G. & Vining, B.A. (eds): Petroleum Geology: North-West Europe and Global Perspectives: Proceedings of the 6th Petroleum Geology Conference. Geological Society, London, 1461 - 1470.

Jóhansson H. & Saemundsson, K. 1998: Geological Map of Iceland. 1:500 000. Bedrock Geology. Icelandic Institute of Natural History, Reykjavík (2nd edition).

Jørgensen, O. 1984: Zeolite zones in the basaltic lavas of the Faroe Islands – A quantitative description of the secondary minerals in the deep wells of Vestmanna-1 and Lopra-

1. In: Berthelsen, O. Noe-Nygaard, A. & Rasmussen, J. (eds) The deep drilling project 1980-1981 in the Faeroe Islands. Føroya Frodskaparfelag, Torshavn, 71–91.

Kanestrøm R. 1999: Acoustic velocities in basalts from log data and core samples from Iceland. Norsk Hydro E&P Research Centre Bergen R-091058 (confidential).

Larsen, L. M., Waagstein, R., Pedersen, A. K. & Storey, M. 1999: Trans-Atlantic correlation of the Palaeogene volcanic successions in the Faeroe Islands and East Greenland. Journal of the Geological Society 156, 1081–1095.

Mavko, G. & Japsen, P. 2005: Rock physics analysis of sonic velocities in wells Lopra-1, Glyvursnes-1 and Vestmanna-1. Danmarks og Grønlands Geologiske Undersøgelse Rapport Rapport 2005/17. 29 pp.

Mavko, G., Japsen, P. & Boldreel, L.O. 2004: Preliminary rock physics analysis of basalts in the Lopra-1 well. GEUS rapport 2004/96, 11 pp.

Nielsen, P. H., Stefánsson, V. & Tulinius, H. 1984: Geophysical logs from Lopra-1 and Vestmanna-1. In: Berthelsen, O., Noe-Nygaard, A. & Rasmussen, J. (eds) The deep drilling project 1980–1981 in the Faeroe Islands. Føroya Frodskaparfelag, Torshavn.

Nur, A., Mavko, G., Dvorkin, J. & Galmundi, D. 1998: Critical porosity; a key to relating physical properties to porosity in rocks. Leading Edge 17, 357–362.

Olsen, D. 2005: Special Core Analysis for the SeiFaBa Project. Ultrasonic velocity measurements on plug samples from the Vestmanna-1 and Glyvursnes-1 wells, Faroe Islands. Danmarks og Grønlands Geologiske Undersøgelse Rapport Rapport 2005/10 (confidential), 65 pp (1 cd).

Olsen, D., Jørgensen, M. & Guvad, C. 2005: Special Core Analysis for the SeiFaBa Project. Ultrasonic velocity measurements on 12 plug samples from the Lopra-1, Vestmanna-1 and Glyvursnes-1 wells, Faroe Islands. Danmarks og Grønlands Geologiske Rapport 2005/76 (confidential), 32 pp, Appendix A (1 cd).

Petersen, U.K., Andersen, M.S., White, R.S. & SEIFABA GROUP 2006: Seismic imaging of basalts at Glyvursnes, Faroe Islands: hunting for future exploration methods in basalt covered areas. First Break 24, pp. 45-52.

Rasmussen, J. & Noe-Nygaard, A. 1970: Geology of the Faroe Islands. Danmarks Geologiske Undersøgelse, First Series 25.

Vilmundardóttir, E.G, Gudlaugsson, S.T. & Fridleifsson, G.Ó. 1999a: Borehole HH-01. Haukholt í Hreppum. Geological report. Orkustofnun, OS-99009 (prepared for Norsk Hydro), 22 pp.

Vilmundardóttir, E.G, Gudlaugsson, S.T. & Fridleifsson, G.Ó. 1999b: Borehole LL-03. Laugalandi í Holtum. Geological report. Orkustofnun, OS-99008 (prepared for Norsk Hydro), 22 pp.

Waagstein R. 1983: Vestmanna well No. 1, Streymoy, Faroe Islands. Danmarks Geologiske Undersøgelse, intern rapport, København, 40 pp.

Waagstein, R. 1988: Structure, composition and age of the Faeroe basalt plateau. In: Morton, A. C. & Parson, L. M. (eds) Early Tertiary Volcanism and the Opening of the NE Atlantic, Geological Society, London, Special Publications 39, 225–238.

Waagstein, R. & Andersen, C. 2004: Well completion report: Glyvursnes-1 and Vestmanna-1, Faroe Islands. Contribution to the SeiFaBa project funded by the Sindri Group. GEUS rapport 2003/99, 67 pp.

Waagstein, R. & Japsen, P. 2005: Comparison of wire-line logs and core data from the flood basalt succession of the Faroe Islands. In: Japsen, P. (Ed) 2005. Seismic and

petrophysical properties of Faroes basalt. SeiFaBa workshop September 29 2005. GEUS rapport 2005/57, 22-24.
Waagstein, R., Boldreel, L.O. & Andersen, C. 2003: An integrated petrophysical approach to the sub-basalt imaging problem using well logging data to link measurements from cores and seismic surface experiments. Geophysical Research Abstracts 5, No. 09388.
Walls, J. D., Dvorkin, J. & Smith, B. A. 1998: Modeling seismic velocity in Ekofisk Chalk. Society of Exploration Geophysicists 68th annual conference. 1016–1019.

# Appendix A. Cross plots of log and core data

**Lithology classification in the studied wells.**

| Lithology | Color | LP-1 | GL-1 | VM-1 | LL-3 | HH-1 | LA-10 |
|---|---|---|---|---|---|---|---|
| Undefined | Yellow | 1 | | | | | |
| Transition | Yellow | | 2 | 2 | | | |
| Sediments | Green | 3 | 3 | 3 | 3 | 3 | 3 |
| Top flows / crust | Red | 4 | 4 | 4 | | | |
| Breccia | Red | | 5 | 5 | | | |
| Massives / core | Blue | 6 | 6 | 6 | | | |
| Dolerites | Magenta | 7 | | | 7 | 7 | 7 |
| Hyaloclastites | Cyan | 8 | | | 8 | 8 | 8 |
| Tuff | Yellow | | | | 9 | 9 | 9 |
| Basalt undefined | Blue | | | | 5 | 5 | 5 |
| (no value) | Black | | | | | | |

**Assumed matrix (or grain) densities:**

Sediment, Faroes: 2.8 g/ccm,
Sediment, Iceland: 3.05 g/ccm (reworked tuffs and lavas),
Dolerite: 3.02 g/ccm,
Basalt: 3.05 g/ccm (irrespective of facies)

**Legend**

[1, 0.3, 0.1, 0.03, 0.01]: Predicted aspect ratios of the ellipsoidal inclusion model for K = 83.4 GPa, G = 40.1 GPa and the assumed values of matrix density (eq. 1).

MUHS: Modified upper Hashin-Shtrikman model (eqs 2, 4)
MLHS: Modified lower Hashin-Shtrikman model (eqs 3, 4)
median: mean of the upper and lower models (eqs 4, 5)

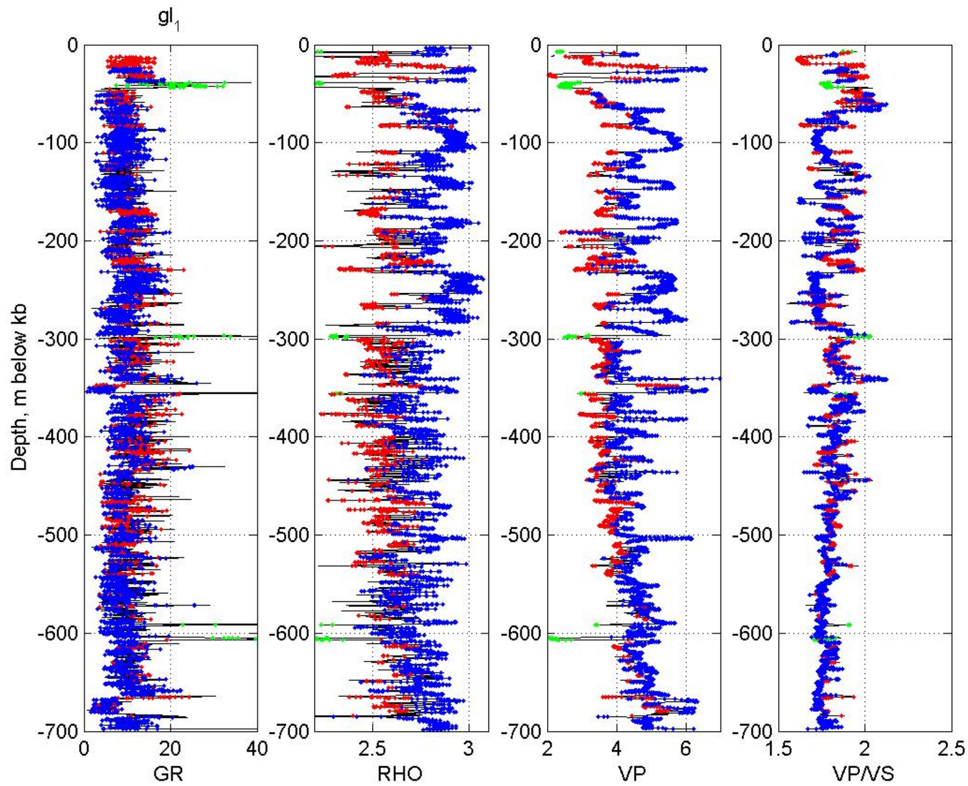
gl1
Depth, m below kb
GR
RHO
VP
VP/VS

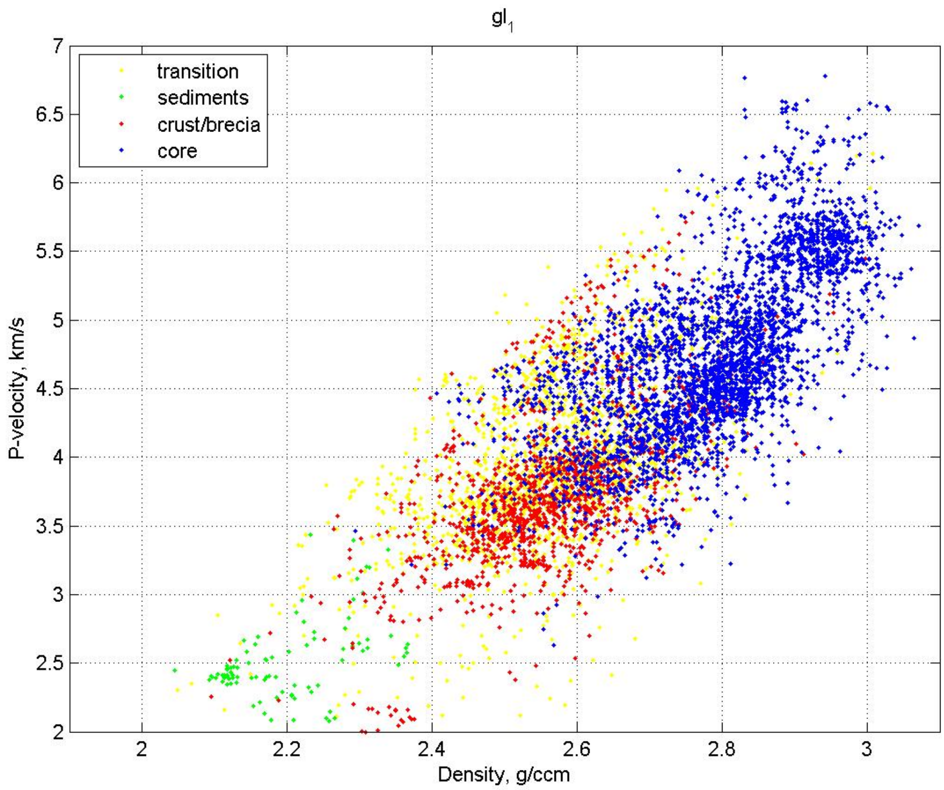
gl1
transition
sediments
crust/brecia
core
P-velocity, km/s
Density, g/ccm

GL-1

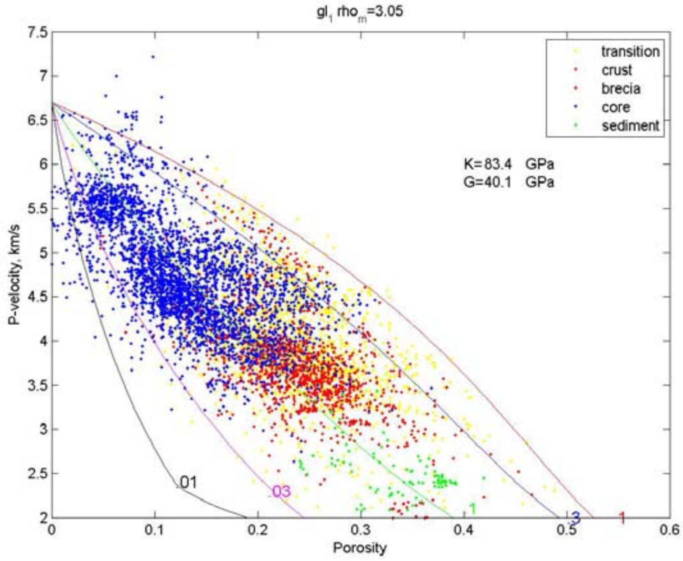
gl1 rhom=3.05
transition
crust
brecia
core
sediment
K=83.4 GPa
G=40.1 GPa
P-velocity, km/s
Porosity
.01
.03
.1
.3
1

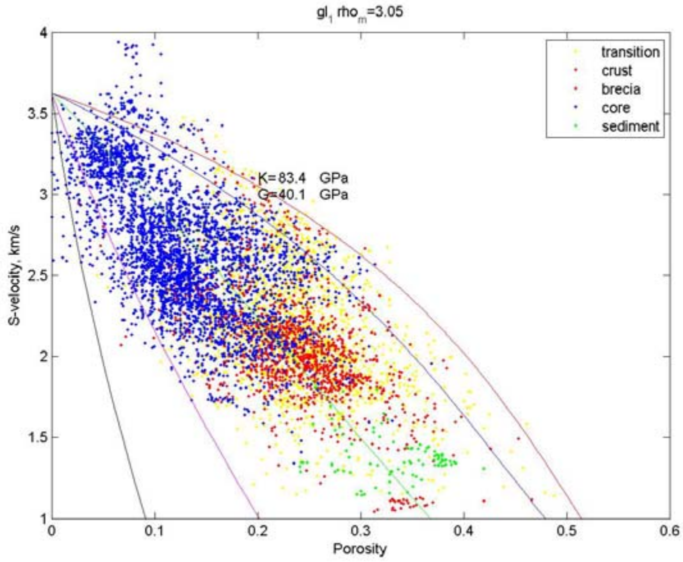
gl1 rhom=3.05
transition
crust
brecia
core
sediment
K=83.4 GPa
G=40.1 GPa
S-velocity, km/s
Porosity

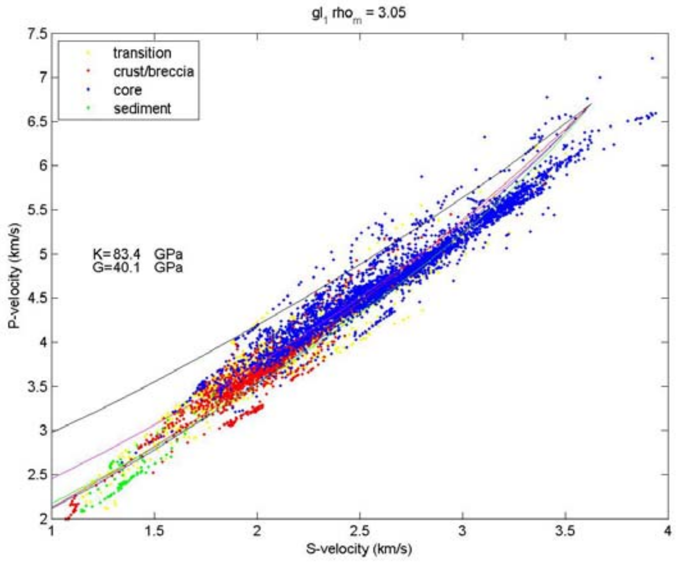
gl1 rhom = 3.05
transition
crust/breccia
core
sediment
K=83.4 GPa
G=40.1 GPa
P-velocity (km/s)
S-velocity (km/s)

GL-1

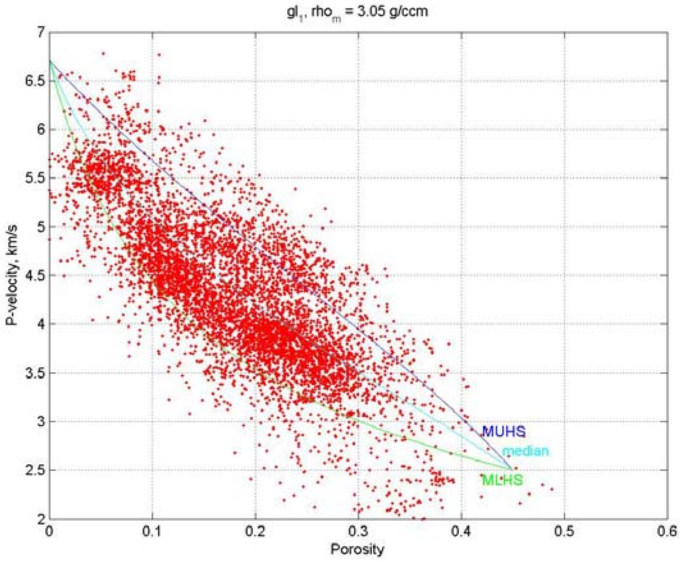
gl1, rhom = 3.05 g/ccm
P-velocity, km/s
Porosity
MUHS
median
MLHS

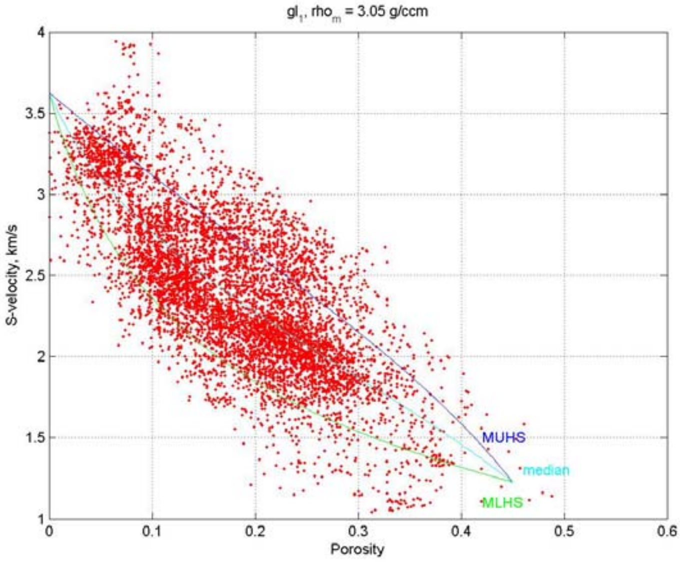
gl1, rhom = 3.05 g/ccm
S-velocity, km/s
Porosity
MUHS
median
MLHS

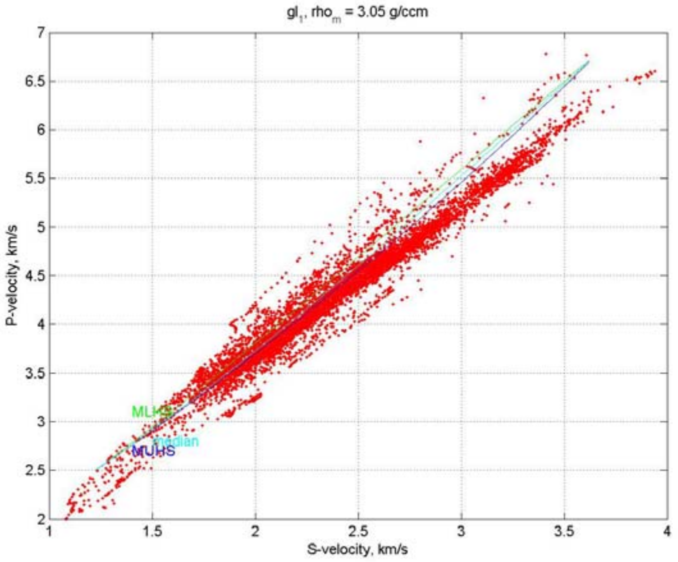
gl1, rhom = 3.05 g/ccm
P-velocity, km/s
S-velocity, km/s
MLHS
median
MUHS

GL-1

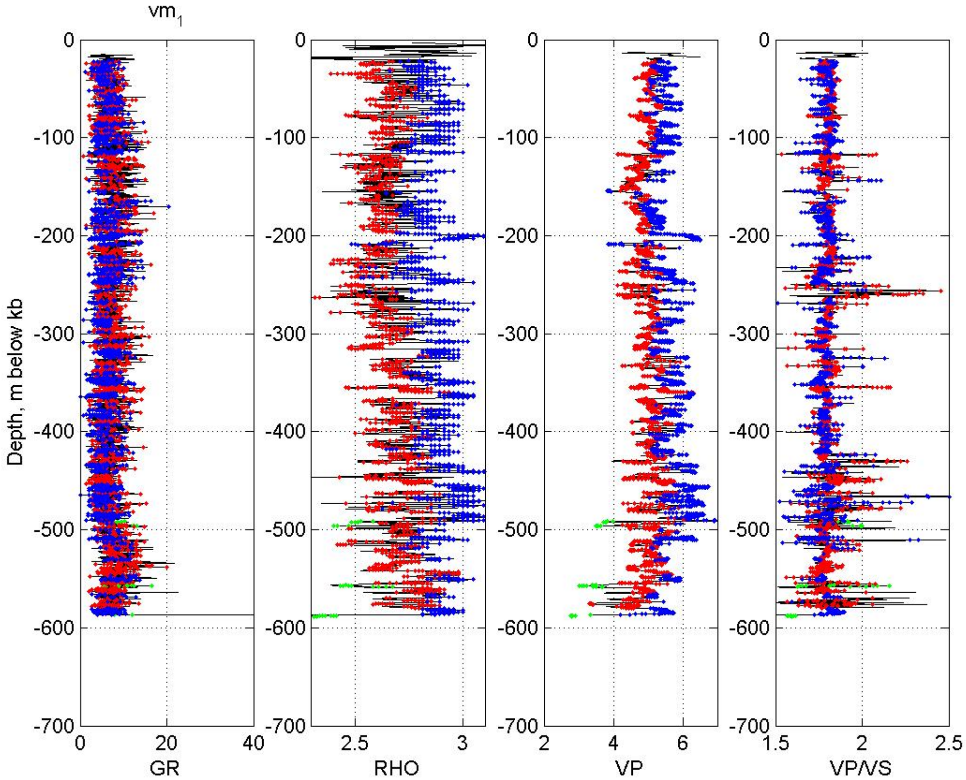
vm1
Depth, m below kb
GR
RHO
VP
VP/VS

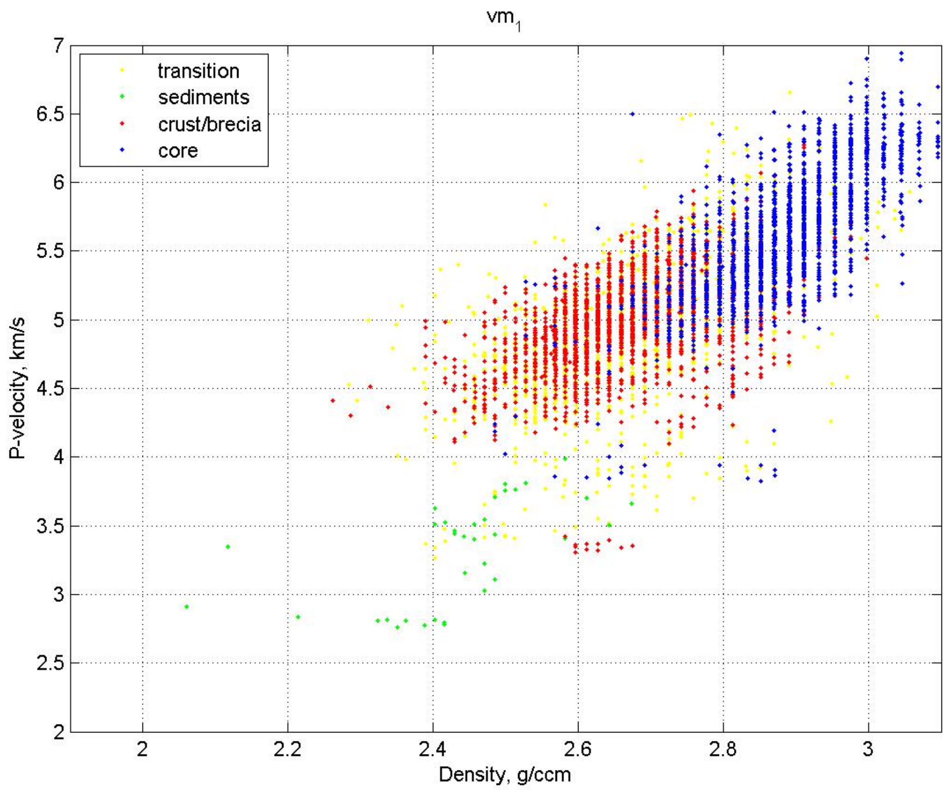
vm1
transition
sediments
crust/brecia
core
P-velocity, km/s
Density, g/ccm

VM-1

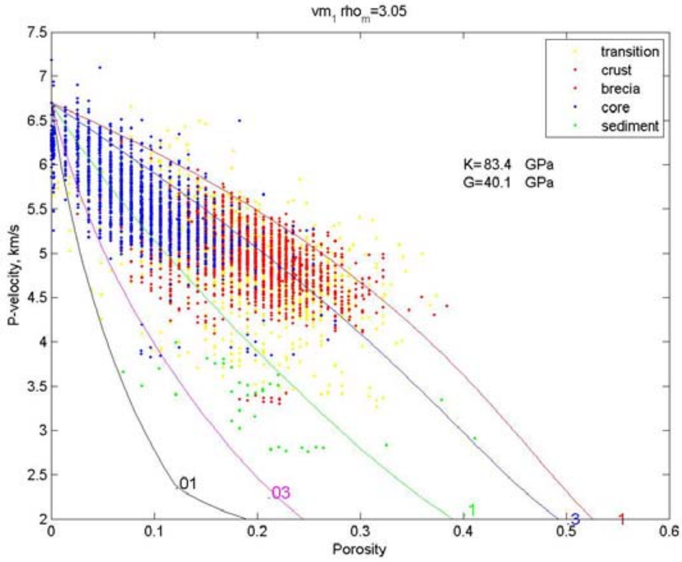
vm$_1$ rho$_m$=3.05
transition
crust
brecia
core
sediment
K=83.4 GPa
G=40.1 GPa
P-velocity, km/s
Porosity
.01
.03
.1
.3
1

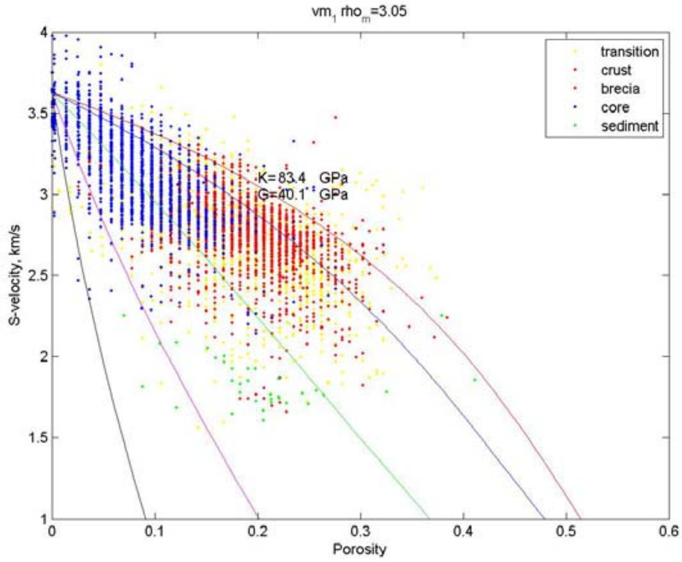
vm$_1$ rho$_m$=3.05
transition
crust
brecia
core
sediment
K=83.4 GPa
G=40.1 GPa
S-velocity, km/s
Porosity

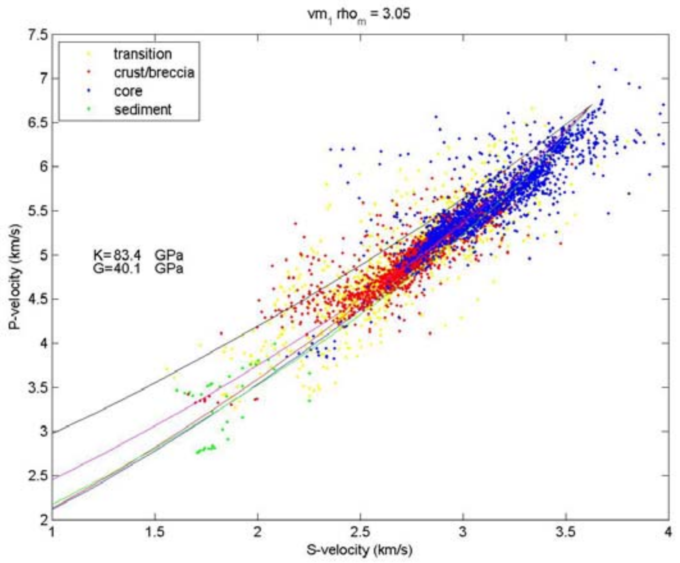
vm$_1$ rho$_m$ = 3.05
transition
crust/breccia
core
sediment
K=83.4 GPa
G=40.1 GPa
P-velocity (km/s)
S-velocity (km/s)

VM-1

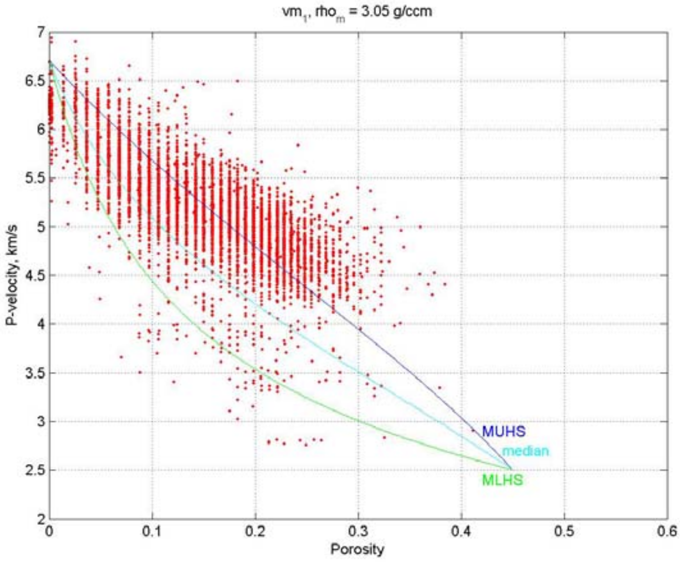
vm$_1$, rho$_m$ = 3.05 g/ccm
P-velocity, km/s
Porosity
MUHS
median
MLHS

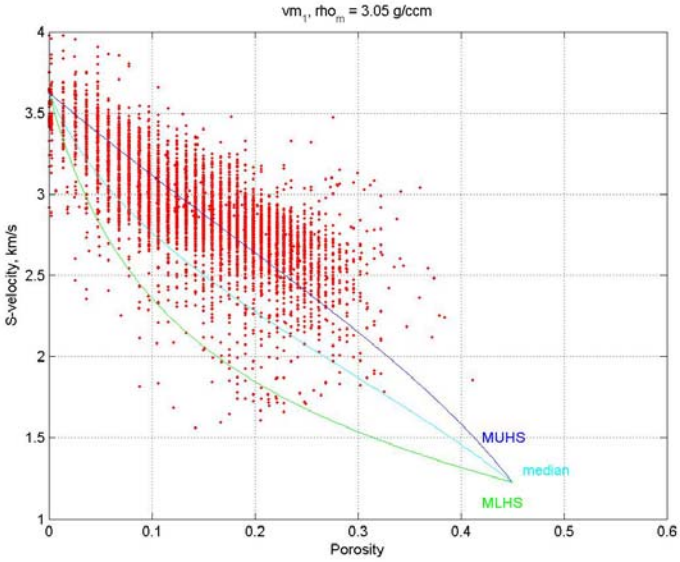
vm$_1$, rho$_m$ = 3.05 g/ccm
S-velocity, km/s
Porosity
MUHS
median
MLHS

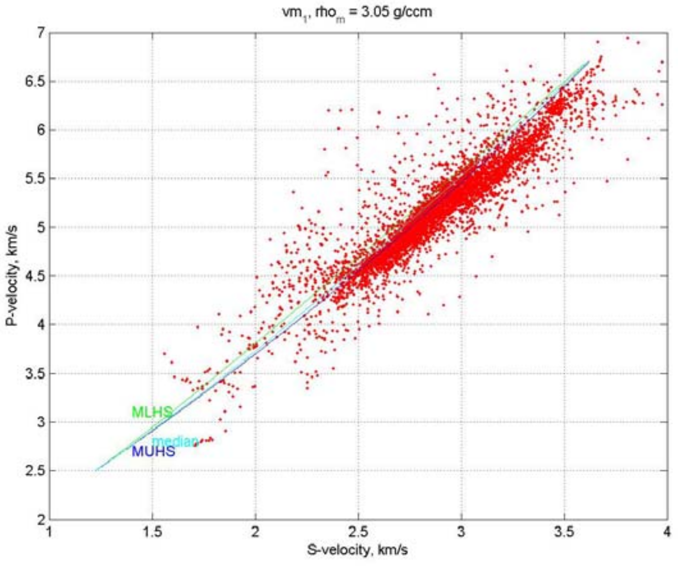
vm$_1$, rho$_m$ = 3.05 g/ccm
P-velocity, km/s
S-velocity, km/s
MLHS
median
MUHS

VM-1

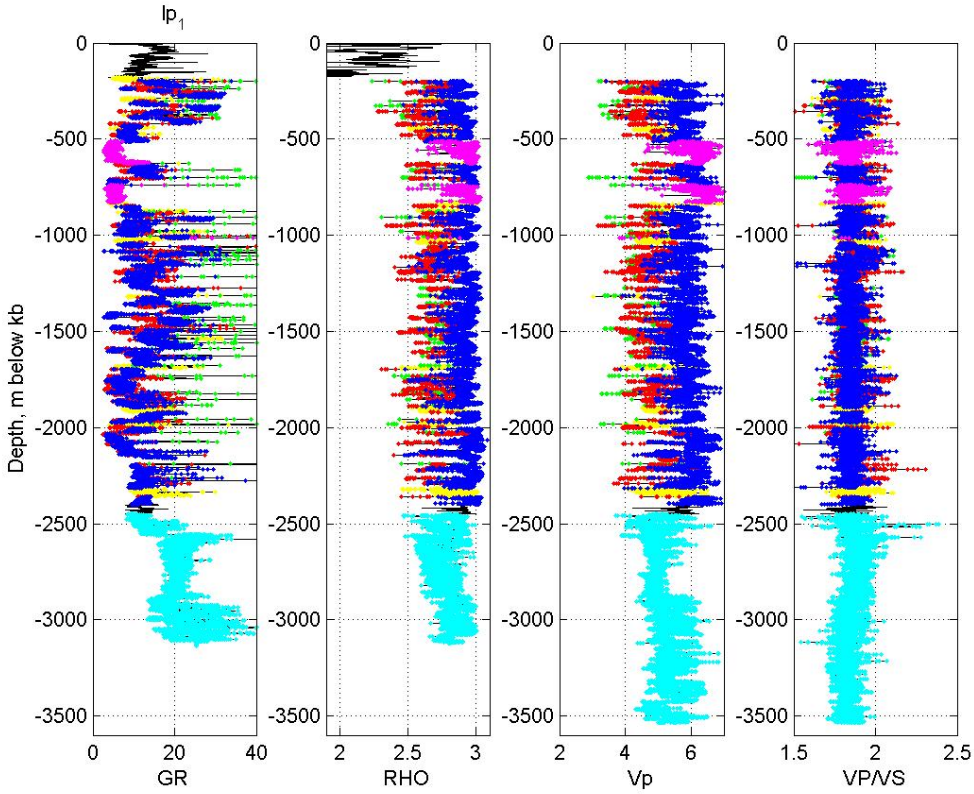
lp1
Depth, m below kb
GR
RHO
Vp
VP/VS

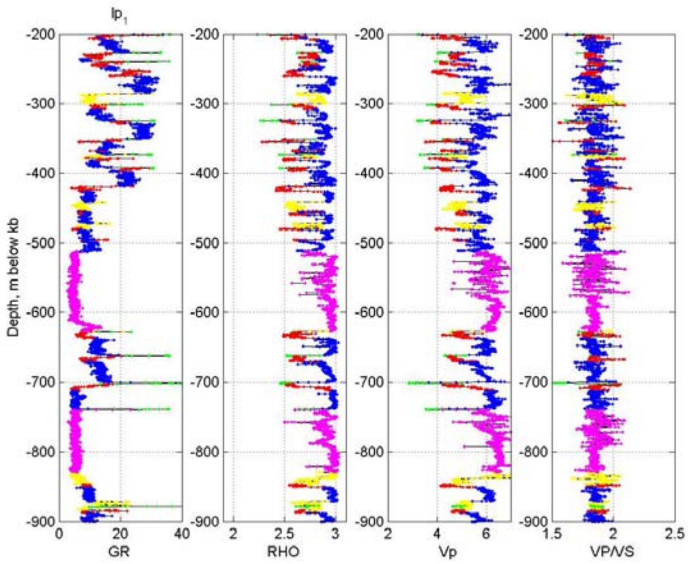
lp1
Depth, m below kb
GR
RHO
Vp
VP/VS

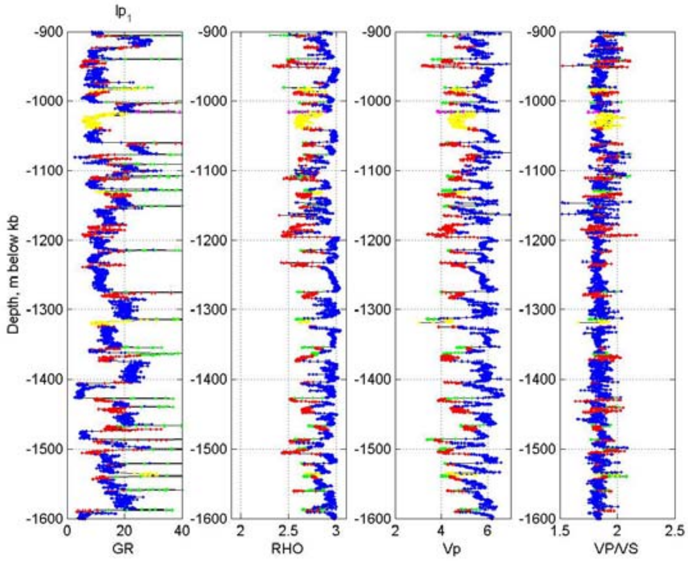
Ip1
Depth, m below kb
GR
RHO
Vp
VP/VS

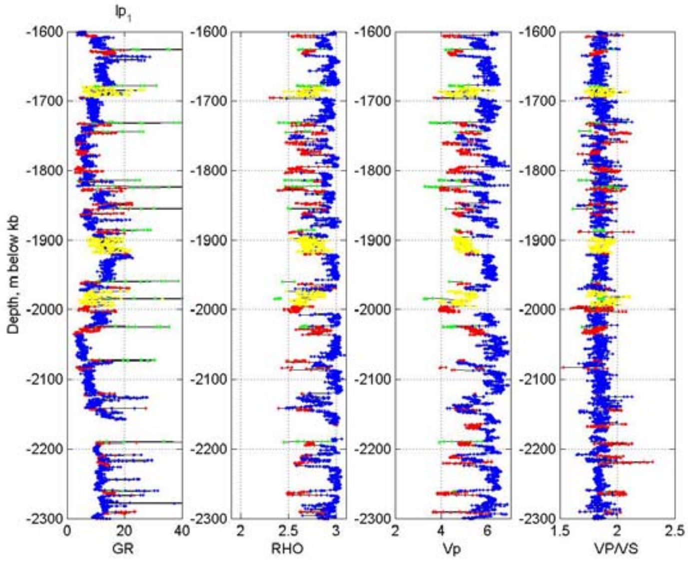
Ip1
Depth, m below kb
GR
RHO
Vp
VP/VS

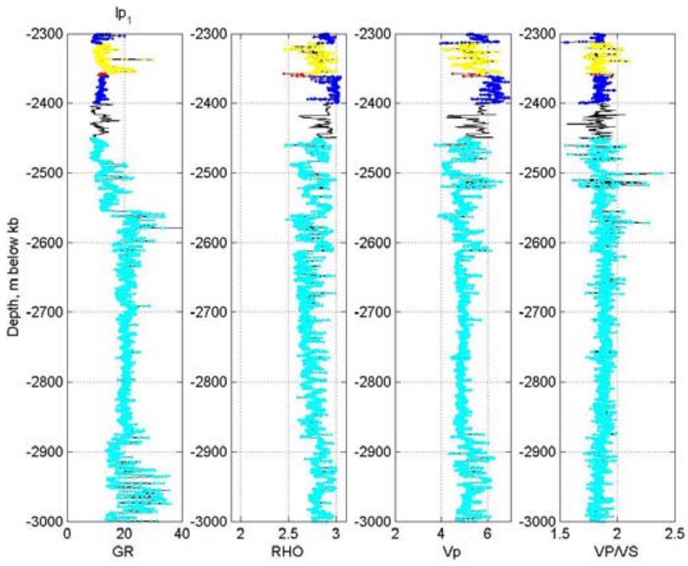
Ip1
Depth, m below kb
GR
RHO
Vp
VP/VS

LP-1

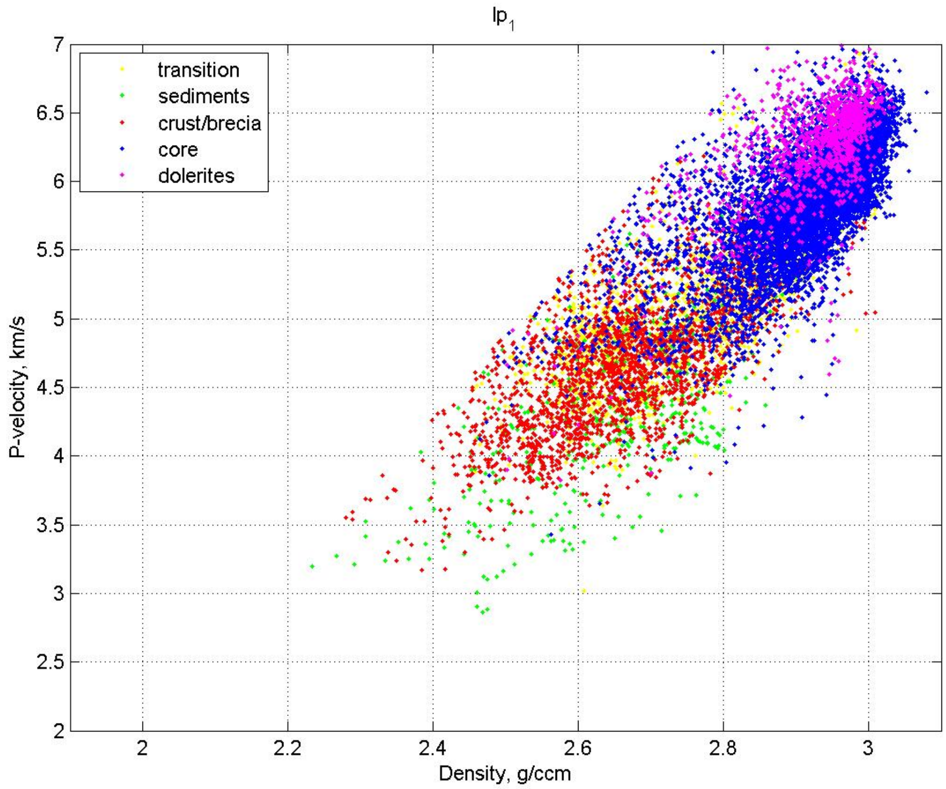
lp1
transition
sediments
crust/brecia
core
dolerites
P-velocity, km/s
Density, g/ccm
7
6.5
6
5.5
5
4.5
4
3.5
3
2.5
2
2.2
2.4
2.6
2.8


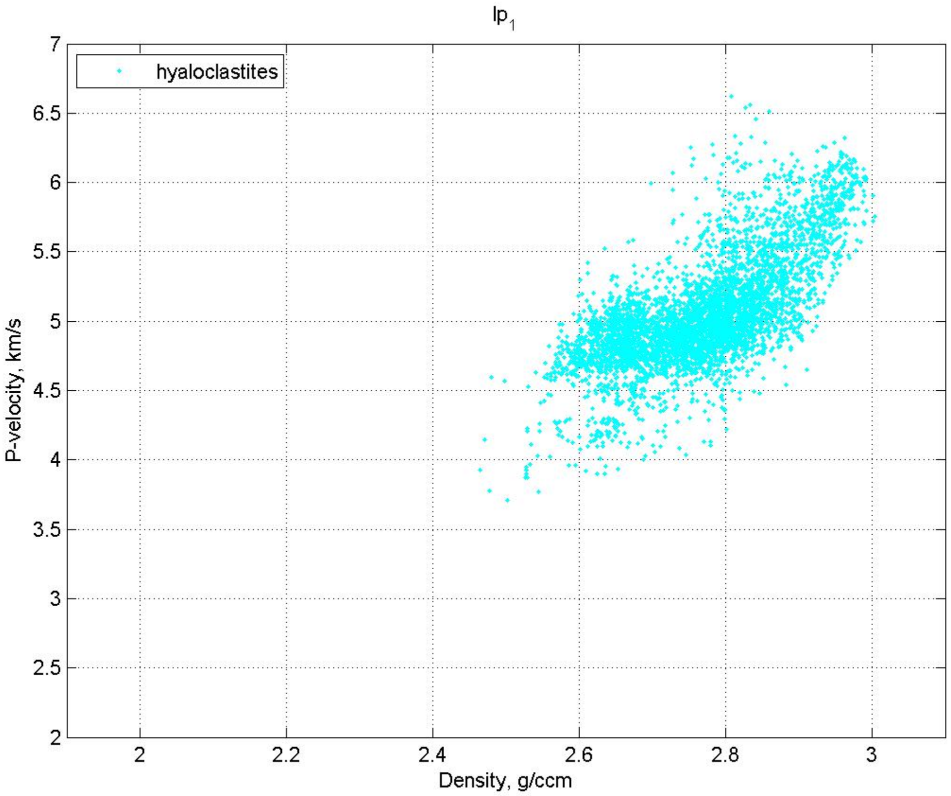
lp1
hyaloclastites
P-velocity, km/s
Density, g/ccm
7
6.5
6
5.5
5
4.5
4
3.5
3
2.5
2
2.2
2.4
2.6
2.8


LP-1

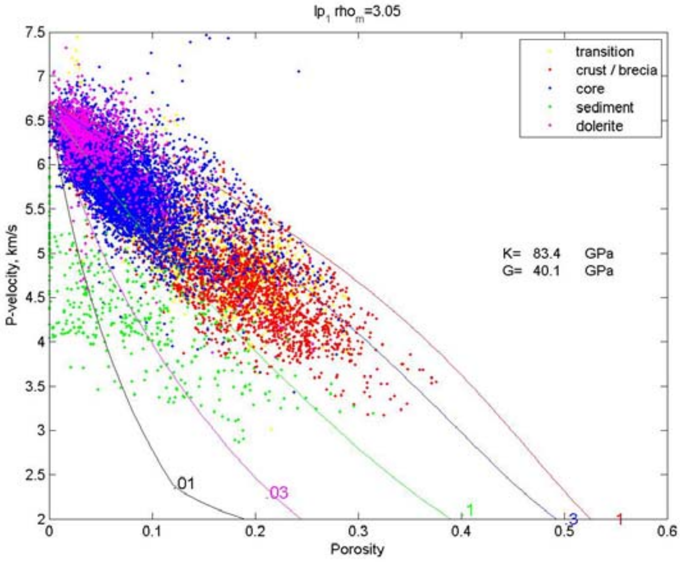
lp1 rhom=3.05
transition
crust / brecia
core
sediment
dolerite
K= 83.4 GPa
G= 40.1 GPa
P-velocity, km/s
Porosity
.01
.03
.1
.3
1

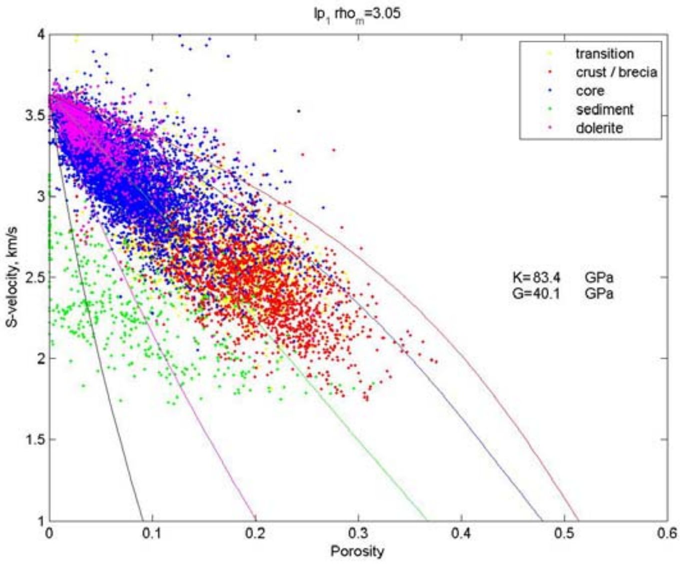
lp1 rhom=3.05
transition
crust / brecia
core
sediment
dolerite
K=83.4 GPa
G=40.1 GPa
S-velocity, km/s
Porosity

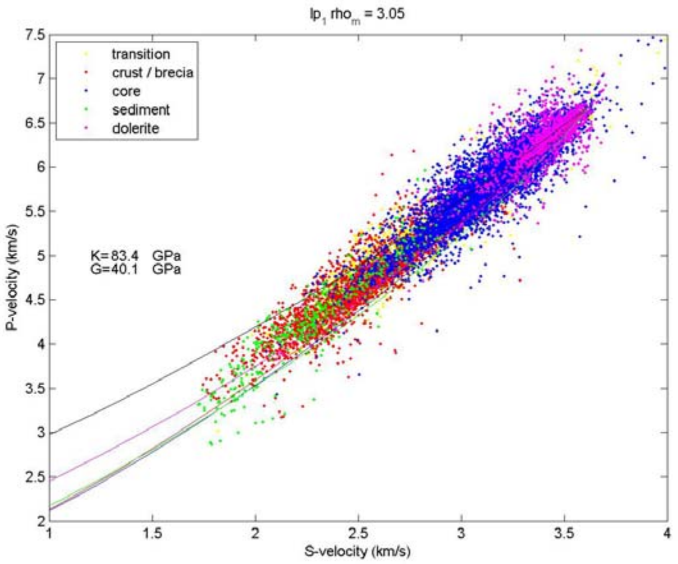
lp1 rhom = 3.05
transition
crust / brecia
core
sediment
dolerite
K=83.4 GPa
G=40.1 GPa
P-velocity (km/s)
S-velocity (km/s)

LP-1

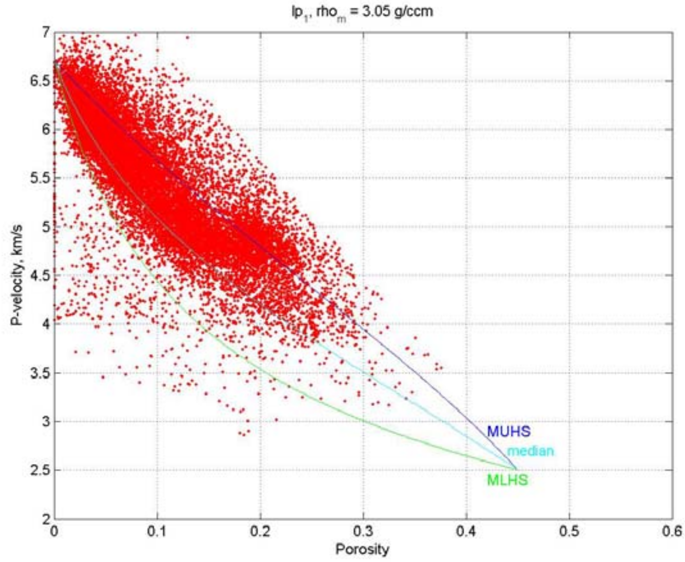

$lp_1$, $rho_m$ = 3.05 g/ccm
P-velocity, km/s
Porosity
MUHS
median
MLHS


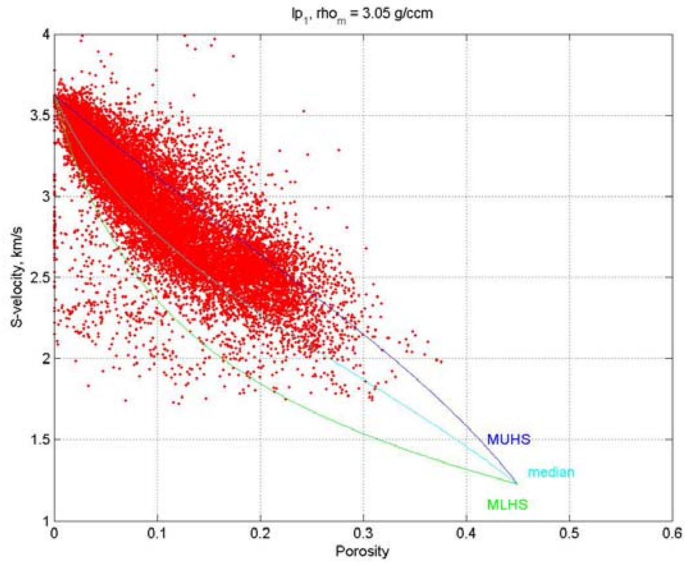

$lp_1$, $rho_m$ = 3.05 g/ccm
S-velocity, km/s
Porosity
MUHS
median
MLHS


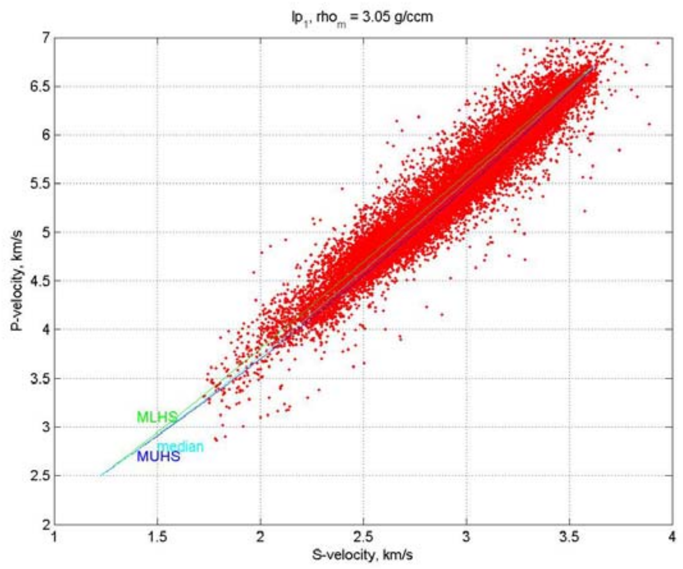

$lp_1$, $rho_m$ = 3.05 g/ccm
P-velocity, km/s
S-velocity, km/s
MLHS
median
MUHS


LP-1

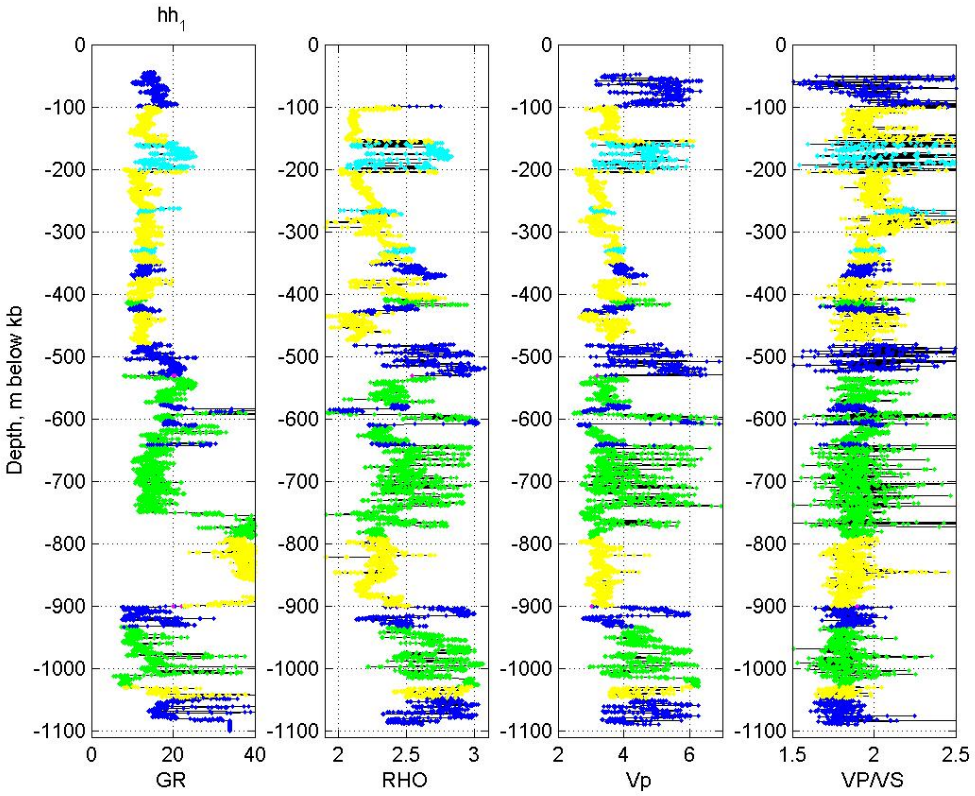
hh1
Depth, m below kb
GR
RHO
Vp
VP/VS

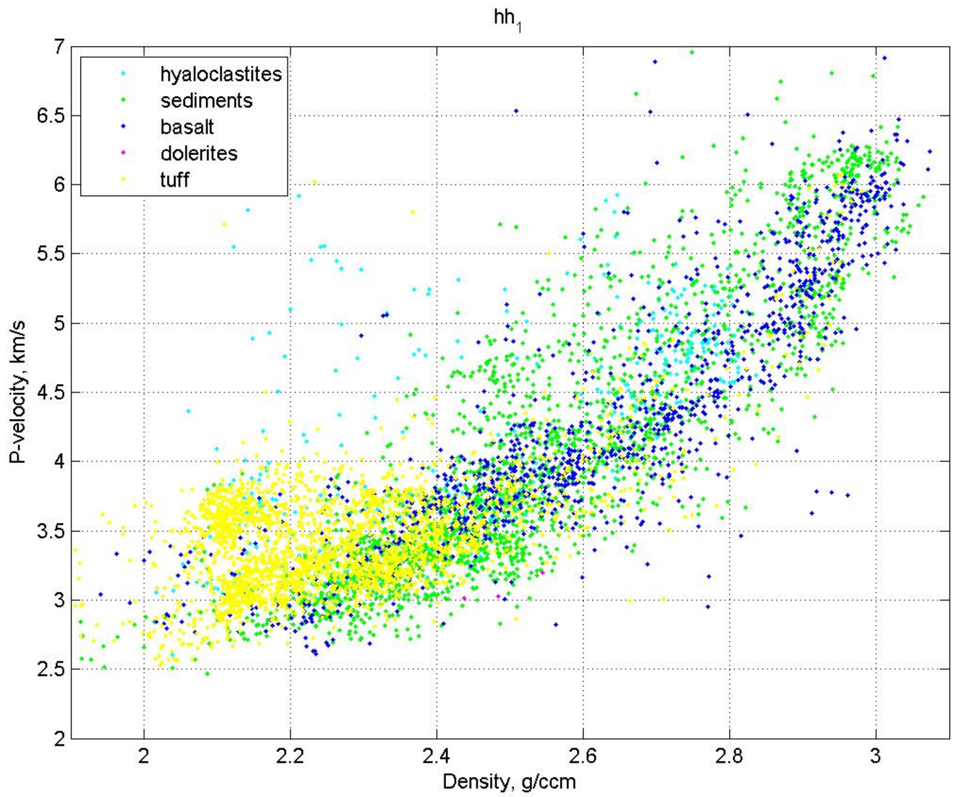
hh1
hyaloclastites
sediments
basalt
dolerites
tuff
P-velocity, km/s
Density, g/ccm

HH-1

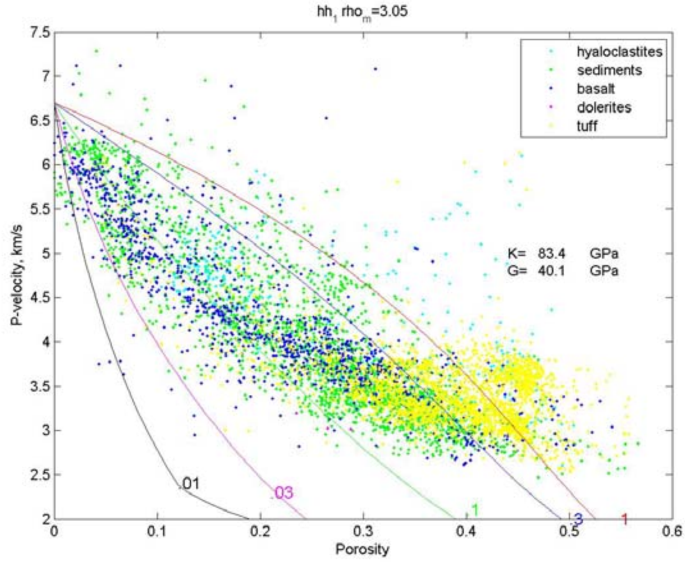
hh1 rhom=3.05
hyaloclastites
sediments
basalt
dolerites
tuff
K= 83.4 GPa
G= 40.1 GPa
P-velocity, km/s
Porosity
.01
.03
.1
.3
1

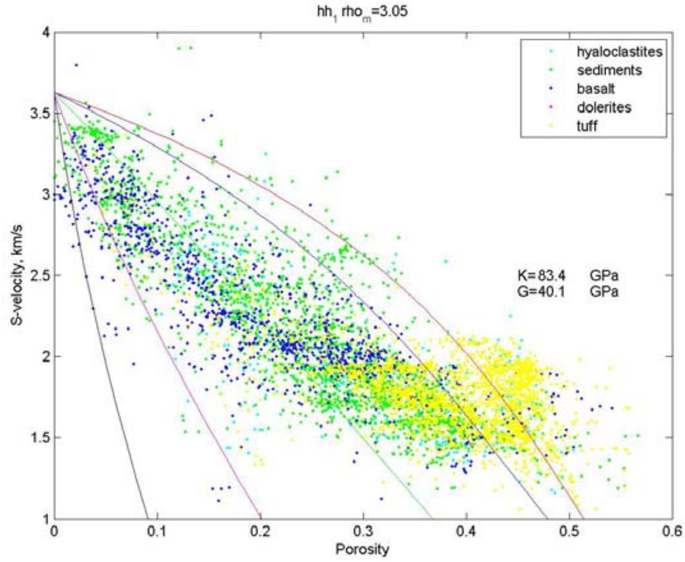
hh1 rhom=3.05
hyaloclastites
sediments
basalt
dolerites
tuff
K=83.4 GPa
G=40.1 GPa
S-velocity, km/s
Porosity

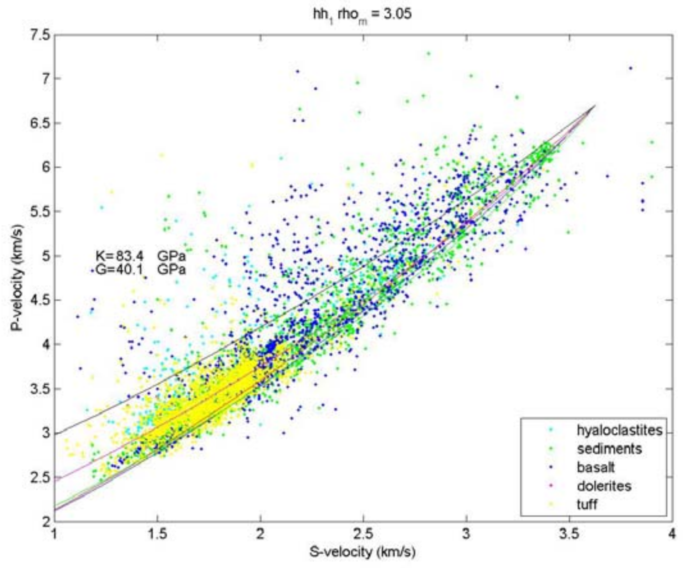
hh1 rhom = 3.05
K=83.4 GPa
G=40.1 GPa
hyaloclastites
sediments
basalt
dolerites
tuff
P-velocity (km/s)
S-velocity (km/s)

HH-1

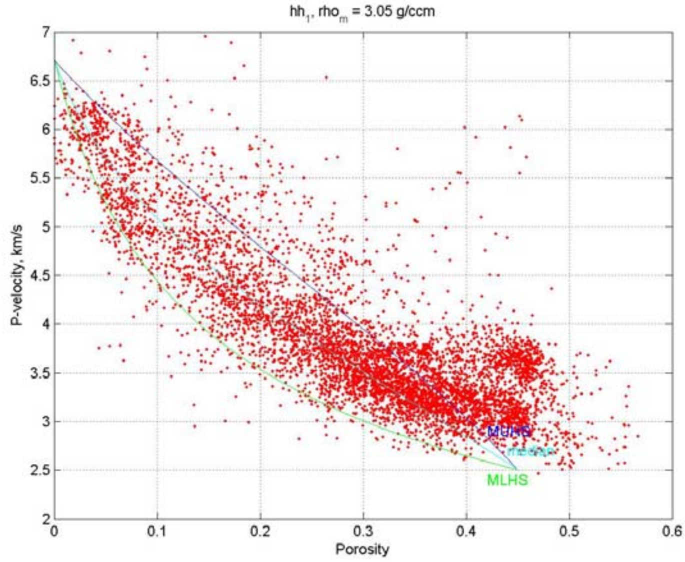
hh1, rhom = 3.05 g/ccm
P-velocity, km/s
Porosity
MUHS
median
MLHS

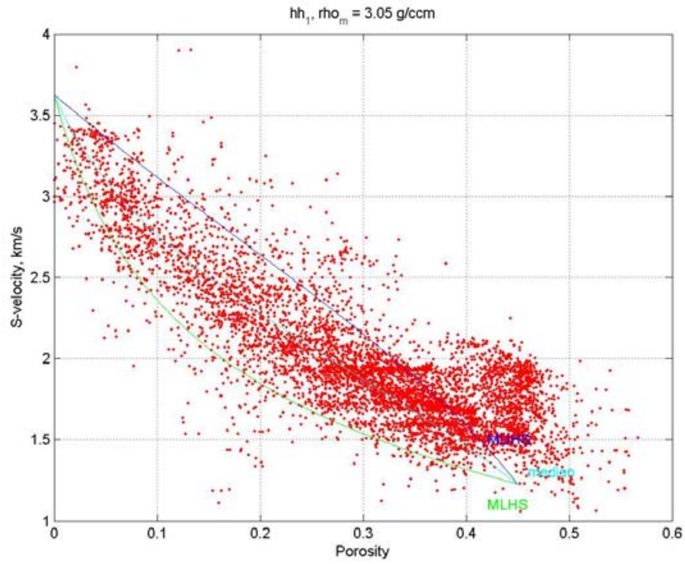
hh1, rhom = 3.05 g/ccm
S-velocity, km/s
Porosity
MUHS
median
MLHS

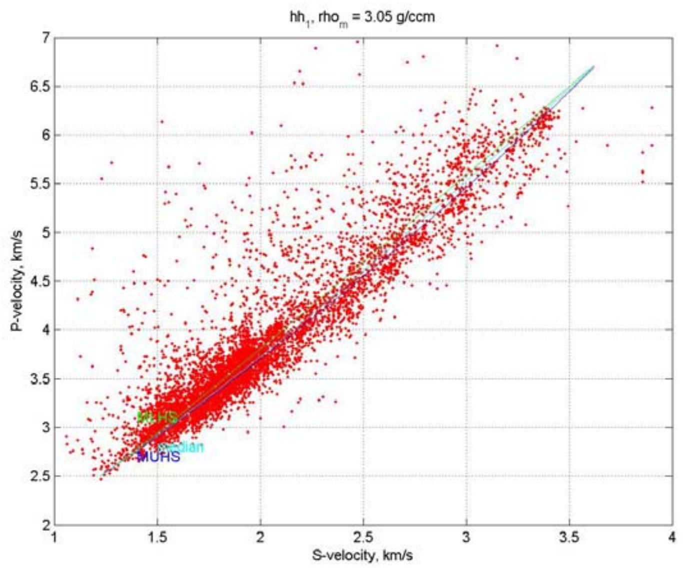
hh1, rhom = 3.05 g/ccm
P-velocity, km/s
S-velocity, km/s
MLHS
median
MUHS

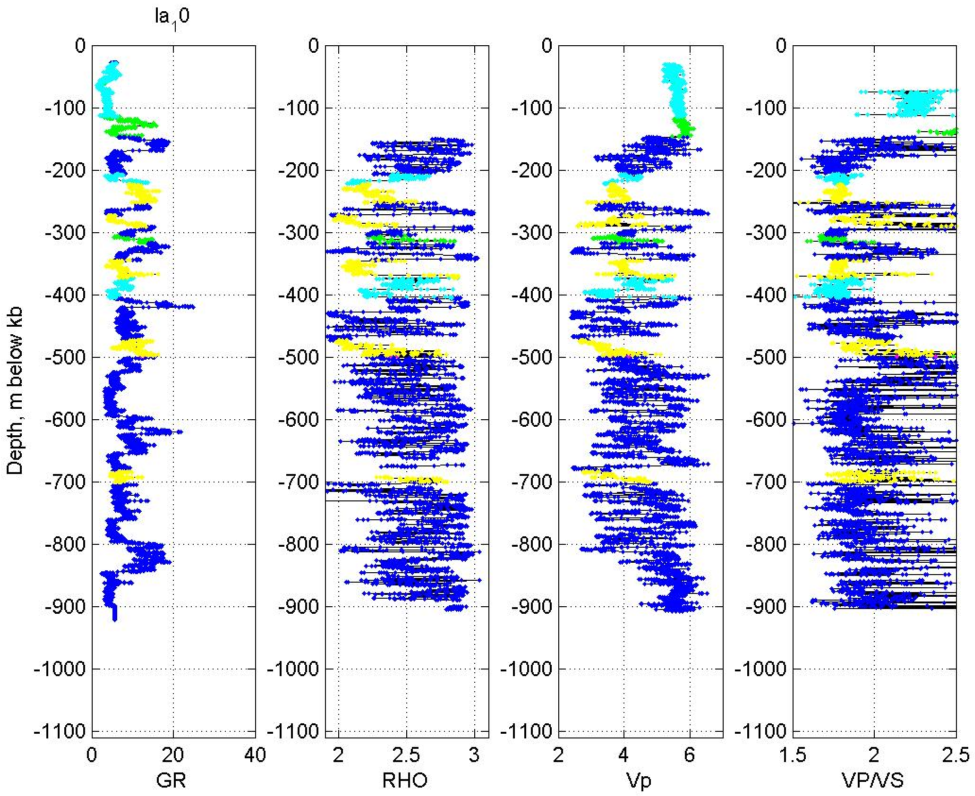

la10
Depth, m below kb
0
-100
-200
-300
-400
-500
-600
-700
-800
-900
-1000
-1100
GR
RHO
Vp
VP/VS


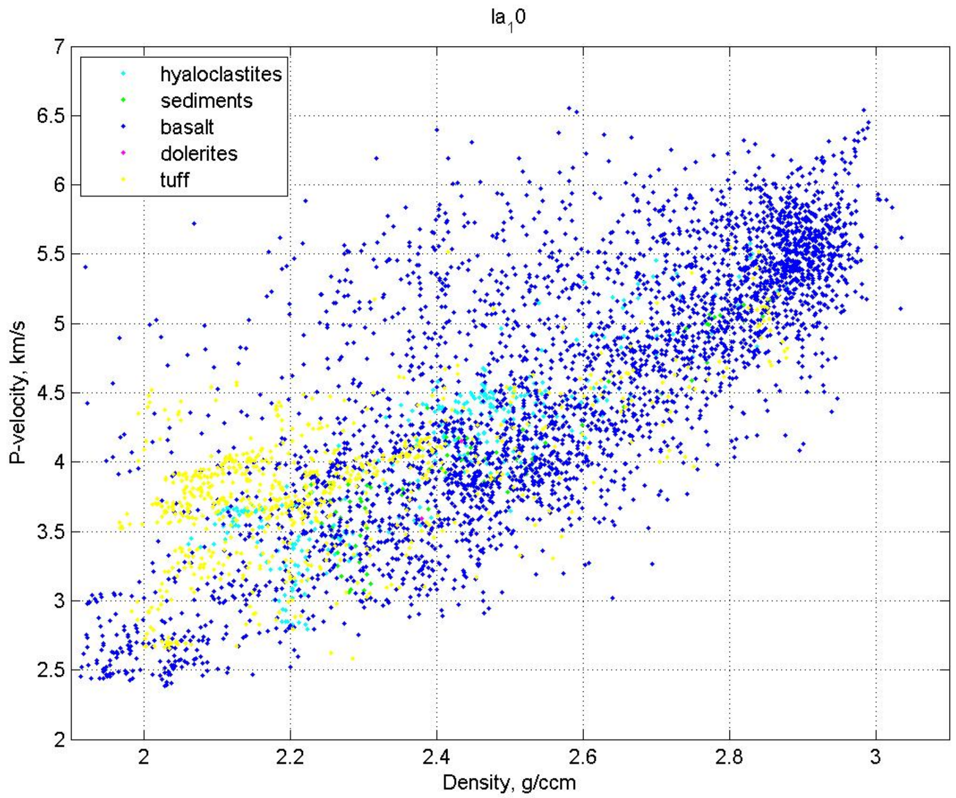

la10
hyaloclastites
sediments
basalt
dolerites
tuff
P-velocity, km/s
Density, g/ccm


LA-10

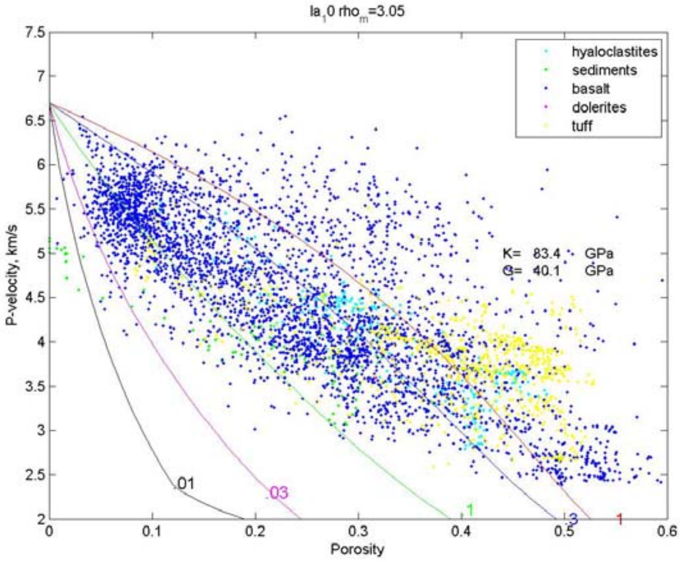
la$_1$0 rho$_m$=3.05
P-velocity, km/s
Porosity
hyaloclastites
sediments
basalt
dolerites
tuff
K= 83.4 GPa
G= 40.1 GPa

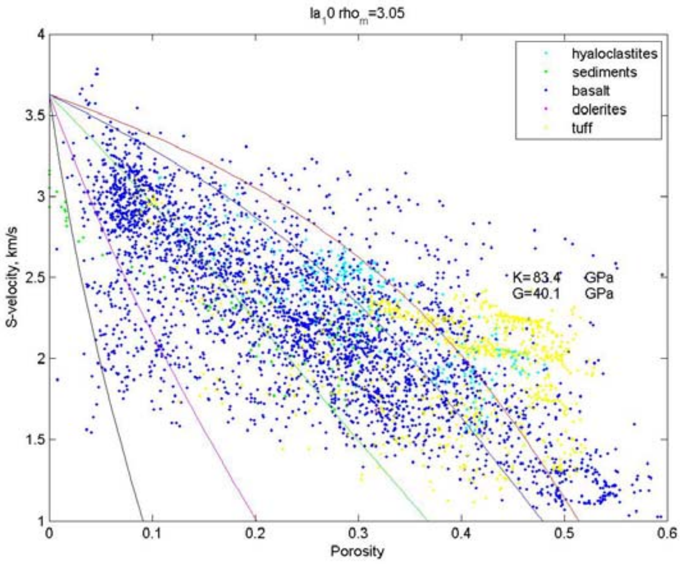
la$_1$0 rho$_m$=3.05
S-velocity, km/s
Porosity
hyaloclastites
sediments
basalt
dolerites
tuff
K=83.4 GPa
G=40.1 GPa

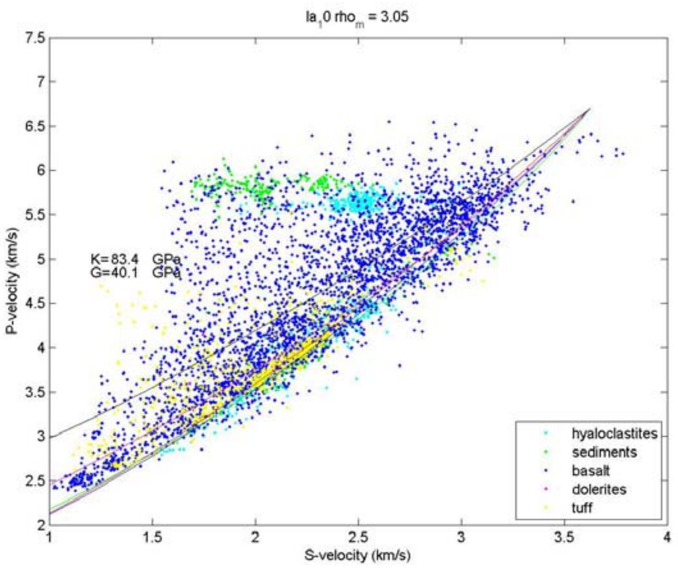
la$_1$0 rho$_m$ = 3.05
P-velocity (km/s)
S-velocity (km/s)
K=83.4 GPa
G=40.1 GPa
hyaloclastites
sediments
basalt
dolerites
tuff

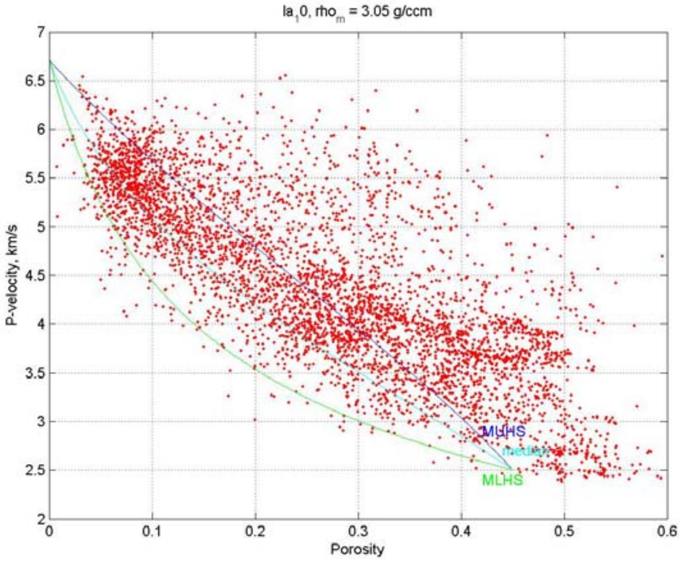
la10, rho_m = 3.05 g/ccm
P-velocity, km/s
Porosity
MUHS
median
MLHS

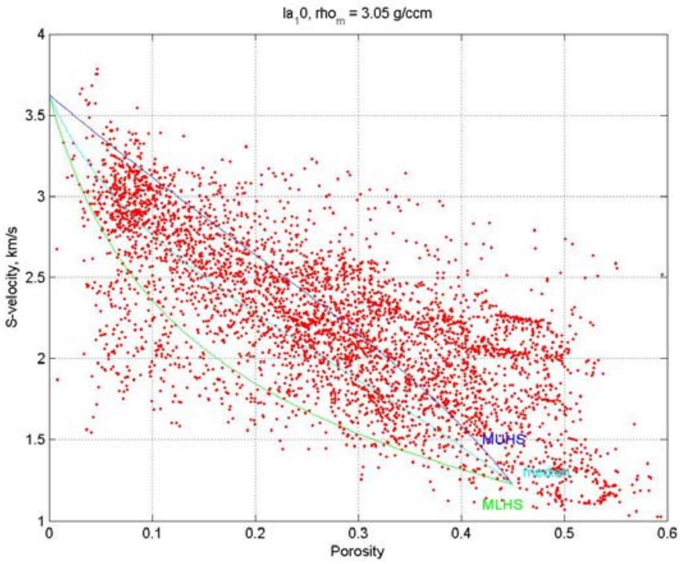
la10, rho_m = 3.05 g/ccm
S-velocity, km/s
Porosity
MUHS
median
MLHS

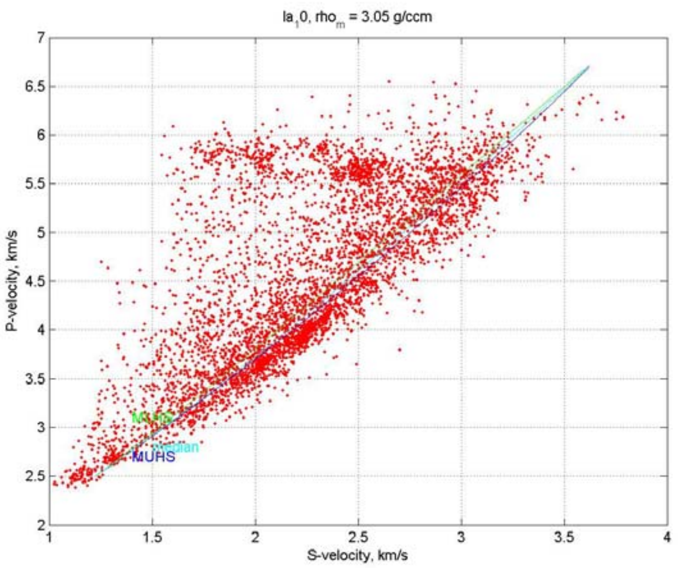
la10, rho_m = 3.05 g/ccm
P-velocity, km/s
S-velocity, km/s
MLHS
median
MUHS

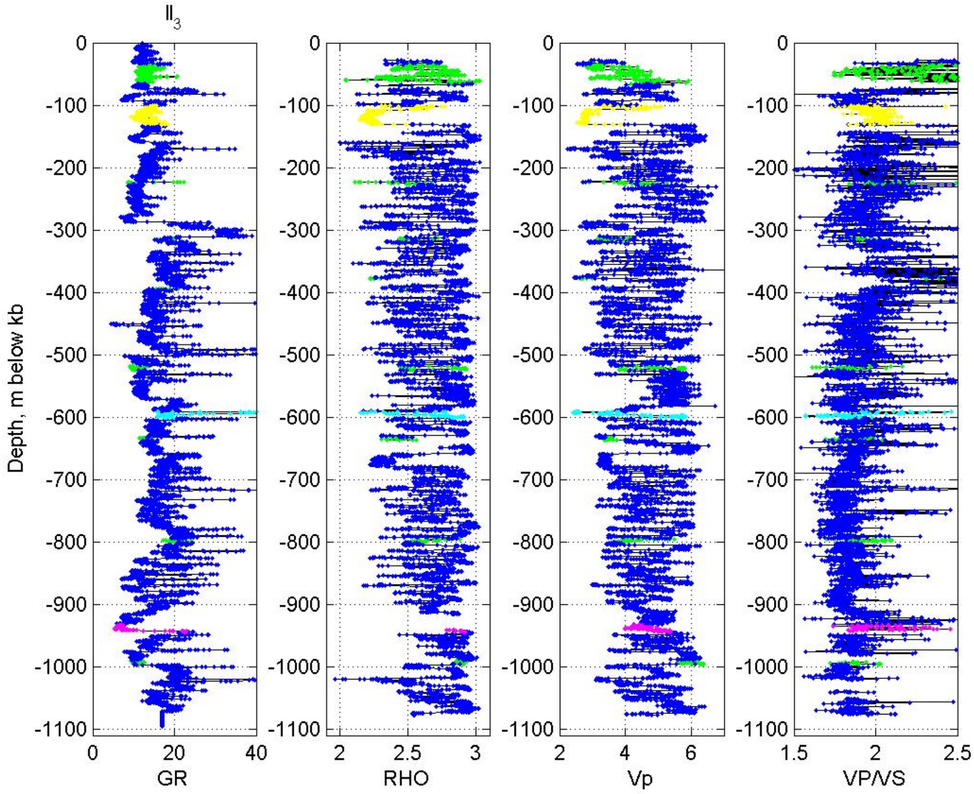

ll3
Depth, m below kb
GR
RHO
Vp
VP/VS


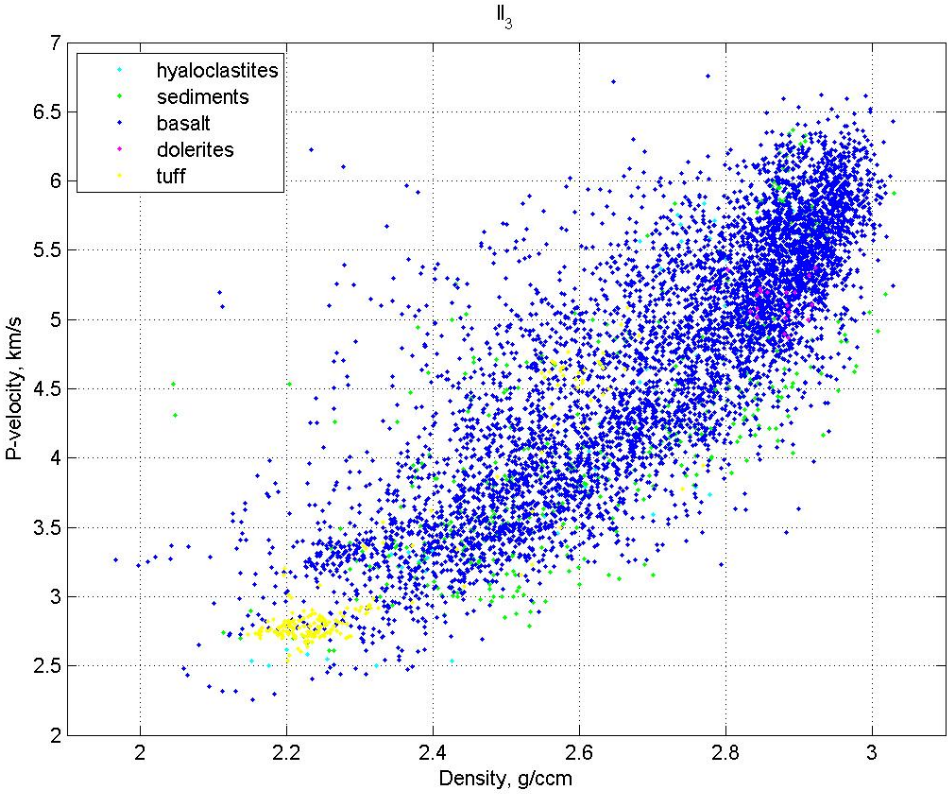

ll3
hyaloclastites
sediments
basalt
dolerites
tuff
P-velocity, km/s
Density, g/ccm


LL-3

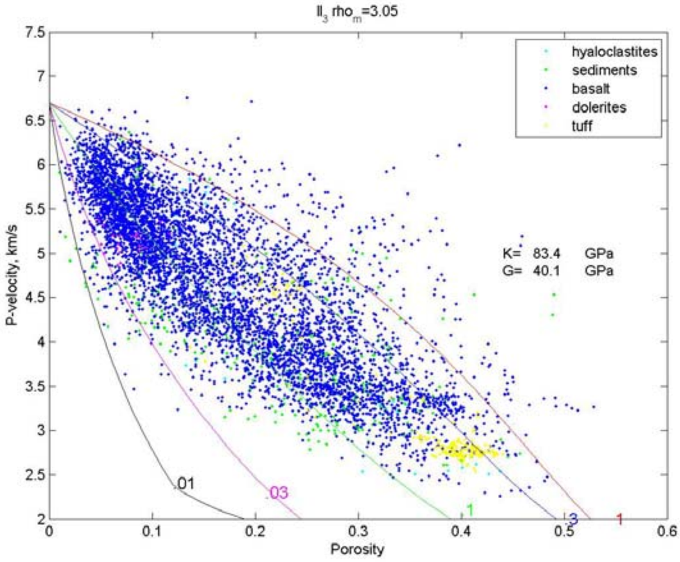
ll$_3$ rho$_m$=3.05
hyaloclastites
sediments
basalt
dolerites
tuff
K= 83.4 GPa
G= 40.1 GPa
P-velocity, km/s
Porosity
.01
.03
.1
.3
1

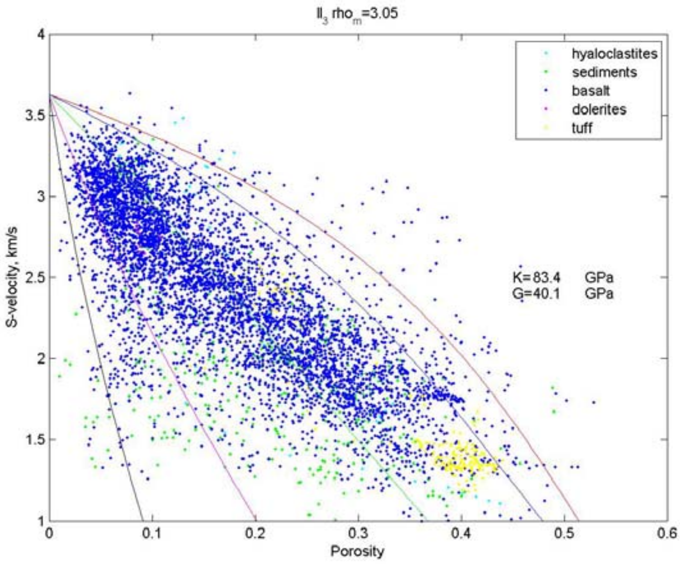
ll$_3$ rho$_m$=3.05
hyaloclastites
sediments
basalt
dolerites
tuff
K=83.4 GPa
G=40.1 GPa
S-velocity, km/s
Porosity

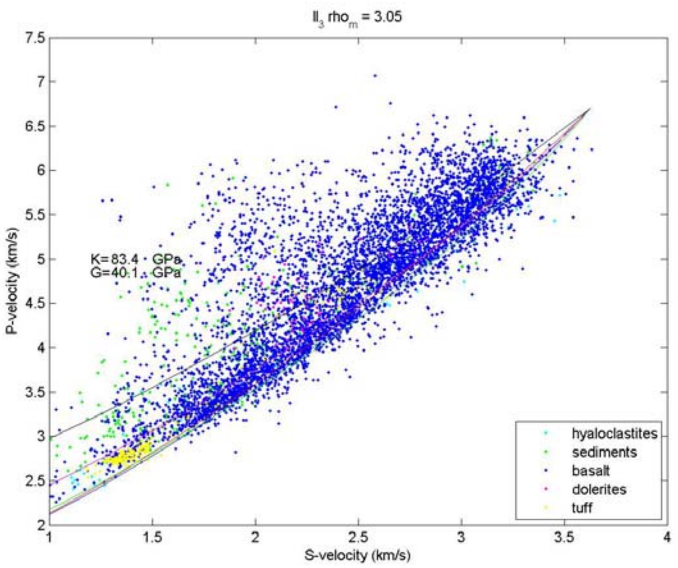
ll$_3$ rho$_m$ = 3.05
K=83.4 GPa
G=40.1 GPa
hyaloclastites
sediments
basalt
dolerites
tuff
P-velocity (km/s)
S-velocity (km/s)

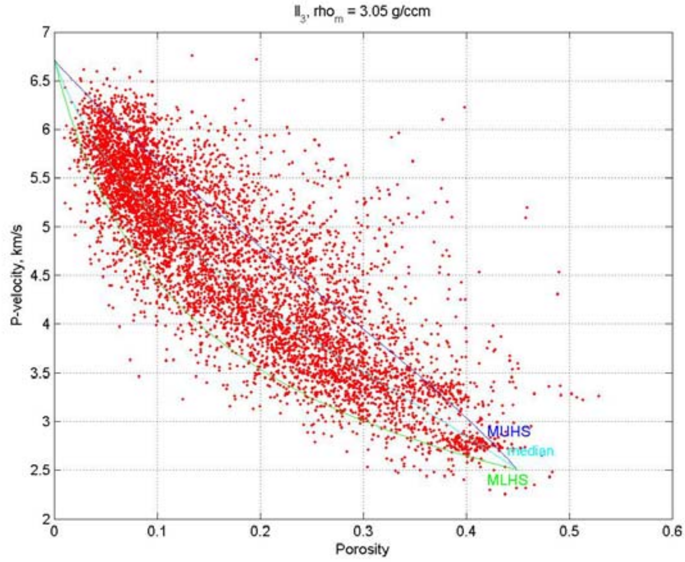
II$_3$, rho$_m$ = 3.05 g/ccm
P-velocity, km/s
Porosity
MUHS
median
MLHS

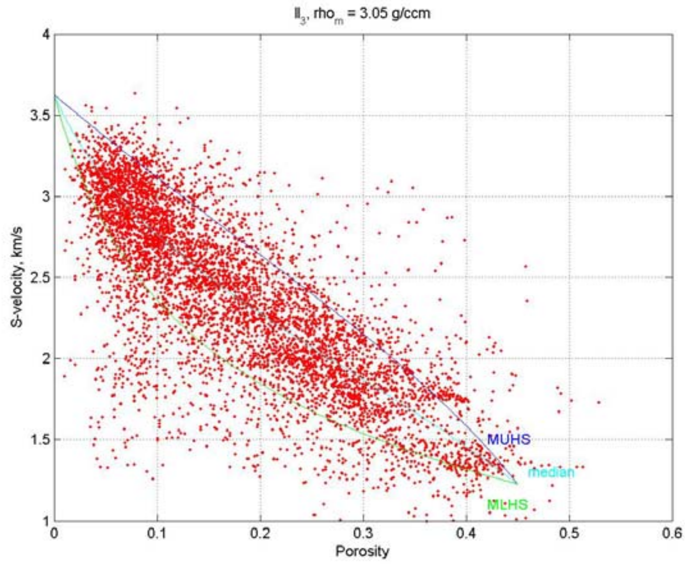
II$_3$, rho$_m$ = 3.05 g/ccm
S-velocity, km/s
Porosity
MUHS
median
MLHS

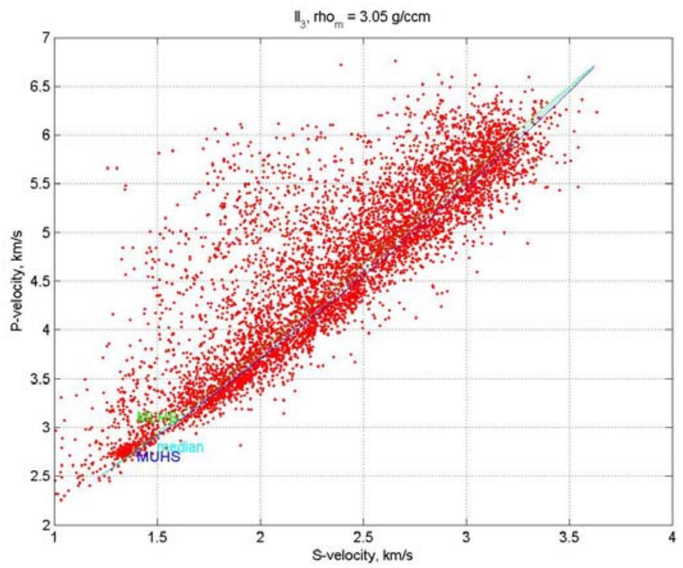
II$_3$, rho$_m$ = 3.05 g/ccm
P-velocity, km/s
S-velocity, km/s
median
MUHS

LL-3

# Appendix B. Stratigraphy of Icelandic wells

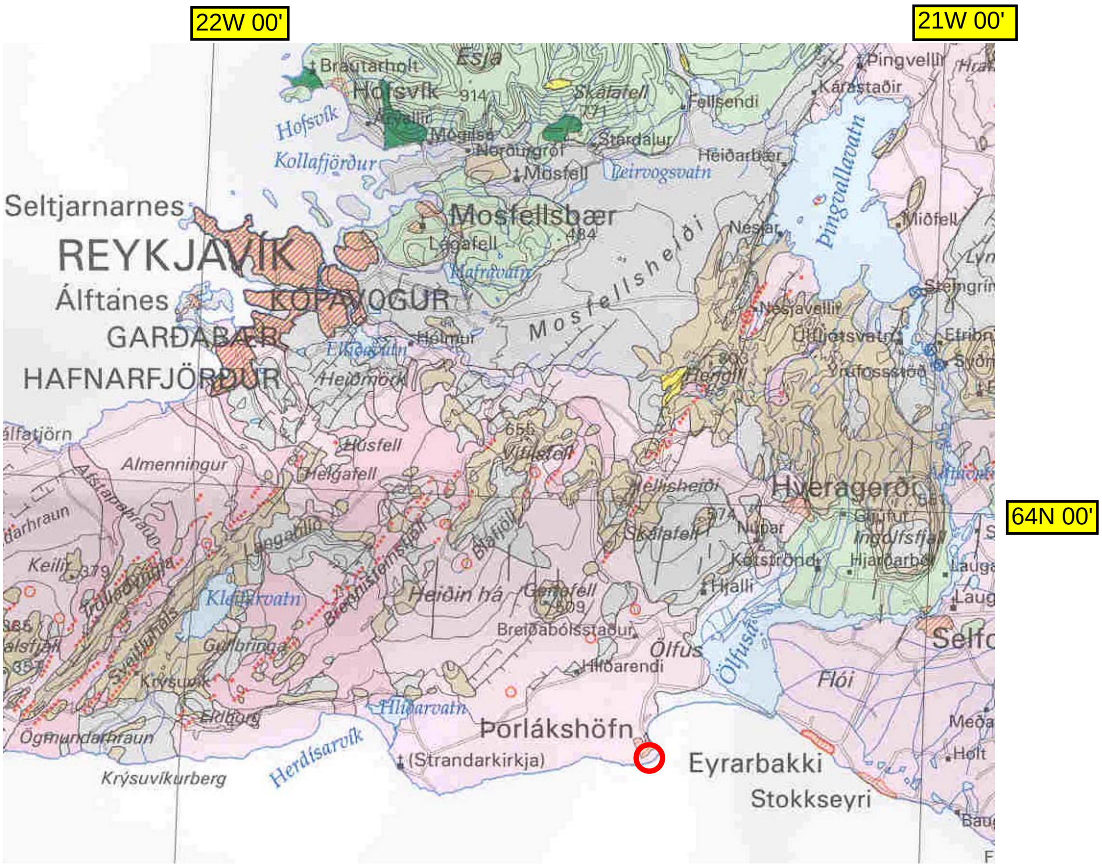


Location of the LA-10 well in Thorlákshöfn (red circle). 1:1 detail of the Geological Map of Iceland (Jóhanneson & Saemundsson 1998).

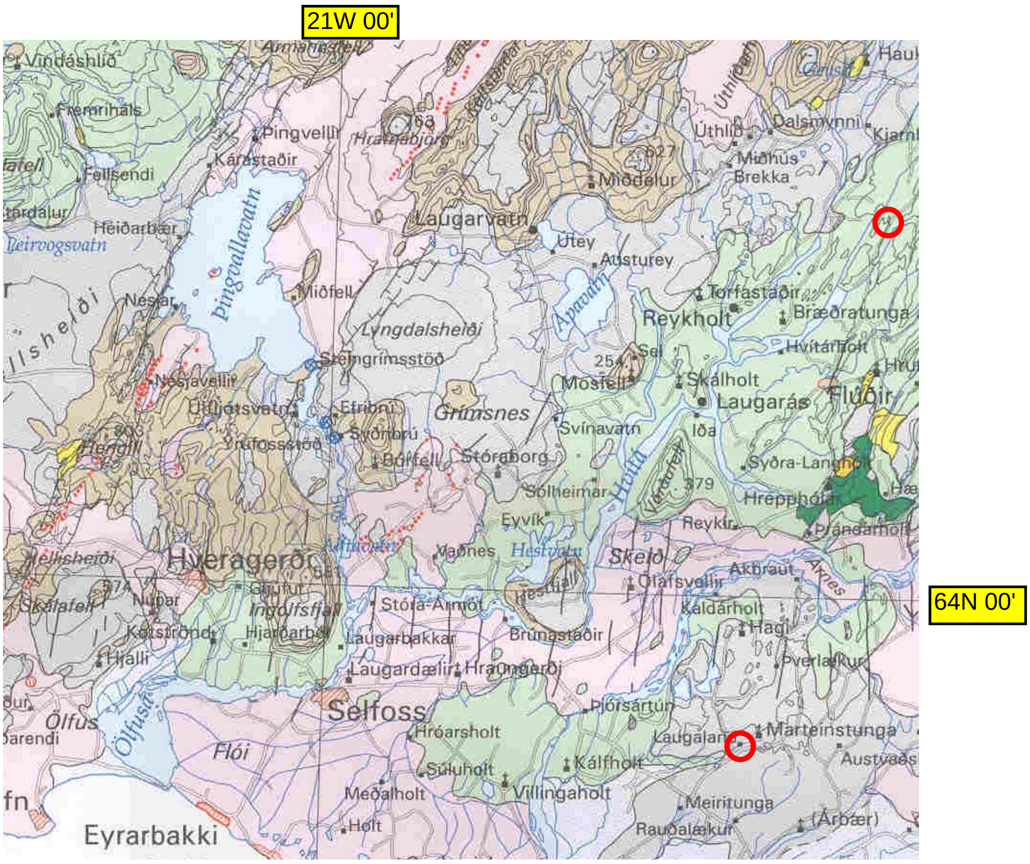


Location of the HH-1 well at Haukholt í Hreppum (upper red circle) and the LL-3 well at Laugaland (lower red circle). 1:1 detail of the Geological Map of Iceland (Jóhanneson & Saemundsson 1998).

# Borehole LL-03, Laugalandi í Holtum, Geological report

Elsa G. Vilmundardóttir
Steinar Thór Gudlaugsson
Gudmundur Ó. Fridleifsson
Orkustofnum 1999, 05-99008

## Abstract

The report is a shortened geological account on borehole data from well LL-03 in Laugaland í Holtum. It is prepared as part of a VSP-experiment carried out by Norsk Hydro in three Icelandic wells in 1998. Well LL-03 was drilled in 1977 to 1308 m depth to provide hot water to a district heating system. The borehole was selected for the experiment mainly because it provides easy access to a typical, regularly developed pile of basaltic lavaflows. The Laugaland area is located on the western flank of the active Eastern rift zone in South Iceland. The bedrock belongs to the oldest part of the Hreppar formation and is considered to be 2.5-3.0 m.y. old. Based on correlation between boreholes, the dip at Laugaland is estimated to be 1-4° to the NW. Two nearly vertical dykes striking NE-SW have been detected in the vicinity of well LL-03 by surface magnetic measurements. Two fracture zones, one striking N15°E and the other N75°E, have also been detected by surface resistivity measurements. The rocks penetrated by the borehole are mostly basaltic lavaflows with thin red, sedimentary interbeds. Hyaloclastites are quite rare in the well and mostly composed of reworked tuffs and breccias. The secondary minerals place the field in the mesolite/scolesite alteration zone.

**Table 1.** *Well LL-03, overview.*

| | |
|---|---|
| Year drilled | 1977 |
| Total depth | 1308 m |
| Drillbits used | 15” to 16 m, 7 7/8” to 1308 m |
| Casing | 14” to 16.2 m |
| Cemented interval | 884.2 m to 932.6 m |
| Borehole geology | Regular pile of subaerial lavaflows containing less than 5% sedimentary interbeds, hyaloclastite, breccia and dikes |
| Cuttings | Every 2 m |
| OS logs | Temperature, caliper, natural gamma ray, neutron-neutron and normal resistivity (16” and 64”) |
| Logs by Geoforschungszentrum Potsdam | Borehole compensated sonic (BCS), dual induction log (DIL), natural gamma ray and borehole televiewer (BHTV) |

# Borehole LN-10, Thorlákshöfn, Geological report

Gudmundur Ó. Fridleifsson
Steinar Th. Gudlaugsson
Orkustofnum, 1998, 05-98071

## Abstract

The report is a shortened geological account on borehole data from well LN-10 in Thorlákshöfn. It is prepared in relation to Norsk Hydro's 1998 VSP-experiment. Two other wells in Iceland will be studied in the project. Well LN-10 was drilled in 1987 to 1096 m depth in an attempto to acquire geothermal water for fishfarming but results were negative. Geologically Thorlákshöfn is sited on a postglacial lava on the eastern flank of the active rift zone in western Iceland. The drilling and design of LN-10 is described along with lithological and geophysical logs and temperature profiles of the well, acquifers or feed points encountered during drilling, injection packer and pumping tests as well as chemistry of the water. LN-10 yields 27°C hot brackish water from acquifers below 150 m depth, but a very limited amount of water can be obtained by pumping. According to well test and model a steady watertable will be reached within a day for a pumping rate of 10 l/s. A neighbouring well, LN-8, is also shortly described for comparison and complementation.

**Table 1.** *Borehole LN-10*

| | |
|---|---|
| Year drilled | 1987 |
| Drillbit to | 1096 m |
| Borehole geology based on cuttings | 2-20 m Relatively coarse-grained fresh basalt lava<br>22-28 m Cuttings lacking<br>28-58 m Unaltered pillow lava formation<br>58-60 m Thin sedimentary layer with molluscs<br>60-114 m Pillow lava formation<br>114-146 m Layered shallow marine sediment<br>146-206 m Relatively unaltered coarse-grained lava flows<br>206-222 m Pillow lava base from the same lava as above<br>222-252 m Layered sedimentary tuff, with sand and silt lenses<br>252-272 m Two coarse-grained olivine tholeiite lava flows separated by a thin, brown and dense sedimentary layer<br>272-290 m Again, an exceedingly dense and fine-grained sedimentary tuff<br>290-304 m Lava flow, scoriaceous at top<br>304-316 m Layered basaltic sediment<br>316-344 m Apparently 2-3 lava flows<br>344-372 m Layered fine-grained tuff sediment<br>372-404 m Pillow lava underlain by tuffaceous sediment<br>404-472 m Coarse-grained lava flows<br>472-498 m Layered dense sedimentary tuff<br>498-682 m Lava pile<br>682-700 m Tuff layer, cemented<br>700-1075 m Lava pile. |

# Borehole HH-01, Haukholt í Hreppum, Geological Report

Elsa G. Vilmundardóttir
Gudmundur Ó. Fridleifsson
Steinar Thór Gudlaugsson
Orkustofnum, 1999, 05-99009

## Abstract

The report provides geological background information for the interpretation of a VSP-experiment carried out in 1998 by Norsk Hydro in well HH-01 at Haukholt in South Iceland. Well HH-01 was selected for the experiment mainly because it provides easy access to a typical pile of volcano-clastic rocks formed subaquatically/subglacially. Haukholt is located within volcanics belonging to the Plio-Pleistocene Hreppar formation. At Haukholt, the volcanics dip approximately 8° to the NW and some 400-500 m have been eroded from the original depositional surface. Well HH-01 encountered an exceptionally high, near linear geothermal gradient of 130-140°C/km indicating a stagnant (convection free) fluid system. The succession of rocks penetrated by the well consists of primary hyaloclastite formations, reworked (sedimentary) tuffs and lavas. Based on the analysis of cuttings, 59 rock units have been identified. They have been grouped into 13 volcanic formations: five lava formations (totalling 330 m in thickness), four primary hyaloclastite formations (480 m) and four formations of reworked tuff (536 m). A cursory study of the hydrothermal alteration minerals indicates that the wellhead is located within the chabazite-thomsonite alteration zone, whereas most of the remaining succession falls within the mesolite-scolecite zone. The deepest part of the well, below 1265 m, lies within the laumontite zone.

**Table 1.** *Well HH-01, overview*

| | |
|---|---|
| Year drilled | 1997 and 1998 |
| Rigs | Ýmir and Azi |
| Total depth | 1346 m |
| Drillbits used | 10 ¾" to 5.4 m (cussion) Ýmir<br>9 7/8" to 101.5 m (cussion) Ýmir<br>7 ¼" to 452,5 m (cussion) Ýmir<br>7" to 606.5 m (cussion) Azi<br>6 ¾" to 1346 m (rotary) Azi |
| Casing | 10 ¾" to 5.4 m cemented<br>8 5/8" to 101.1 m cemented |
| Cemented interval | None below casing |
| Borehole geolog | 0-100 m Lavas<br>100-350 m Hyaloclastites<br>350-374 m Lavas<br>374-478 m Hyaloclastites with lava interbeds<br>478-530 m Lavas<br>530-790 m Reworked tuffs and volcanoclastic sediments<br>790-900 m Hyaloclastites<br>900-932 m Lavas<br>932-1046 m Volcanoclastic sedimentary rocks<br>1046-1168 m Lavas<br>1168-1312 m Volcanoclastic sedimentary rocks<br>1312-1328 m Hyaloclastite<br>1328-1346 m Volcanoclastic sedimentary rocks |
| Cuttings | Every 2 m |
| OS logs | Temperature |